Modeling, controlling and optimizing the application of photovoltaic energy on CDI cells

by

Alaa GHAMRAWI

MANUSCRIPT-BASED THESIS PRESENTED TO ÉCOLE DE TECHNOLOGIE SUPÉRIEURE
IN PARTIAL FULFILLMENT FOR THE DEGREE OF
DOCTOR OF PHILOSOPHY
Ph.D.

MONTREAL, 8 SEPTEMBER 2023

ÉCOLE DE TECHNOLOGIE SUPÉRIEURE
UNIVERSITÉ DU QUÉBEC

BOARD OF EXAMINERS

THIS THESIS HAS BEEN EVALUATED

BY THE FOLLOWING BOARD OF EXAMINERS

M. Maarouf Saad, Thesis supervisor
Department of Electrical Engineering, École de technologie supérieure

M. Imad Mougharbel, Thesis Co-Supervisor
Department of Electrical Engineering, École de technologie supérieure

M. Robert Hausler, Chair, Board of Examiners
Department of Construction Engineering, École de technologie supérieure

M. Ambrish Chandra, Member of the Jury
Department of Electrical Engineering, École de technologie supérieure

M. Gene Shelp, External Examiner
CEO Current Water technologies inc.

THIS THESIS WAS PRESENTED AND DEFENDED

IN THE PRESENCE OF A BOARD OF EXAMINERS AND THE PUBLIC

ON 31 AUGUST 2023

AT ÉCOLE DE TECHNOLOGIE SUPÉRIEURE

FOREWORD

Water is one of the essential elements for life. However, billions of people around the world experience a shortage of drinking water resources and struggle to find a clean source to meet their basic needs. The exact number varies depending on the source, but it is estimated that over 2 billion people already live in areas subject to water stress, and 3.4 billion people, 45% of the global population, lack access to safely managed sanitation facilities.In addition, millions of children die each year by preventable diseases transmitted by water. With an actual world population of over 8 billion, the planet is expected to host a population forecast between 9 and 10 billion by the end of 2050. These numbers represent a population growth of 80 million people per year (WWAP, 2018). This necessarily increases water requirements. Knowing that, in 2050, approximately 2/3 of the world's population will live in large cities, mainly in developing countries such as China and India, access to water risks being made even more difficult than currently. This is because these geographical areas are already in a situation of water deficit, as reported by the United Nations World Water Development Report 2018 (WWAP, 2018).

According to economic theory, the value of a good is determined by its scarcity, which is the gap between limited resources and unlimited needs. Humans certainly use water as if it was limitless: an estimated 80% of all industrial and municipal wastewater, for example, is released into the environment without prior treatment.But fresh water is in fact scarce, and becoming scarcer. Over 2 billion people already live in areas subject to water stress, and 3.4 billion people, 45% of the global population, lack access to safely managed sanitation facilities. According to independent assessments, the world will face a global water deficit of 40% by 2030. This situation will be worsened by global challenges such as COVID-19 and climate change (UNESCO, 2021).

As the water use is expected to continue to increase globally, driven by population growth, economic development and changing consumption patterns, among other factors, the developed Photo-CDI will be a realistic solution based on the renewable solar energy and an eco-friendly desalination system.

ACKNOWLEDGEMENTS

The work presented in this thesis was carried out at the Ecole de technologie Supérieure (ETS) in Montreal, within the department of electrical engineering, under the direction of Professor Maarouf SAAD.

I would like first to express my deepest gratitude to my Supervisor , Dr. SAAD, whose sincerity and encouragement I will never forget. Dr. SAAD has been an inspiration as I hurdled through the path of this PhD degree. He is the true definition of a leader and the ultimate role model.

This thesis would not have been possible without Dr. Imad MOUGHARBEL, whose guidance from the initial step in research enabled me to develop an understanding of the subject for his precious help, his scientific and human qualities.

I am pleased to be able to express my gratitude to Dr. Robert HAUSLER, professor at the ETS, for the honor that has been done to us by accepting to be president of the jury.

Deepest thanks to Dr. Ambrish CHANDRA, professor at ETS, for accepting to examine this work and to participate in my thesis jury.

I also extend my sincere thanks to Dr. Gene SHELP, founder and CEO of *Current Water Technologies inc.* for his advice and also for agreeing to participate in my thesis jury. Beside the team at *Current Water Technologies inc.* for collaborating with my project and being able to benefit from their experiences in the field of MCDI cells.

Finally, I owe my deepest gratitude to all the members of the Electrical Engineering Department at Valleyfield College and the Toromont Energy team, for the help and support they provided me during the completion of this thesis.

I am forever thankful for the unconditional love and support throughout the entire thesis process and every day to my wife and my children who endured my long absences in the laboratory, and who waited impatiently for this moment.

To the soul of my father, to my mother and all the members of my family, I say thank you.

Alaa GHAMRAWI

L'ÎLe Perrot 27 April 2023

Modélisation, commande et optimisation de l'application de l'énergie photovoltaique sur des cellules CDI

Alaa GHAMRAWI

RÉSUMÉ

L'énergie était traditionnellement la composante la plus coûteuse dans la plupart des technologies de dessalement de l'eau. La technologie de l'osmose inversée a diminué son empreinte énergétique jusqu'à 50% grâce aux systèmes modernes thermodynamiques pour le traitement de l'eau de mer. Cependant, cette efficacité énergétique tombe jusqu'à 10% pour le traitement de l'eau moins concentrée tel que l'eau saumâtre. Selon les chiffres de l'industrie de traitement de l'eau, on estime que cette énergie représente plus de 65% du coût de la production de l'eau. Le condensateur dé-ionisateur (CDI) est une méthode de dessalement qui affecte directement les ions dans la solution et les attire vers les doubles couches électriques pour libérer l'eau qui sort pure de la cellule. Les CDI ont été découverts depuis plus de 50 ans, mais ils ont reconnu récemment un développement croissant, grâce au développement des électrodes au carbone et la consommation énergétique de cette technologie. De plus, les récentes études sur les CDI ont attribué un grand avantage énergétique sur cette technique surtout pour les applications des solutions à faible concentration.

En outre de cet aspect énergétique réduit, les besoins de l'eau filtrée/potable sont plus pressants dans les pays les plus ensoleillés (absence des rivières, fleuves, lac. . .) et que les travaux d'électrification au point de production et de traitement constituent un fardeau non seulement énergétique, mais aussi monétaire pour les états en charge.

Dans cette recherche, un modèle d'exploitation de l'énergie photovoltaïque est développé non seulement pour alimenter la cellule CDI, mais aussi pour profiter de l'incidence du contrôle du débit de l'eau pour optimiser l'énergie apportée par le panneau solaire, tout en respectant une concentration stable à la sortie de la cellule.

Mots-clés: Énergie, CDI, photovoltaïque, cellule, Photo-CDI, osmose inversée, contrôle du débit, dessalement.

Modeling, controlling and optimizing the application of photovoltaic energy on CDI cells

Alaa GHAMRAWI

ABSTRACT

Energy has traditionally been the most expensive component in most water desalination technologies. Reverse osmosis technology has reduced its energy footprint by up to 50%, thanks to modern thermodynamic systems for the treatment of seawater. However, this energy efficiency drops to 10% for treatment less concentrated water such as brackish water. According to figures from the water treatment industry, it is estimated that this energy accounts for more than 65% of the cost of producing water. The Capacitive De-Ionizer (CDI) is a desalination method that directly affects the ions in the solution and attracts them to the electric double layers which release the pure water from the cell. CDIs have been discovered for more than 50 years, but they have recently recognized an increasing development, due to the carbon electrodes development and the reduced energy consumption for salt removal. Recent studies on CDI have attributed a great energy advantage to this technique, especially for applications of low concentration solutions.

Add to this reduced energy aspect, that the needs for filtered / potable water are more pressing in the sunniest countries (absence of rivers, lakes, etc.) and that the electrification works at the point of production and treatment remains not only an energy consumption challenge, but also a monetary burden for the states in charge.

In this research, we present a model for the application of the photovoltaic energy not only to supply the CDI cell, but also to take advantage of the flow control impact on the cell to optimize the solar panel energy behavior considering a stable concentration on the product water.

Keywords: Energy, CDI, photovoltaic, cell Photo-CDI, reverse osmosis, flow control, desalination.

TABLE OF CONTENTS

Page

LIST OF TABLES

LIST OF FIGURES

LIST OF ALGORITHMS

Page

LIST OF ABBREVIATIONS

ASAR : Average Salt Adsorption Rate (mol/g/s).

CDI: Capacitive De-ionization.

EBM: Energetic Based Model.

EDL: Electrical Double Layer.

i-CDI: inverted Capacitive De-ionization.

F-CDI: Flow Capacitive De-ionization.

MCDI: Membrane Capacitive De-ionization.

n: Maximum number of samples during the charging phase.

OC: Operational Conditions.

WR: Water Recovery.

LIST OF SYMBOLS AND UNITS OF MEASUREMENTS

AC_E : Average Energetic Capacitance during an adsorption/desorption cycle (Farad/Second).

C_0 is the feed-water molar concentration (mol/l).

$C_{cha,ef}$(t) is the effluent salt molar concentration in charge cycle (mol/l).

C_E : Energetic Capacitance (Farad).

C_T : Traditional Capacitance (Farad).

TC: A charging and discharging cycle (seconds).

E_{stored}: Stored energy inside the cell (wh).

$E_{consumed}$:Consumed energy by the cell during the charging phase (wh).

E_{lost}: Lost energy inside the cell (wh).

E_{cell}: Cell Energy calculated based on V_{cell} and I_{cell} (volt).

I_{ads}: Adsorption or Charging current (Ampere).

I_{des}: Desorption or Disharging current(Ampere).

I_{cell}: Cell current(Ampere).

$m_{electrode}$: The electrode mass(gram).

R_E: Energetic Resistor(ohm).

R_{SC}: Series resistor(ohm).

t_{ads}: Adsorption or Charging period (seconds).

t_{des}: Desorption or Disharging period (seconds).

t_{cycle}: Sum of charging and discharging periods (seconds).

V_{cell}: Cell voltage(volt).

Φ: Constant water effluent flow-rate through the cell (ml/min).

INTRODUCTION

Water is at the heart of sustainable development and is essential for socio-economic development, energy and food production, healthy ecosystems and human survival. Water is also at the heart of climate change adaptation – a crucial link between society and the environment. Water is also a matter of rights. As the world's population grows, it is essential that a balance be struck so that communities have enough water for their needs. At the human level, the issue of water cannot be considered separately from that of sanitation. They are essential for reducing the global burden of diseases linked to lack of fresh water and improving people's health, education and economic productivity. According to UNICEF, the World Health Organization (WHO), UNESCO and FAO (UN, 2018):

- 2.1 billion people do not have access to safely managed drinking water services.
- 4.5 billion people lack safely managed sanitation services.
- 340,000 children under the age of five die each year from diarrheal diseases.
- Water scarcity affects four out of ten people.

0.1 Energy requirement of CDI cells

Desalination is the most effective solution nowadays. However, the energy gluttony of these processes such as thermal distillation, reverse osmosis and electrodialysis has limited the diffusion of these techniques. A quick comparison of the energy consumption of these desalination processes shows that reverse osmosis, for example, is around 4 kWh/m3, while CDI technology only consumes 1 kWh/m3 without taking into consideration that these traditional techniques are based on polluting sources based governed by high fuel consumption that generates greenhouse gas emissions (Welgemoed *et al.*, 2005a; Oren, 2008).

0.2 Problem with CDI cells

Despite the reduced energy requirement for the operation of CDI cells, many questions regarding their application currently remain unanswered due to the nascent state of these cells. Will these systems compete with seawater reverse osmosis in terms of energy requirements? How many charge-discharge cycles will these systems be able to achieve without significant performance degradation? It is clear that CDI cells will be important research topics in the near future, with their most appropriate applications yet to be determined. However, in our research work, we will focus our study on the energy aspect of the cell in order to design a solar model, taking advantage of a photovoltaic source for the treatment of water and the regeneration of electrical power. To achieve our objective, we will divide our design problem into three sub-problems which we had developed as part of our research:

0.2.1 Energy model

The modeling of CDI cells makes it possible to predict their behavior in different applications, based on the analysis of the main physical phenomena appearing during adsorption/desorption phase within the component. The majority of the proposed model of the CDI cell is interested in its aspect of water treatment, or the instantaneous evolution of the components of the model. However, the new developed model should be energy target in order to evaluate energetic profile of the cell during the full desalination cycles. An energetic model will let us to:

1. evaluate the energy inside the cell for a given time in the cycle.
2. Analyze the cell electrical/energetical behavior once connected to a renewable source.
3. simulate the cell behavior by using the developed mode and the experimental values in a simulation software.
4. be used for troubleshooting, diagnostic of the cell beside determining the aging of the electrodes.

0.2.2 Controllability of the CDI

Once the model of the CDI had been accomplished and tested, it is more important to validate the controllability of the cell. Determining the controllability will allow to optimize the suitable parameters to achieve the best performance and optimize by the end the cell salt removal capacity. The application of a closed loop control is applied for the first time on the cell, taking into account a stable concentration of the effluent at the output of the cell. Based on that control four points should be respected in the cell operation:

1. To validate that the CDI desalination process is controllable.
2. To develop the state matrix that could be used in any future research for optimization of the CDI operation
3. To produce a stable water quality at the output of the cell.
4. Finally, to verify the impact of such control on the cell performance in terms of the quantity of removed salt , the quantity of consumed energy , . . .

0.2.3 Application of Solar Energy

Once the controllability of the CDI is proven, its supply by means of solar energy should consider three main objectives:

1. A stable predefined output concentration.
2. An optimization of the solar power that could be used in the desalination process.
3. Elimination of the use of batteries as an inter-media for energy storage purpose.

We aim in this application to profit from each received photon on the solar panel for the production of a drop of desalinated water.

CHAPTER 1

STATE OF THE ART ON CDI CELLS

1.1 Introduction

Capacitive De-ionization (CDI) cell is an emerging technique for removing dissolved and charged species from aqueous solutions, that has already been applied to brackish water desalination (Gabelich *et al.*, 2002), seawater desalination (Jeon *et al.*, 2013), wastewater treatment (Lee *et al.*, 2009a), and water softening (Seo *et al.*, 2010). The last decade has seen a remarkable number of innovations in the exponentially growing field of CDI, including important theoretical (Biesheuvel *et al.*, 2011a,b, 2014), architectural (Jeon *et al.*, 2013; Lee *et al.*, 2009a; Suss *et al.*, 2012; Lee *et al.*, 2014), materials (Porada *et al.*, 2012b; Leonard *et al.*, 2009) experimental methods (Zhao *et al.*, 2012a; Avraham *et al.*, 2011a), and performance optimization (Duduta *et al.*, 2011; Avraham *et al.*, 2011b). In this literature review, we briefly review major aspects of CDI, such as cellular architecture, materials, applications, and theory with an emphasis on major recent advancements. We also try to project the work done that is directly related to our work. The CDI shares many commonalities with other electrochemical systems such as supercapacitors and flow batteries: a CDI cell consists of a pair of porous electrodes (static or flow electrodes), with a separator (open channel or porous dielectric material) in between. The electrodes are generally made of carbon and the feed water circulates between or through the charging electrodes. The pair of porous electrodes is charged with an applied voltage difference typically 1 to <2V (called cell or charge voltage), and the salt ions present in the supply migrate in electrical double layers (EDL) along the pore surfaces at the carbon/water interface, removing salt from the water supply (a process called "electrosorption"). The salt ions are held electrostatically in the double layer until the discharge stage. During discharge, the release of ions results in a flow of brine, and the charge leaving the cell can be used to recover energy (similar to the energy of an electrical discharge capacitor) (Dlugolecki *et al.*, 2013). The first work on a CDI-like system was published by Blair *et al.* (1960a,b), and the next four decades saw only intermittent advances in this technology. Examples of progress during this period include the development of the first macroscopic theory applied to CDI in 1971 (Johnson *et al.*,

1971), and the use of carbon aerogels as CDI electrode material in the mid-1990s (Farmer *et al.*, 1996a). In relation to naming, the term 'CDI' was not used until 1996 when it was introduced by Farmer *et al.* (1995a,b). In contrast to the slow initial development of CDI, the past decade has seen advancements including the development of the CDI membrane (Lee *et al.*, 2009a; Li *et al.*, 2008a), flow electrodes (Suss *et al.*, 2012), flux electrodes (Jeon *et al.*, 2014; Porada *et al.*, 2014; Hatzell *et al.*, 2014), CDI hybrid cells (Lee *et al.*, 2014), Donnan's modified mathematical model for CDI (Biesheuvel *et al.*, 2011b), and the discovery of correlations between pore size and electrosorption performance (Suss *et al.*, 2012). These scientific advances are accompanied by the increasing commercial development of products using CDI technology by several companies around the world.

1.2 Advantages of desalination by CDI cells

As a salt ion removal technology, CDI offers several unique advantages. First, CDI allows salt removal at low (sub-osmotic) pressures and ambient temperatures, the main input being a small cell voltage (about 1 V) and an electric current whose magnitude depends on the system size. So, unlike reverse osmosis or distillation-based desalination systems, the CDI does not need to be coupled to high-pressure pumps or heat sources, allowing an easy scale-up of the system. Second, in CDI, the few salt ions (compared to the many water molecules) are directly transported out of the feed water, as in the case of electrodialysis. This enables potentially very energy efficient desalination of low salinity feed waters, such as brackish water (Zhao *et al.*, 2013a). Third, the operating principle of CDI shares many features with electrochemical capacitors, also known as supercapacitors (Béguin *et al.*, 2014) , including reversible operation and energy storage capability (CDI can be roughly thought of as "desalination with a supercapacitor"). Thus, CDI systems have the unique ability to simultaneously store energy (similar to a supercapacitor) and desalinate water when charging (Suss *et al.*, 2015). Even if this energy storage capacity is not used, the charge once invested for ion removal is almost fully recovered upon discharge of the electrode material, capitalizing on the very high inherent Coulomb efficiency to EDL technologies (Suss *et al.*, 2015). As such, CDI has the potential to be an important part of future

water purification solutions as well as potentially contributing to next-generation distributed power grids.

1.3 Architecture and Material of the cell

In recent years, there has been a proliferation of new architectures for CDI cells, and these have introduced several unique features and new functionalities to this field. In this section, we will briefly review the architectures that have been developed previously (Figure 1.1). The first and most widely used CDI cell architecture consists of a pair of porous carbon electrodes separated by a gap through which the feed water flows (the feed water flows perpendicular to the direction of the field power applied, see figure 1.1 A). This architecture is often called flux architecture (Bouhadana *et al.*, 2010; Porada *et al.*, 2013b), and has also been called CDI with flux between electrodes (Suss *et al.*, 2012). The circulation cell was first seen in the pioneering work of Blair & Murphy (1960a), was revisited in the 1970s and 1980s by Golub *et al.* (1987); Oren *et al.* (1983), and again in the 1990s with the work of Farmer *et al.* (1996b). This architecture has subsequently been used in a wide variety of work, including those demonstrating the removal of salt from various feed waters (Xu *et al.*, 2008), examining the performance of new electrode materials (Porada *et al.*, 2012b; Li *et al.*, 2010) , or performing fundamental studies on salt sorption on porous electrodes (Avraham *et al.*, 2009; Zhao *et al.*, 2012b). Early work on CDI-like systems in the 1970s by Johnson & Newman (1971) developed a cell in which the power flow was directed directly through the electrodes themselves and parallel to the direction of the applied electric field (figure 1.1 B). Work on such CDI cell (Avraham *et al.*, 2009) or continuous flow electrode (Suss *et al.*, 2012) architectures was apparently abandoned for nearly 40 years until Avraham *et al.* (2009, 2011a) and Cohen *et al.* (2011) used flow-through electrodes in a three-electrode cell to study fundamental performance parameters, such as charging efficiency. The authors of the latter work noted that through-electrodes allowed faster charging of cells compared to systems with flow between the electrodes (Avraham *et al.*, 2009). In 2012, Suss et al. investigated the performance of a CDI cell with a flow-through electrode architecture and novel monolithic hierarchical carbon airgel (HCAM) electrodes, and demonstrated a reduction

in concentration down to 70 mM of a power supply. NaCl when operated in stopped-flow mode (no flow during cell recharge), with an average sorption rate of nearly 1 mg/g.min. (Suss *et al.*, 2012). The main advantage of this architecture is to eliminate the need for a separator layer which also serves as a feed flow channel, thus allowing a minimization of the separator thickness (typically 200-500 mm to about 10 mm) (Suss *et al.*, 2012). This reduced spacer thickness may allow for more compact cells with lower cell ionic strength and potentially faster desalination by reducing the diffusion timescale governing salt removal between the electrodes (Suss *et al.*, 2014). This architecture requires the use of multi-scale porous electrodes, with both micrometer-scale pores to allow flow through the electrodes at moderate fluid pressures, and micropores (nanometer-scale pores) to allow strong salt sorption (Suss *et al.*, 2012; Avraham *et al.*, 2009).

A major variation in the basic architecture of CDI cells (a cell with two porous electrodes and a separator) occurred with the development of the CDI membrane (MCDI), with the first scientific demonstration of an MCDI system in 2006 by Lee *et al.* (2009a). This architecture uses ion exchange membranes on the separator side of each electrode (Figure 1.1C). As in electrodialysis cells, the feedwater channels in MCDI cells are bounded by an anion exchange membrane (AEM) and a cation exchange membrane (CEM). In MCDIs, the configuration most often used is a stand-alone CEM placed at the cathode, and a stand-alone AEM placed at the anode. Alternatively, by using the porous electrode as a structural scaffold, it is possible to directly coat the membrane over the electrode, which may allow for a thinner membrane layer than when using a stand-alone membrane. (Kim *et al.*, 2010a).The main benefit of adding membranes to the CDI cell is the improved charging efficiency (which is related to the energy efficiency of the cells), as the membranes prevent co-ions (ions having the same charge as the local electrode) to carry stray current and can increase salt storage in the electrode macropores (Biesheuvel *et al.*, 2011b). Additionally, the membranes can be designed to have selectivity between different ions of the same charge sign, which provides an additional level of capability suitable for complex multi-ion systems (Kim *et al.*, 2012; Yeo *et al.*, 2013).

Furthermore, the advantage of charging a CDI cell with constant current I than constant voltage, namely that constant current allows constant cell effluent concentration, was first demonstrated on an MCDI cell (Zhao *et al.*, 2012a). The latter cell achieved a concentration reduction of nearly 20 mM and an average salt adsorption rate (ASAR) of up to 2.3 mg/g/min with optimized operational parameters (Zhao *et al.*, 2013b). Recently, the CDI flow cell has been modified through the use of a surface-treated carbon anode, leading to the case of the inverted CDI (i-CDI, Figure 1.1 D) (Gao *et al.*, 2015). This latter cell used a carbon xerogel anode impregnated with a negative surface charge via chemical surface treatment and virgin carbon xerogel as the cathode. The cell demonstrated reversed behavior, with cell charging causing desorption of EDL ions from the electrodes and cell discharging causing ion electrosorption. The sorption performance of i-CDI cells was maintained over 600 hours of continuous operation at 0.8 V cell voltage, in contrast to the relatively rapid decay observed for a CDI cell with only pristine carbon xerogels (Gao *et al.*, 2015). In 2013, a new architectural class for CDI was demonstrated, which uses carbon flux electrodes or carbon slurry electrodes that can be pumped through the electrode compartments (Figure 1.1 F) (Jeon *et al.*, 2013). This concept of flux electrode CDI, or FCDI, follows that of mud-based electrodes developed for electrochemical energy storage systems such as the electrochemical flux capacitor (Presser *et al.*, 2012), and semi-solid batteries lithium-ion (Duduta *et al.*, 2011; Brunini *et al.*, 2012).The FCDI cell offers two major advantages over CDI systems with non-fluid or static electrodes.

First, in FCDI, the feed water flowing through a single cell can be continuously desalinated, since the discharge of activated carbon particles (brine formation) can occur as a separate process downstream of the cell (Jeon *et al.*, 2013). In all previous CDI architectures based on static electrodes, the cell can only desalinate for a finite time until the EDLs of the porous electrodes are fully charged, then desalination must cease while the cell is discharged to allow cycles desalination plants (Porada *et al.*, 2013b). This intermittent operation can also require complicated fluid manipulation as desalted streams (during loading) and brine streams (during unloading) emerge, at different times, from the same spacer between the electrodes.

A second major advantage is that FCDI, by continuously introducing uncharged carbon particles into the load cell, can effectively increase the capacity available for desalination above that of static electrode CDI systems. Thus, the FCDI can desalinate higher salinity flows than static CDI systems, and desalination of high salinity water (with a total dissolved salt concentration approximately that of seawater) has been achieved with the FCDI by Jeon *et al.* (2013) when using a total suspension flow rate of 50 ml/min and a feed flow rate of 3 ml/min (Jeon *et al.*, 2013). In 2014, an FCDI architecture was proposed that desalinates without ion exchange membranes or feed streams between the electrodes (Figure 1.1 G) (Hatzell *et al.*, 2014). This latter architecture can potentially enable compact and low-resistance systems (similar to the benefits of continuous flow vs. flow-through CDI) (Hatzell *et al.*, 2014). Linked to FCDI, Porada et al. introduced in 2012 another form of moving electrodes through the use of moving wires to perform desalination (Porada *et al.*, 2012a). In this system, the wires consist of a graphite rod coated with porous activated carbon and an optional outer coating of an ion exchange membrane. The mechanical movement of wires occurs between a feed and brine stream, where the wire is loaded into the feed stream and unloaded into the brine stream. Operation of this system with multiple wires running between the feed and brine streams can allow continuous desalination of the feed stream. In 2015, another advanced research was carried out which combines a battery electrode (sodium manganese oxide) and a capacitive electrode (porous carbon) in a single desalination cell (Lee *et al.*, 2014), Figure 1.1 E) inspired by the previously developed desalination battery (Figure 1.1 G) (Pasta *et al.*, 2012). Such a ”hybrid CDI” system allowed a high salt sorption of about 31 mg/g (Lee *et al.*, 2014), compared to purely capacitive CDI cells which reach up to about 15 mg/g (Porada *et al.*, 2015).

1.4 Electrical capacity

One of the most interesting metrics for the CDI cell researches is charge storage capacity, a metric shared with the supercapacitor community. This metric can be obtained from measured data for current versus time during charging and discharging. Current data in units of Amps (A = C/s) can be integrated as a function of time to obtain the electric charge transferred between the

A

The first common architecture of the CDI cells consists of on pair of porous carbon electrodes separated with a space. The feed water pass through this space perpendicularly to the applied electrical field on the cell.
That architecture is called FLUX architecture and so the flux electrode CDI.
The circulation cell was introduced for the first time in Blair and Murphy works in 1960, and revised between 1970 and 1980 by Oren and Soffer and finally, in 1990 in Farmer et al.

1960

1970

The first works on the CDI systems in the middle of 70's was initiated by Johnson et al., who introduced the parallel flux cells where the water flux pass through the electrodes in the same direction of the applied electrical field on the cell.
The works were left after that for 40 years before Avraham et al. reinstated the concept in their research. In 2012, Sus et al. had noticed the advantage of such architecture in eliminating the need of the separation layer as a flow channel. This approach had contribute in minimizing the thickness of the pacer resulting in more compact cell with a reduced ionic resistance and a faster potential desalination due to the time

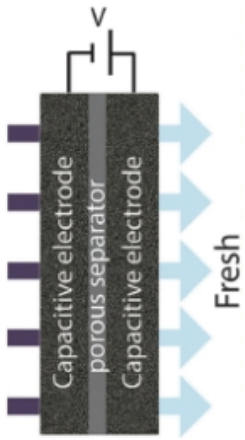

B

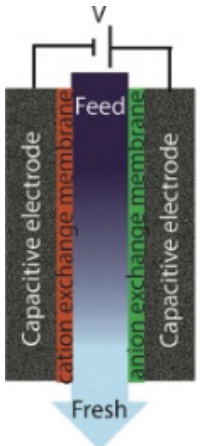

C

The major development of the basic architecture of the CDI cells (a cell with two electrodes and a spacer in between) was the introduction of the membrane and the so called MCDI in 2006 by Lee et al. in 2006.
Two ions exchange membranes are placed beside each electrode. As for the electrodialysis cells, the water flow is delimited by an Anion Exchange Membrane (AEM) and a Cation Exchange Membrane (CEM).
The main advantage of adding the membrane in the CDI cell is the improvement in the charge efficiency since the membranes were able to prevent the co-ions to flow the parasitic current and increase the storage of the salt in the electrodes macro-pores.

2006

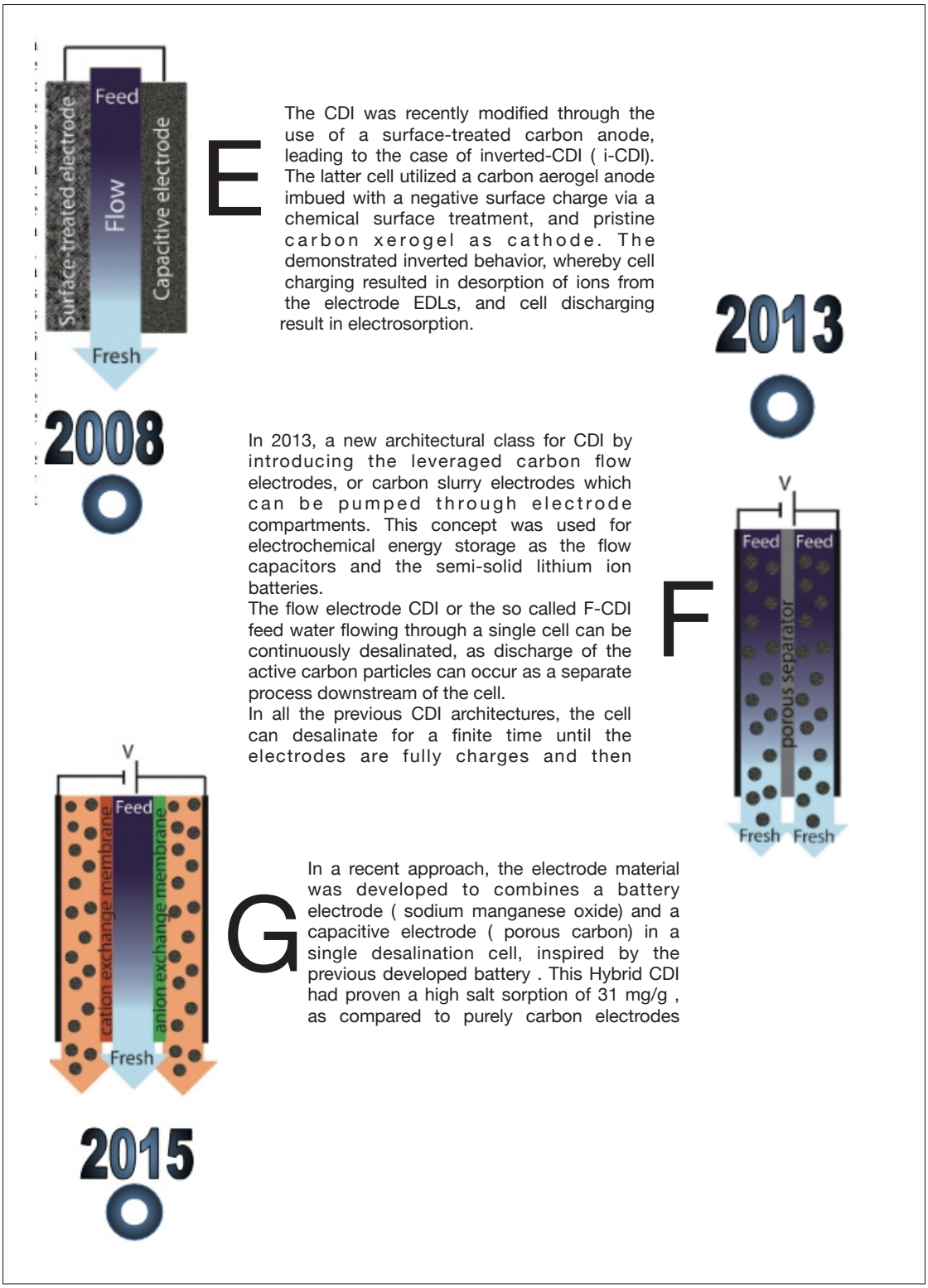

Figure 1.1 Architectures and matriels of the CDI cells based on Suss *et al.* (2015)

cell electrodes (units of Coulombs, C). Additionally, by subtracting the (non-capacitive) leakage current, which is typically greater during charging compared to discharging, the calculated capacitive charge and applied cell voltage can be converted to cell or electrode capacitance by F/g (Zhang *et al.*, 2015) the capacitance of a single electrode, the capacitive load at C must be divided by the mass of a single electrode and by half the cell voltage (assuming cell symmetry), leading to a conversion factor (Seo *et al.*, 2010; Stoller *et al.*, 2010; Zhang & Pan, 2015). This single electrode capacitance is often called 'specific capacitance' in the field of supercapacitors (Béguin *et al.*, 2014; Stoller & Ruoff, 2010). Equivalently, the 'volumetric capacitance' in the supercapacitor community for single electrodes, which is four times larger than the cell volumetric capacitance (the capacitance of the cell divided by the volume of the two electrodes).

Although many similarities exist between the supercapacitor and CDI fields, the focus and key performance parameters are different. Thus, although charge storage is a key performance metric for supercapacitors (energy storage), we treat this metric within the framework of specific environmental conditions such as concentration, temperature,...

1.4.1 Electrical and salt removal relation

The electrical charge that builds up in a pair of electrodes during charging (and is released during discharge) can simply be divided by the Faraday number, F = 96,485 C/mol, to arrive at the charge expressed as units of moles, and this value can be compared to the measured salt adsorption per cycle (also expressed in moles). This leads to the definition of charge efficiency, Λ, as the ratio of adsorbed salt to charge. The concept and significance of the ratio of salt removed to invested electrical charge stored was first described by Johnson & Newman (1971), and the terminology 'charge efficiency' was used for the first time by (Avraham *et al.*, 2009) and Zhao *et al.* (2010) proposed the Λ symbol for charging efficiency, and provided the first comprehensive dataset for Λ as a function of cell voltage and food salinity. The metric Λ is used in CDI static electrode cycle analysis as an integral property of the entire cycle, and Λ must be less than unity (but can approach unity). Λ is a function of the cell voltage during charging and discharging, as well as the salt concentration of the feed water. Generally, Λ increases with

higher charge and discharge voltages and with decreasing supply concentration (Zhao *et al.*, 2010). Λ is a critically important parameter when evaluating CDI cells because of two important implications. First, the electrical power requirements of a CDI cell are determined by the value of Λ, and generally higher values of Λ result in lower power consumption.

CHAPTER 2

OPERATION, MODEL AND EQUATIONS

2.1 Introduction

In this chapter we will resume the different approaches and equation that have been used in the development of the thesis and the essential points in the literature review that we served in our model elaboration and the proposed operation method for the application of the solar energy on the CDI cells.

2.2 Operating principle

Capacitive Deionization Cells (CDI) is a water desalination technology based on the application of a potential difference between two porous electrodes placed opposite each other and separated by a layer of membranes and a space for circulation water to be treated. In the desalination phase, the ions are absorbed on the carbon-water interface with the micropores of the porous carbon electrodes. Once the electrodes reach a saturation level of adsorption capacity, the voltage across the electrodes will be reduced and even reversed, allowing ions to abandon the electrode. The ions will be accumulated between the electrodes, or a highly concentrated salt solution will be eliminated by a flow of water released during the cleaning or flushing phase. So CDI technology is based on two modes of operation: purification (adsorption) and cleaning (desorption).

Figure 2.1 shows that the application of the direct current voltage applied to the electrodes of the CDIs ensures the elimination of the ions in the flow of water passing by absorption of these ions in the inversely charged plate to the charge carried by these ions: thus positively charged ions such as Na+ will be picked up on the negative electrode and negatively charged ones such as Cl- will be attracted by the positive electrode. This mode of phase is called purification or absorption which takes place until the saturation of the electrodes by the concentration of the accumulated ions. The detection of the saturation phase is determined by comparing the level of conductivity of the incoming flux with respect to that leaving. If the conductivity is slightly

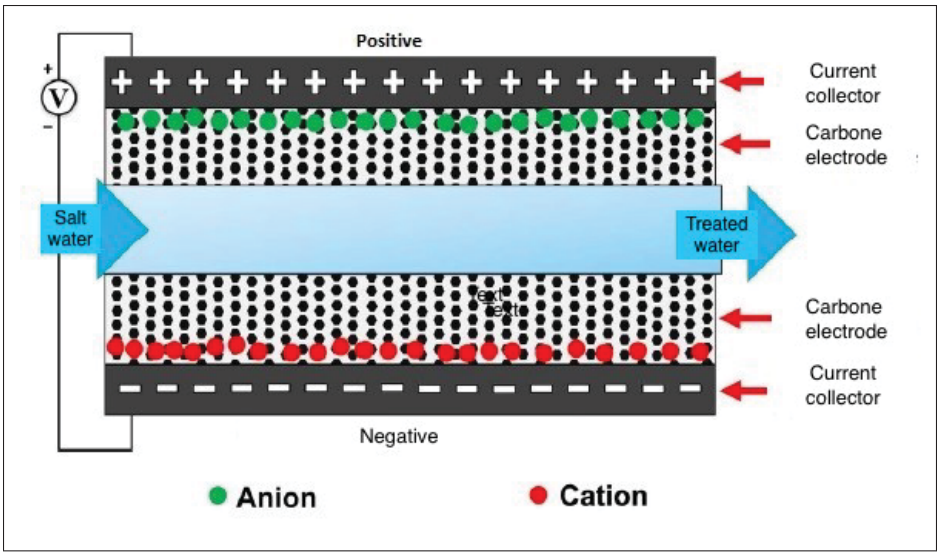

Figure 2.1 Fundemental basic of operation of a CDI cell

changed between the two points, it seems that the saturation phase has been reached since the electrodes are not able to retain the new incoming ions. The cleaning phase then begins by reversing the polarity on the electrodes or by transferring the stored energy to a new cell or a system to exploit this energy on the distribution network. At the same time as this phase, the outlet valves change the destination of the product from the desalinated water tank to the waste water tank, as well as the water flow cleaning the saturated electrodes (Welgemoed & Schutte, 2005a). The energy stored in the CDIs during the purification phase process can be recovered by power converters. The efficiency of the CDI desalination process is improved using advanced energy recovery techniques. Energy storage is due to the existence of two charged electrodes separated by a barrier of brackish water which plays the role of the electrolyte.

2.3 Comparison CDI Vs Supercapacitor

As mentioned before: there are many similarities between supercapacitor cells for energy storage and CDI cells. Architecturally, both consist of a pair of conductive porous electrodes (static or flow electrodes) that are capacitively charged to store ions in EDLs at the interface between the solid carbon matrix and the electrolyte liquid. The dynamics of supercapacitors are often

modeled via linear circuits, the most common circuit being the transmission line model (Rizoug *et al.*, 2010). This circuit model can capture the charge/discharge of a porous medium composed of two continuous interpenetrating conductive media, such as an electrically conductive solid carbon material (the pore walls), and an electrolyte filling the void volume of the pores. For supercapacitor applications, the charge is stored capacitively at the carbon/electrolyte interface. Generally, for the sake of simplicity, the resistance in electron-conducting carbon is assumed to be negligible (Stoller & Ruoff, 2010), although the treatment of carbon as an ideal metal is in fact incorrect. A supercapacitor is normally modeled by a series of capacitor branches and resistors, the resistive elements represent the ionic resistance of the electrolyte in the pores, while the capacitive elements represent the EDLs forming at the pore walls. Nomenclature for micropores and macropores (for ion transport pathways through the electrode) goes back to Johnson & Newman (1971), and it is different from the IUPAC definitions for the sizes of pores. From this circuit model, a simple partial differential equation can be formulated to describe the dynamics of the local electric potential in the electrolyte (Biesheuvel *et al.*, 2011a,b, 2014) :

$$\frac{\partial \phi}{\partial t} == \frac{1}{RC}\frac{\partial^2 \phi}{\partial x^2} \tag{2.1}$$

where ϕ is the electric potential in the electrolyte of the pores, R represents the ionic resistance of the electrode (Ohm.m), C is the EDL capacity of the electrode per unit volume (F/m3) and x is a position coordinate in the electrode. Equation 2.1 assumes a 1-dimensional (1D) planar geometry but can be easily adjusted to describe any geometry. The transmission line model serves as a useful approximation to the charging dynamics of a supercapacitor even though it has significant limitations, for example, EDL often cannot be modeled exactly with a linear capacitor element (because EDL capacitance typically varies with applied voltage) (Barrade, 2002), and this model may not be appropriate for describing charging in porous media with nanoscale pores (Biesheuvel *et al.*, 2012). In supercapacitor cells, the ion concentration in the electrolyte is usually very high (1 M or more), and so during charging the ion concentration in the pore volume (outside the EDLs) remains at little almost unchanged and therefore R can be considered as a constant. Although similar in architecture, significant differences in

charging dynamics can be observed between supercapacitors and CDI cells. In a CDI cell, the ion concentration is significantly lower than in supercapacitors (typically 1–100 mM), so that during charging the pore mass is significantly depleted of ions (i.e. desalinated). Thus, a key difference between supercapacitors and CDI cell dynamics is that in CDI cells the dynamic cannot be captured by linear circuit elements equation 2.1, because the desalination process necessarily introduces time-varying electrolytic resistances in the system (Zhang & Pan, 2015). Additionally, modeling salt concentration dynamics requires an additional parameter called charging efficiency. CDI models must also take into account the complexities associated with ionic mixtures, for example containing multiple species of cations (Zhao *et al.*, 2012b). As a result, the dynamics of CDI cells can be considerably more complex than it is in the supercapacitor, but, nevertheless, understanding supercapacitors provides an excellent foundation upon which to build an understanding of CDI cells.

2.4 Electrical modeling of the CDI cell

2.4.1 Basic RC Model

Obviously, modeling with a simple capacitive element is not sufficient for these capacitors. Indeed, in particular because of the liquid electrolyte ensuring the contact between the dielectric and the cathode, this type of element has a non-negligible resistive part. Thus the simplest modeling is that composed of a capacitor in series with a resistor as in Figure 2.2

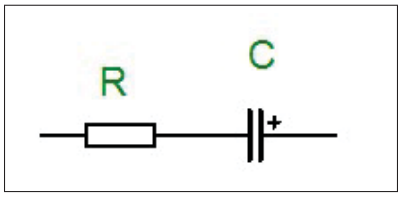

Figure 2.2 Simple RC model

2.4.2 Basic RC model with a leakage resistor

Figure 2.3 shows a basic diagram representing the electrical behavior of CDI cells through the two main phenomena appearing in storage systems:

1. the injection or extraction of charges over generally relatively short durations is quantified through (R, C) type parameters.
2. the presence of a permanently stored charge induces secondary phenomena generating pressure losses and often represented by a leakage resistance (Rl) noted parallel resistance (Rp) or (Rf) sometimes.

There are also some models taking into account the leakage resistance of the components themselves. The latter comes from the resistivity of the dielectric which, as defined in some supercapacitors works (Rizoug *et al.*, 2010).

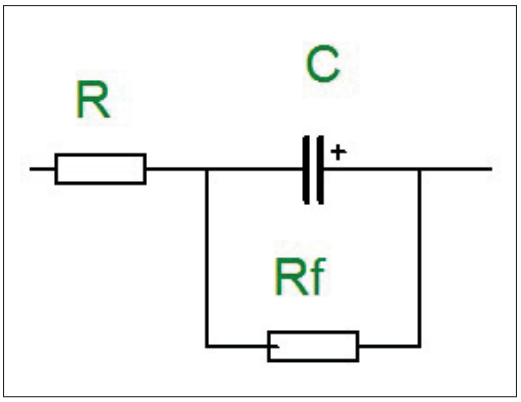

Figure 2.3 RC model with a parallel leak resistance

2.4.3 Model of the transmission line

To manage to represent the temporal phenomena of recharging/discharging of CDI cells, models equivalent to the transmission line are used. Thus, the cell is represented by a finite representation of Ri–Ci type components. These are defined by choosing different time constants adapted to the intended use; it is then necessary to characterize these elements by identifying the Ri-Ci branches used. In this case, instead of taking a linear resistance R and a capacitance C (homogeneous

medium) as defined in the previous part, we take circuits Ri-Ci independent of each other from the point of view of identification thanks to the differences imposed time constants. This type of model was notably proposed by Andres *et al.* (2008).

This model describes the behavior of the system by decomposing its response into several parts; each part is represented by a different time constant as shown in Figure 2.4.

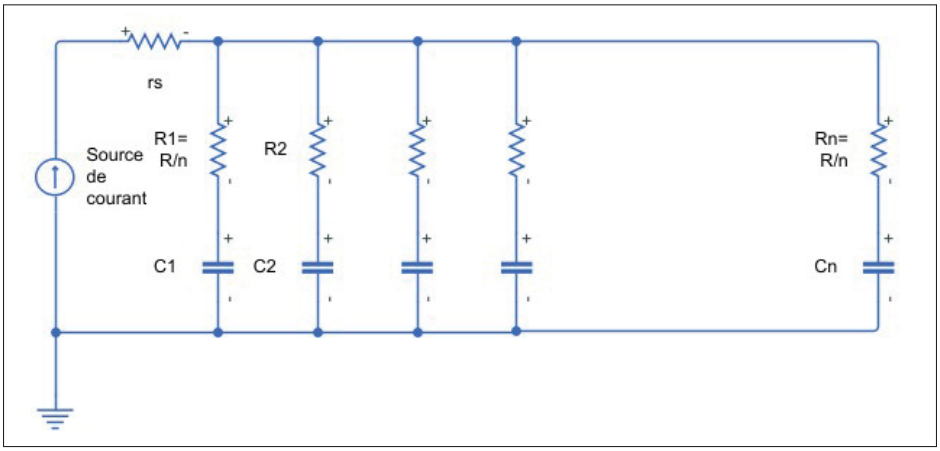

Figure 2.4 Transmission line model

2.5 Operating Conditions

The models presented previously implicitly assumed a constant series resistance (R), but in CDIs, this is not the case. Indeed, firstly this resistance is composed of about 80% of the resistance due to the electrolyte. However, this electrolyte (like many ionic conductive liquids) sees its resistivity vary greatly with temperature. The higher the water temperature, the more the resistivity decreases due to molecular agitation. It could therefore be admitted that the above-named resistance is constant for a given temperature. In addition, there is another phenomenon which makes this resistance variable: it is its sensitivity to the concentration of salt water which affects the resistivity. Indeed, for a given temperature, the value of R decreases with the increase in the input concentration since the conductivity of the ions will increase. This is called the Debye-Falkenhagen (Anderson, 1994) effect which occurs during our study when a modification of the treated concentration is applied. Thus, rather than denoting R, it

would be more appropriate to denote R(Ci), or even R(Ci, T) with Ci the concentration and T the temperature. By convention, the notation used is ESR for Equivalent Series Resistance. Another factor also affects the operation of the CDI cell or the values of the parameters of the model, it is the flow rate of the water entering inside the cell. In fact, as flow increases until saturation, the amount of salt retained in the cell increases (Gasperi, 2005), which makes flow another important factor to consider when operating the system.

2.6 Mode of operation

CDI cells can be operated in different charging modes, the main modes of which are those of constant voltage (CV) charging (Hemmatifar *et al.*, 2015; Bian *et al.*, 2016; Kim *et al.*, 2015; Duduta *et al.*, 2011) and those for constant current charging (CC) (Zhao *et al.*, 2013b, 2012a). Until now, the most common method in CDI technology is the application of a constant voltage (the difference in electrical potential between the two porous electrodes) during the charging phase (absorption of ions) and also in phase the discharge (ion repulsion) of the electrodes. For example, during absorption, the typical value of voltage applied per cell Vcell=1.2V applied to absorb ions and produce drinking water, also during discharge, the two electrodes are short-circuited in the common practice to reduce the voltage to 0 V. However, studies have shown that constant voltage operation has an impact on the change of the outlet flow concentration over time, for example, the ion concentration of the produced water (drinking water) changes over time, as ion removal step. This phenomenon is due to the start of the absorption phase where the EDL (double layer electrode) are initially uncharged, and since the flow force in the channel is at a maximum (No loss of cell voltage in the EDL). This means that a large part of the ions are directed towards the electrodes. As the absorption in the electrodes progresses, the voltage of the electrodes gradually increases and the remaining voltage passing through the membranes begins to decrease over time.

In this way, the salt concentration in the outlet water initially begins to decrease and then gradually increases again. This gradual change in concentration over time is undesirable in

practical applications unless the produced water is stored in large tanks. We then speak of production at a constant level of desalination.

Another method was proposed in a previous study (Zhao *et al.*, 2012a) in order to obtain a lower salt concentration. The idea is to apply a constant current (CC) between the two electrodes instead of the constant voltage (CV). Indeed, the applied external electron current I will also be diffused as a large ionic current in the cell, following the contribution of the ionic fluxes of positive ions (such as Na+) and negative ions (such as Cl -). Studies have shown that the application of constant current generates a constant concentration product over time, either in the ion absorption phase or in the repulsion phase. Another advantage of applying direct current is the ability to effectively and easily control the concentration to a certain value by varying the current level.

2.7 Energy Profile

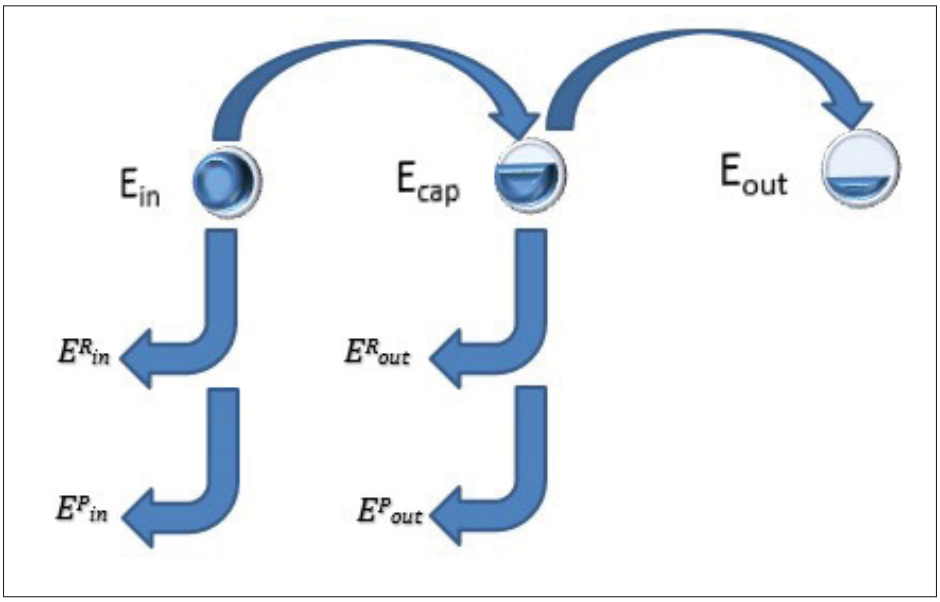

Figure 2.5 Energy diffusion inside CDI cell

The diagram in Figure 2.5 shows the energy path in a typical CDI cell. To understand this, we first note that the purpose of any CDI system is to increase the potential energy of the electrode

stack from its base level and, therefore, to attract ionic species to the electrodes with electrostatic forces. This is done by transferring electrons to the cell via an external voltage and/or current source. This input energy is denoted E_{in} in Figure 2.5. However, not all of the transferred potential energy is used for the storage of ionic charges (capacitive energy or E_{cap}), because there are different loss mechanisms during the charging process. Namely, the resistive and parasitic energy losses are denoted by E^R and E^P respectively in Figure 2.5. The charging process continues until one or more charging criteria are met, such as a specified maximum cell voltage or a predefined amount of electronic charge transferred. Then the regeneration or discharge process begins and gradually lowers the potential energy level to its minimum level. The extractable or recoverable energy E_{out} is less than E_{cap}, however, because there are also resistive and parasitic energy losses in the discharge process: E^R_{out} and E^P_{out}, respectively. Ein is measured as the (unsigned) magnitude area under the curve of voltage versus time during charging times current during charging. E_{out} is measured as the (unsigned) magnitude area under the voltage-time curve during discharge multiplied by current during discharge. Part of E_{in} is dissipated (by internal resistance and parasitic feedback losses) and the rest of E_{in} is stored as capacitive energy. The energy loss in the entire charging and discharging phase is therefore equal to E_{in} - E_{out}. The two equations (2.6) and (2.3) can then describe the flow of energy in CDI systems.

$$E_{in} - E_{out} = (E^R_{in} + E^R_{out}) + (E^P_{in} + E^P_{out}) \tag{2.2}$$

$$E_{cap} = E_{in} - (E^R_{in} + E^P_{in}) \tag{2.3}$$

The resistive loss is defined also as :

$$E^R_{in} = E^{R,NS}_{in} + E^{R,S}_{in} = E^{R,S}_{in} + \int_0^{t_{charge}} I_0^2.R_s(t)dt \tag{2.4}$$

$$E^R_{out} = E^{R,NS}_{out} + E^{R,S}_{out} = E^{R,S}_{out} + \int_{t_{charge}}^{t_{cycle}} I_0^2.R_s(t)dt \tag{2.5}$$

Where $E^{R,S}_{in}$ and $E^{R,S}_{out}$ are series resistive losses during charging and discharging, respectively. The series resistance here corresponds to the contact resistance, the ionic resistance of the

solution in the separators and the resistance of the wires. Similarly $E_{in}^{R,NS}$ and $E_{out}^{R,NS}$ are energy losses due to the network of distributed ionic resistances of the solution inside the electrode pores during charging and discharging. The abbreviation NS stands for non-series resistor. In most research, electrode array resistances tend to be neglected, since these tend to be negligible in CDI (e.g., compared to ionic resistance in electrodes) (Dykstra *et al.*, 2016; Qu *et al.*, 2015). In the work of Hemmatifar *et al.* (2015), they separated the resistive loss contributions into series and non-series resistances due to their distinct behavior as described below. The equivalent circuit of a CDI cell can be described as a network of nonlinear resistors and capacitors (Qu *et al.*, 2015; Suss *et al.*, 2013). Some of these resistors are electrically in series and some are parallel to the capacitors. The series resistances include the resistances of the outer conductors, the current collector and the non-series resistance associated with the electrolyte inside the pores of the spacers (porous dielectric). It can be assumed that the voltage (in current) response of these series resistors to rapid changes in current (in voltage) is instantaneous. In contrast, the distributed resistor/capacitor network of porous CDI cell electrodes exhibits significant characteristic RC (resistance-capacitance) delays associated with charge (order greater than or equal to 10 seconds for significant charge penetration into the electrode). Therefore, due to its fast time response, series resistances can be measured every time during charging and discharging, while it is impossible to directly measure the values of $E_{in}^{R,NS}$ and $E_{out}^{R,NS}$ in situ and independently. Also in the work of Hemmatifar *et al.* (2015), they focused directly on the series resistive loss and also quantified the parasitic loss with a separate experiment.

2.8 CDI efficiency

The experimental results for CDI and MCDI reported in the work of (Zhao *et al.*, 2012a) for constant voltage operation and constant current operation were analyzed for power consumption per removed ion ("kT/ion") and for charging efficiency. The line drawn from these two measurements is a simple inverse proportionality that captures both the magnitude and the functional dependence of the data, according to: Energy (kT / ion) = α / Λ , with α = 1/2.Vch/VT, and VT is the thermal voltage. This relationship holds for all constant voltage experiments that

are at the same cell voltage during charging and discharging. Constant current experiments also closely match this dependency. The work of (Zhao *et al.*, 2010) also shows that charging efficiency determines power consumption (for a certain charging voltage), that higher values of charging efficiency lead to lower power consumption , and therefore that MCDI (higher charging efficiency) generally requires lower electrical energy inputs than CDI (lower charging efficiency). Second, in an equilibrium cycle, where salt adsorption and stored charge reach equilibrium values, equilibrium EDL theory can be used to predict Λ, or vice versa, data for Λ can be used to validate an EDL model. As indicated in Zhao *et al.* (2010), Λ is well suited for fundamental studies of EDL, because it is independent of the volume (area) of the pores in which EDLs are formed, and therefore independent of the electrodemass. Related to charging efficiency, Λ, is the ratio of salt adsorption rate (in mol/s) to current (in A/s) divided by Faraday's constant, which is called the current efficiency (Porada *et al.*, 2014). The current efficiency is for two streams and can be used instead of Λ in a steady state CDI process such as constant current MCDI (CCMCDI) or FCDI (i.e. , where all the process parameters, such as the current concentration and the salt concentration of the effluent, do not vary hourly). This metric comes from the field of electrodialysis, but can be used to characterize any FCDI cell, including those without an (Hatzell *et al.*, 2014) ion exchange membrane. Current efficiency is calculated from effluent and inlet salinity, Cout and Cin, water flow F and applied current, I, according to equation 2.6 assuming the use of a 1:1 monovalent salt.

$$\Lambda = \frac{(Cin - Cout)\phi}{I/F} \tag{2.6}$$

For FCDI experiments at the same level of cell voltage, the energy used ("kT/ion") evolves as the inverse of the current efficiency.

2.9 CDI in real application

The most widely studied application for the Capacitive De-Ionization cell is the desalination of brackish water for the production of drinking or agricultural water (Gabelich *et al.*, 2002;

Farmer *et al.*, 1996a; Zhao *et al.*, 2013b; Xu *et al.*, 2008). Compared to established desalination technologies, such as reverse osmosis (RO) and multi-stage flash distillation (MSF), current CDI systems may require less energy for desalination at low levels of salt concentration in feed water (at levels about an order of magnitude less salt than seawater and lower) (Zhao *et al.*, 2012a, 2013b). Like electrodialysis, CDI is a technology that directly transports (relatively few) dissolved salt ions out of the feed water, rather than transporting the (many) water molecules away from the salt, as in RO and MSF. In the case of the CDI, the dissolved salts are transported by electromigration to the EDLs, where they are stored until the end of the desalination step. In the case of RO, water molecules are transported across a semi-permeable membrane, with salt ions remaining in the water upstream feed water, abd ejected in the end of the line (Zhao *et al.*, 2013a). The energy requirements of MCDI and RO setups are compared in (Zhao *et al.*, 2013a) research show a crossover point in salt concentration below which MCDI becomes more energy efficient. CDI systems with static electrodes (Figure 1.1) are characterized by a limited amount of salt that can be absorbed into the EDL per charge, and therefore seawater desalination with CDI systems at static electrodes is impractical from an infrastructure and energy point of view :a ratio of approximately 5:1 between the volume of the electrode and the volume of feed water is necessary to adequately desalinate seawater.

The vast majority of CDI experimental work tests new CDI cell architectures or electrode materials using brackish feed water synthesized in the laboratory. Most commonly, feed water is a solution of sodium chloride in deionized water (Porada *et al.*, 2013b). These latter conditions allow for insightful and controlled experiments for proof-of-concept type work. However, they do not reliably predict performance when continuously treating true brackish source waters, such as river water or saline aquifers. In real-water systems, such as that of Gabelich *et al.* (2002) using carbon airgel electrodes, the natural organic matter present in river water appears to reduce the sorption capacity of the electrodes, indicating some surface fouling. Conversely, field tests by Xu *et al.* (2008) on brackish produced water from natural gas production sites indicated stable performance of the carbon airgel-based CDI system over several hours of continuous operation, indicating no significant fouling of the electrodes in this time scale. In addition, work

by Lee *et al.* (2009a) on the treatment of brackish waste water from thermal power plants using a membrane CDI cell reported no significant degradation in cell performance for 500 desalination cycles. In another work, it was demonstrated that MCDI systems can be applied for the treatment of brackish water containing 5-10 mg/l of petroleum compounds such as octane. Currently, it is difficult to draw general conclusions about the lifetime of CDI cells, because it is clear that the target parameters (water hardness, chemical composition, etc.) play an important role for performance and stability of the resulting CDI (Suss *et al.*, 2015).

The very recent advent of flux electrode CDI (FCDI) and hybrid CDI systems has opened up new areas of application for CDI systems (Jeon *et al.*, 2013; Lee *et al.*, 2014). An advantage of these systems over CDI with two static porous carbon electrodes is to allow desalination of higher salinity feeds which was previously possible. For example, the FCDI, in which both electrodes are composed of a fluid carbon suspension, has demonstrated the desalination of feed water with a total salt concentration approximately equal to that of seawater, with a single cellular charge (Jeon *et al.*, 2013). The hybrid CDI cell, in which one electrode is porous carbon and the other is a battery electrode such as sodium manganese oxide, has demonstrated more than 30 mg/g NaCl salt at equilibrium per charge, almost double that of static electrode CDI systems (Lee *et al.*, 2014).

2.9.1 CDI beyond salt removal

Beyond the application of brackish and seawater desalination, CDI has also been used for other applications that require the removal of ions from an aqueous solution. For example, CDI for water softening has been demonstrated by Seo *et al.* (2010), where CDI cells have been used to remove divalent dissolved minerals such as calcium and magnesium that can scale household appliances and interfere with their cleaning processes. Additionally, CDI systems have been used as a method of removing weak acids, such as boric acid from RO treated water (Avraham *et al.*, 2011b). Other innovative applications of CDI and MCDI relate to the removal of ions from biomass hydrolyzate (Huyskens *et al.*, 2013), acetic and sulfuric acids from biomass hydrolyzate using a hybrid lime addition-capacitive deionization process (Kim *et al.*, 2012),

insulin purifications (Jung *et al.*, 2012), microfluidic sample preparations (Roelofs *et al.*, 2015), elimination of phosphates and nitrates (Macı´as *et al.*, 2014; Huang *et al.*, 2013), chromes (Wang *et al.*, 2014; Farmer *et al.*, 1997) , copper (Huang *et al.*, 2014, 2013), lithiums (Ryu *et al.*, 2015; Liu *et al.*, 2013), lead ions (Yang *et al.*, 2014), and cadmium ions (Chen *et al.*, 2014). It is important to note that some of the applications mentioned above related to the treatment of feed water containing amphoteric ions such as phosphate or bicarbonate ions which, depending on the pH value of the electrolyte, can donate or accept protons. Such processes should be taken into account when performing desalination tests (because the pH of the feed can be disturbed when loading CDI(M) cells) (Porada *et al.*, 2013b; Lee *et al.*, 2010). Still, we hold to point out that certain metal ions, for example copper, can undergo a process of reduction and consequently be deposited in the form of elemental copper on the electrodes (Huang *et al.*, 2014; Grujicic *et al.*, 2002). If this is the case, this process should not be classified as a de-ionizing capacitor but rather a metallic electroplating involving an electron transfer reaction between electrodes and dissolved ions. It should also be noted that CDI systems can be integrated with other technologies to provide synergy to achieve various end goals. One example combines CDI functionality with a microbial environment, the Microbial Integrated Capacitive Desalination Cell (MICDI). In the latter cells, microbes in the anode compartment are reported to oxidize organic matter in the wastewater, producing electrons that can be used to drive a CDI process. Thus, these cells would have simultaneously eliminated organic matter and salts (while generating the energy necessary for desalination). Finally, CDI cells can be coupled with other desalination systems, such as reverse osmosis (RO), where CDI systems have previously been used to treat brine water exiting an RO unit (Suss *et al.*, 2015). In addition, CDI has been studied as a tool for the selective removal or upward concentration of a certain ion from multicomponent electrolytes (Zhao *et al.*, 2012b). The latter method takes advantage of the time-dependent selectivity of the charge of EDLs, which preferentially adsorb species with higher bulk ion concentrations early during charging, while later ions with higher valence are preferentially adsorbed (Zhao *et al.*, 2012b). This concept can even be used to build a cell for so-called controlled potential chromatography with improved separation (and detection) of charged species. An alternative approach to achieve the preferential elimination of a certain ion uses a material with high selectivity towards an ionic

species placed either on the surfaces of the electrodes, or between the carbon particles of the electrodes. This approach has been demonstrated for the preferential removal of nitrates over chloride and sulfate ions (Kim & Choi, 2012; Yeo & Choi, 2013).

2.10 Commercialization of CDI units

In addition to research-level explorations of CDI applications, there have been several commercial efforts based on CDI technologies. The first commercialization efforts emerged from LLNL (Lawrence Livermore National Laboratory, USA) in the 1990s (Farmer *et al.*, 1996a), but ultimately failed. In retrospect, the low salt adsorption capacity of the early carbon aerogels used during this working time may have played a role. Breakthroughs made since then, as described in this perspective, in materials performance, cell design and fundamental understanding, have resulted in great improvements in CDI system performance and energy efficiency. As a result, recent industrial efforts have emerged around the world to commercialize CDI technologies. For example, the company Voltea BV (Netherlands) has developed CDI membrane systems for commercial and domestic applications. Performance data of their MCDI pilot system obtained by treating cooling tower feed water has been published in the work of (van Limpt *et al.*, 2014). In this work, it was claimed that the use of an MCDI system over traditional water treatment technologies is beneficial in terms of saving chemicals, water and waste water. In addition, this work demonstrated a low energy consumption of between 0.1 and 0.2 kWh/m3 of desalinated water produced for the desalination of cooling tower feed water with a total conductivity of 0.37–0.65mS/cm. ENPAR, also developed their first MCDI cells (ESD100) in 2002, to arrive today with their fourth generation of ESD400 cell which presents characteristics as competitive as that of Voltea. EST Water & Technologies (People's Republic of China) develops large-scale CDI systems for desalination that can be applied in a variety of industries. Examples include applications in municipal groundwater, petrochemical industry, steel mills, thermoelectric power plants, coal chemical manufacturing, paper mills, fertilizer production, and brackish waters high in fluorine and arsenic. So far, more than 30 industrial systems are installed in China, where most of the facilities are for the recovery/reuse of industrial/municipal wastewater with treatment

capacities ranging from 100 to 2000 m3/h. In terms of power consumption, EST modules are attractive compared to RO modules, with power consumption values of around 1.0 kW h/m3 for EST CDI and 1.5 kW h/m3 for RO.

CHAPTER 3

ENERGETIC CAPACITANCE OF THE MEMBRANE CAPACITIVE DEIONIZATION CELLS

Alaa Ghamrawi[1] , Maarouf Saad, Imad Mougharbel.

[1] Electrical Department, École de Technologie Supérieure,
1100 Notre-Dame Ouest, Montréal, Québec, Canada H3C 1K3

Paper published in « Cleaner Energy» in June 2022.

3.1 ABSTRACT

The Membrane Capacitive Deionization (MCDI) is a non-faradic, capacitive technology for brackish water desalination. As the applied electrical power charges the porous electrodes, they adsorbe ions from the crossing water stream. The MCDI process is known for its reduced energy footprint rather than its stored energy during the adsorption phase. This energy will be released in a clean and sustainable way at the desorption phase. Since the stored energy is tightly related to the amount of retained ions inside, modeling a cell based on energy will implicate several operational advantages: an instant estimation of the retained salt quantity, the cell behavior, the process performance in addition to the quantity of the stored energy during the cleaning cycle. The modeling approach is based on the cell energetic balance of the consumed energy and the regenerated one. The Energetic Based Model (EBM) is simply represented by a calculated Energetic Capacitance (C_E) serially connected to an Energetic Resistance (R_E). Conversely to the up-to-date models, the EBM's components are based on the cell's electrical parameters only. Electrical approach will give faster and more accurate results than the traditional one. In this paper, the energetic capacity had shown less than 2% error in reproducing the cell energetic profile.The (C_E) reaches its maximum of 32 Farad for an applied voltage of 2.0 V in constant voltage application. However, a similar result of 30 Farad is obtained for a 0.2 A constant current application. The (C_E) is finally presented as an indicator of the cell water recovery, beside the average energetic capacitance (AC_E) as a similar replication of the average amount of adsorbed salt during the cycle.

Keywords: Modeling, MCDI,Energetic,capacitance,stored energy, ASAR,WR.

3.2 Introduction

The capacitive De-Ionization (CDI) had shown interesting results for water treatment quality, specific ions removal and efficiency in energy consumption (Curto *et al.*, 2021). As the process is based on capacitive adsorption (Seo *et al.*, 2010), two main phases will take place: The first phase consists of application of the charging voltage on the cell terminals, so the ions will migrate toward the charged electrode (Gierst, 1966). The resulting electrostatic force on the electrodes will keep those ions onto (Oh *et al.*, 2006). Consequently, it will increase the voltage of the cell, thus the solution is desalted (Yang *et al.*, 2001). After reaching the maximum allowed voltage on the cell terminal, the electrodes reached their maximum capacity of ions and the second phase will take place. Applying a reversed voltage or shorting the terminal will repel the ions from the electrodes and return them into the flushing stream. The phase will end once the cell voltage is zero, so all the ions from the electrodes have been completely desorbed, and the cell is again ready for a new adsorption phase after restoring its adsorption capacity (Lee *et al.*, 2011b). The introduction of the Membrane Capacitive De-Ionization (MCDI) had opened various opportunities and shows many possibilities to overcome key limitations of the conventional CDI with a unique cell architecture using multichannel (Kim *et al.*, 2020). MCDI was achieved by introducing the ion-exchange membranes especially the cation exchange and the anion exchange ones in between the electrodes. Despite the similar functionality of the MCDI and the CDI (Li *et al.*, 2012), the MCDI has proven to have higher performance and better efficiency due to the ion exchange membranes between electrodes (Zhao *et al.*, 2013c). The installation of the anion-exchange membrane on the cathode electrode surface and the cation-exchange membrane on the anode electrode surface had reduced the effect of co-ions (H. Li, 2011). This reduction had given the place of the co-ions to adsorb more counter-ions from the solution and increased the efficiency of the cell salt adsorption (Kwak *et al.*, 2011) and thus dramatically increase the current efficiency of MCDI to about four times of the CDI (Zhao *et al.*, 2013c). In addition,the introduction of the anion exchange membrane had shown

a high advantage to keep high CO2 absorption efficiencies, while the absorption efficiency of the CO2-CDI cell was lower than expected (Legrand *et al.*, 2020). The MCDI process had shown also a supplementary advantage of a practical treatment in nitrate-contaminated water (Çetinkaya, 2020). The circulation of the water through the layers is ensured by special spacer water permeable membranes. The MCDI is also the subject of recent studies in many aspects: Ion-transport mechanism between the cell's electrodes was the interest of Kim and Choi (Kim *et al.*, 2010b) who described those migration during the adsorption and the desorption phases. And while Zhao *et al.* (2013b) proposed their theoretical model of the MCDI process (Zhao *et al.*, 2012a), they were trying also to optimize the parameters to achieve the highest average salt adsorption rate and water recovery (Biesheuvel *et al.*, 2010). As the similarity of the electrical behavior of the CDI/MCDI cell and the supercapacitor was obviously clear, Pernía *et al.* (2012); Álvarez González *et al.* (2016) and Alkuran *et al.* (2008) used for example in their application the basic model of an RC model as a standard representation that will describe the behavior of the MCDI. Their model for the calculation of the capacitance was based on the voltage slope evaluation and the values were more a reflection of the traditional capacitance response of the cell. Another more detailed modeling study used the transmission line model in order to provide a more accurate representation of the electrical behavior of the MCDI cell according to Andres *et al.* (2008). Despite the interesting results of both models, they could not accurately retrace the energetic behavior of the cell, and estimate the stored energy inside. Many of the recent studies of the MCDI had concentrated on the water quality by optimizing the cell construction materials, or on the operational application as a constant current versus voltage charging (Zhao *et al.*, 2012a). Therefore the behavior of the stored energy didn't take the deserved place. The stored energy was used for comparison purpose between water desalination technology or for supplying another cell as per Pernía *et al.* (2012); M.Pernia *et al.* (2014). In this paper, the energetic profile of the cell will define a new electrical parameter able to retrace the stored energy inside the cell. It will be referred as Energetic Capacitance (C_E) since it was calculated based on the energetic profile of the cell and it will contribute in the stored energy estimation. The energetic capacitance was introduced initially to model supercapacitors (Rizoug *et al.*, 2010), and thanks to the high similarities between the MCDI and the supercapacitors electrical behavior

(Suss *et al.*, 2015), this paper will extend the application of energetic capacitance to MCDI cells. As the energetic capacitance is a descriptive figure of the stored energy inside the cell during the charging phase, it resumes the evolution of the energy inside the cell. The paper will also present the main difference between our energetic capacitance and the traditional one and define the field of use of each capacitance. Therefore, we assume that the energetic capacitance is able to give a better figure of evolution of the cell energy than the traditional one. This traditional capacitance C_T has a non constant value during the charging and discharging operations. It is definitely hard to simply measure it in real time.

As for the performance description of the MCDI , most of the recent studies have adopted two performance process indicators. The first one is the water recovery (WR) which indicates the fraction of the salt stream that is recovered as freshwater. Thus, a second important metric to describe MCDI cell performance is the average salt adsorption rate (ASAR), described in detail in ref. (Zhao *et al.*, 2013b). In order to validate our energetic model as a performance indicator, the energetic capacitance will be calculated for different applicable charging constant currents as well as for different constant voltage levels. The results will be compared to an associated ASAR and WR indicator to see the way that the energetic parameters can go along with them. The study will use the energetic capacitance as a reference to optimize the charging period of the MCDI Cell. To do so, the charging current will be fixed at a certain level, and applied for a various charging periods, so the C_E is calculated to conclude the usefulness of a small charging period of time versus a longer charging one. By the end, the energetic capacitance will be evaluated for different current levels at a same charging period.

Although the traditional such Andres *et al.* (2008) was able to reproduce the cell response to an applied voltage or current, the calculation of the equivalent components required an offline test bench. The cell should be removed and installed in a specific operational condition, so the calculation of the model's components can be achieved. Conversely, the energetic model requires only the online measurement of the voltage and current to calculate the parameters of the working cell. On the other hand, the energetic approach becomes more important when the parameters will estimate the stored energy inside the cell, and also the quantity of retained

ions during the adsorption (Landon *et al.*, 2019). This is due to the close relation between the stored energy and the retained counter-ions inside. Furthermore, the energetic parameter monitors the performance of the cell under different operating conditions such as the variation of the influent concentration, the water flow rate and the water temperature. They will help to identify the best operating method of the cell as a constant voltage or a constant current charging. This monitoring leads to estimate the aging of the cell and the necessity to replace the carbon electrode or/and the ions-exchange membranes inside the cell, by supervising the energetic capacitance tumble down. Finally, the evolution of the energetic capacitance will also propose a new procedure to determine the cycle period and contribute to determine the suitable charging period of the cell.

Hence, in this paper the energetic model will allow to :

- Estimate the stored energy inside the MCDI cell
- Evaluate the performance of the cell.
- Determine the optimal cycle period.

3.3 Materials and methods

3.3.1 Test bench

The test bench (Figure 3.1) consists in two MCDI cells installed mounted on the same skid next to each other. The cell itself is the ESD400 from Enpar company, known as current water technologies as well, form Guelph Ontario region[1]. The selection of the cell type is based on the successful industrial profile of the cell upon the application in several water process projects as Sojeco plant of Sawaco company in southern Jeddah, for water desalination. The cells have also seen an interesting advantageous in specific ions removal, in mine water treatment and many others as well. The ESD400 model has a 4 poles electrical connection, two for the positive terminal and the other two adjacent for negative one. The water will be supplied from the bottom orifice and the product will be recapitulated from the upper one. Both cells are fed from the

[1] 70 Southgate Drive, Unit 4, Guelph, ON, Canada, N1G 4P5 https://www.currentwatertechnologies.com/

same solution tank, through manual valves through a peristaltic pump. The peristaltic pump is a 12VDC driven motor pump, that ensures the circulation of the required flow through the cell.

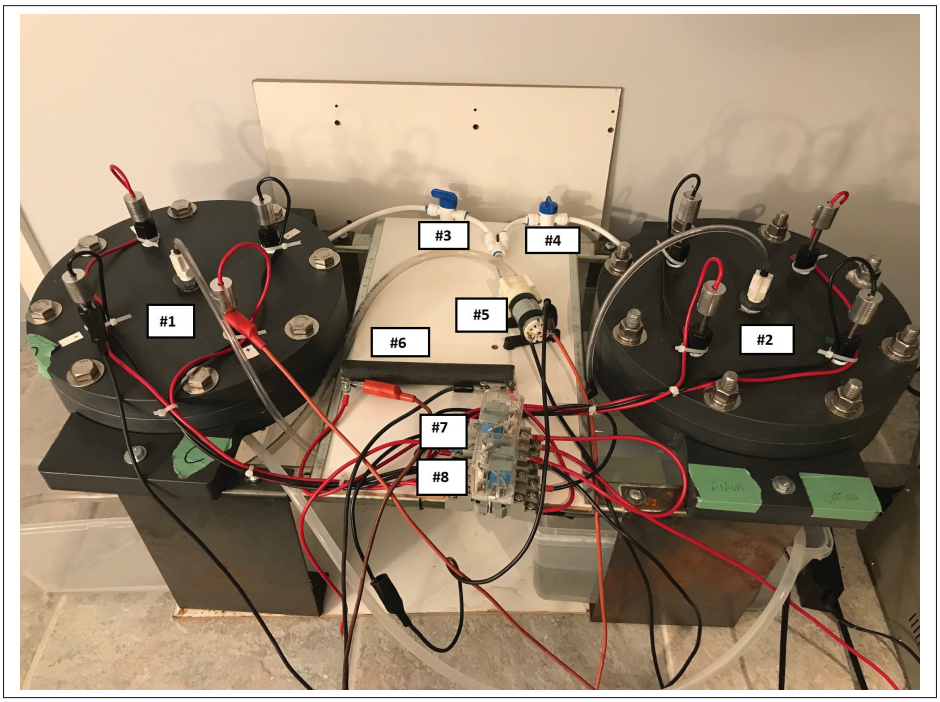

Figure 3.1 Testing bench: (#1):MCDI#1 cell, (#2):MCDI#2 cell, (#3):MCDI#1 feeding valve, (#4):MCDI#2 feeding valve, (#5):Main peristaltic pump, (#6):R_SC resistor (1 ohms), (#7):Relay switch SW1, (#8):Relay switch SW2

The second cell was installed in order to validate the result of the first cell. The electrical connection is shown in Figure 5.8. The operational selection between the cells is made through the relay switch SW2. The activation of the switch relay will power the cell#2 , however the cell#1 will be applied when the switch relay is deactivated. The change from the charging (adsorbing) to the discharging (desorbing) phase is realized by the relay switch SW1. The two relay switches are connected through a power resistor R_SC. This resistor has a double function in the system setup: the first is to contribute in the charging current load and validate the current measurement by a simple reading the voltage on its terminals. The second function is to provide a discharge load releasing the stored energy inside the cell in a regulated way through this resistor. When the relay switch SW1 is in position (1), the adjustable power supply (current or

voltage) based on the desired level, will be supplying the cell and driving the adsorption phase. By switching to position (2), the cell terminals will be short-circuited and the energy will be dissipated through the power resistor R_SC as explained before.

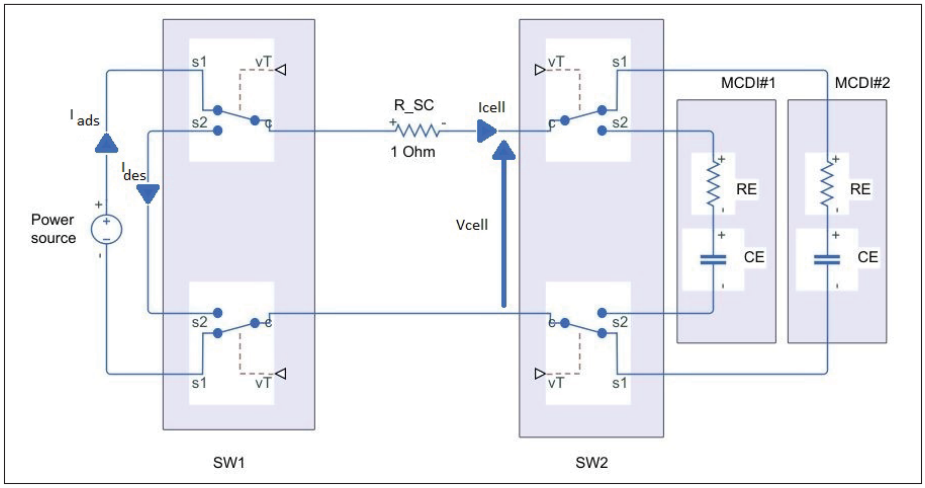

Figure 3.2 Electrical testing bench connection

3.3.2 Modeling method of the MCDI Cell

3.3.2.1 Energy characterization

The energy characterization is based on the use of the energy balance of the MCDI cell on a charge-discharge cycle of the test bench. As we do apply and measure the voltage (V) and the current (A) on the cell during a specific period of time (T) , we will be able to calculate the stored energy and estimate the total losses inside the cell (Figure 5.6).

$$E_{stored} = E_{consumed} - E_{lost} \tag{3.1}$$

This way makes it possible to know, on the one hand, the energy storage capacity and the losses of the system. The separation of these two energies (stored and lost) facilitates the modeling of

the MCDI cell in electrical circuit form. In this case, losses are represented by a resistance (R_E) and the stored energy will be identified by an energy storage capacitance (C_E).

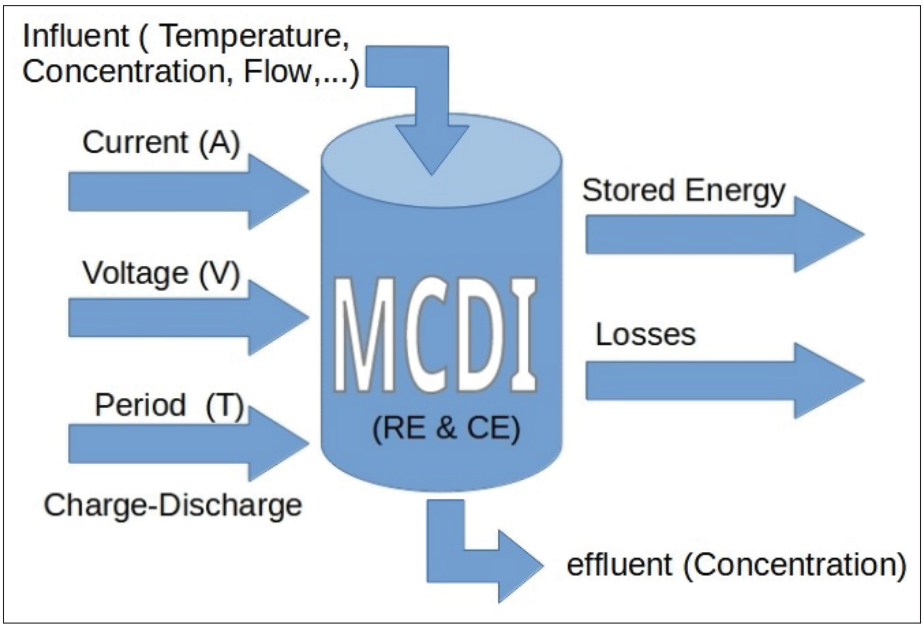

Figure 3.3 Energy characteristics of the simplified energy model

3.3.2.2 Energetic resistance (R_E)

Energetic resistance (R_E) represents losses for a constant charging current or a constant charging voltage during a charge-discharge cycle. Using this type of cycle gives us the ability to have the same energetic state at the end of the cycle that existed before the cycle. The difference between the energy stored (charge phase) and that released (discharge phase) represents the energy lost. This energy is calculated by integrating the power at the input of the MCDI cell throughout the cycle which is the application period of charging and discharging the cell.

$$E_{lost} = \int_{t_{cycle}} V_{cell}.I_{cell}\, dt = \int_{t_{cycle}} R_E.I_{cell}^2\, dt \tag{3.2}$$

Developing the equation for a charging /discharging period will give :

$$E_{lost} = \int_{t_{ads}} V_{cell}.I_{ads}\,dt - \int_{t_{des}} V_{cell}.I_{des}\,dt \tag{3.3}$$

$$= \int_{t_{ads}} R_E.I_{ads}^2\,dt + \int_{t_{des}} R_E.I_{des}^2\,dt \tag{3.4}$$

As (R_E) is considered constant during this cycle:

$$E_{lost} = \int_{t_{ads}} V_{cell}.I_{ads}\,dt - \int_{t_{des}} V_{cell}.I_{des}\,dt \tag{3.5}$$

$$= R_E.(\int_{t_{ads}} I_{ads}^2\,dt + \int_{t_{des}} I_{des}^2\,dt) \tag{3.6}$$

Using Equation 5.10 , the energetic resistance will be :

$$R_E = \frac{\int_{t_{ads}} V_{cell}.I_{ads}\,dt - \int_{t_{des}} V_{cell}.I_{des}\,dt}{\int_{t_{ads}} I_{ads}^2\,dt + \int_{t_{des}} I_{des}^2\,dt} \tag{3.7}$$

The R_E depends of the applied charging conditions as the influent concentration, the water flow and the charging current/voltage.

3.3.2.3 Energetic capacitance (C_E)

The energetic capacitance will be defined as :

$$E_{stored} = C_E.\frac{V_{cell}^2}{2} \tag{3.8}$$

C_E is a parameter which should make it possible to easily determine the stored energy, knowing that this relation is not applicable to the traditional capacity since it depends on voltage (V). The value of the energetic capacitance can be calculated using a low current full load test. The temporal response should start at null voltage, as this capacitance gives the image of the stored energy versus the empty state of the MCDI cell. So the energetic capacitance will be calculated

as follows :

$$C_E = \frac{2E_{stored}}{V_{cell}^2} \tag{3.9}$$

As for the R_E, the C_E is also tight to the applied charging/discharging conditions as the influent concentration, the water flow, temperature, charging period and the charging current/voltage. Considering those Operational Conditions as (OC), the stored energy will be estimated as :

$$E_{stored}(OC) = E_{Consumed}(OC) - E_{lost}(OC) \tag{3.10}$$

and

$$E_{Consumed}(OC) = \int_{t_{ads}} V_{cell}.I_{ads}\, dt \tag{3.11}$$

$$E_{lost}(OC) = \int_{t_{ads}} R_E.I_{ads}^2\, dt \tag{3.12}$$

3.4 Results and discussions

The experience discussion will be divided into three main topics. The first one will try to calculate the energy inside the cell using the energetic capacitance and the standard traditional one. The results will be compared to the actual stored energy of the cell, so it will be so far easier to determine which capacitance is able to give a more accurate figure of that energy. The next topic compares the EBM parameters to the existing cell performance indicators especially the ASAR and the WR, in order to prove the efficiency of those parameters in cell performance identification. Finally, the effect of the charging period on the stored energy through the energetic capacitance will be verified, so it determines one that can optimize that energy. Each operating condition was repeated twice on each cell to make sure that the resulting information is reflecting the actual case of the cell and not a result to an uncontrolled operational condition. All the following experiments were conducted at a fix influent concentration of 50PPM, a flow of 0.25L/min and a water temperature of 12°C.

3.4.1 Energetic Vs Traditional capacitance:

In order to highlight to the importance of the energetic capacitance in the stored energy estimation, we will first calculate the real stored energy inside the cell. The calculation method is shown in Figure 3.4, and since we were using a numerical signal with a fix sample time T_s, the cell energy will be written as :

$$E_{cell} = \sum_{k=1}^{n} V_k . I_k . T_s \tag{3.13}$$

Where n is the maximum number of voltage samples during the charging phase. And since the cell is applied to a fixed current (I) and a fixed sampling period is fixed, the equation will be :

$$E_{cell} = I.T_s . \sum_{k=1}^{n} V_k . \tag{3.14}$$

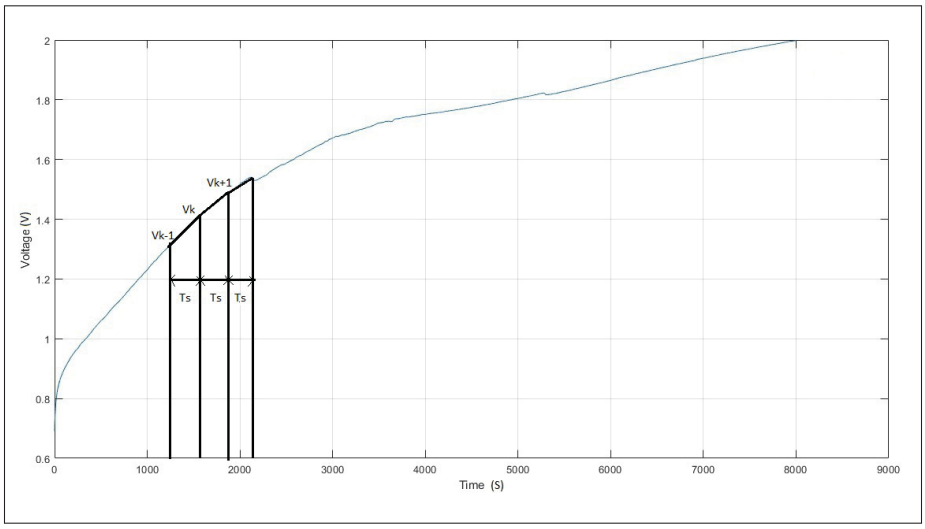

Figure 3.4 Total energy calculation

This amount will be compared to the theoretical amount of the calculated capacitance:

$$E = C.V_{cell}^2/2 \tag{3.15}$$

where C could be the traditional capacitance C_T or the energetic one C_E, and V_{cell} is the maximum voltage of the cell during the charging phase. The application of the energetic capacitance and the traditional one will lead to two resulting of energy profile.

3.4.1.1 Traditional capacitance

the traditional capacitance is defined as the capacitance value for each applied charging period. Normally, the values of this capacitance are calculated as the evolution of the voltage on the cell terminals for a given charging current:

$$I_{cell} = C_T \frac{dV_{cell}}{dt} \tag{3.16}$$

So, the definition of the traditional capacitance in the numerical application for Ts as sampling time, will be defined as a slope of the voltage evolution due to the applied constant current. C_T will be given by :

$$C_T(k) = I.\frac{k.T_s}{\Delta V_k} \tag{3.17}$$

where k is the sample that goes from 1 to the number of samples of the charging phase (n).

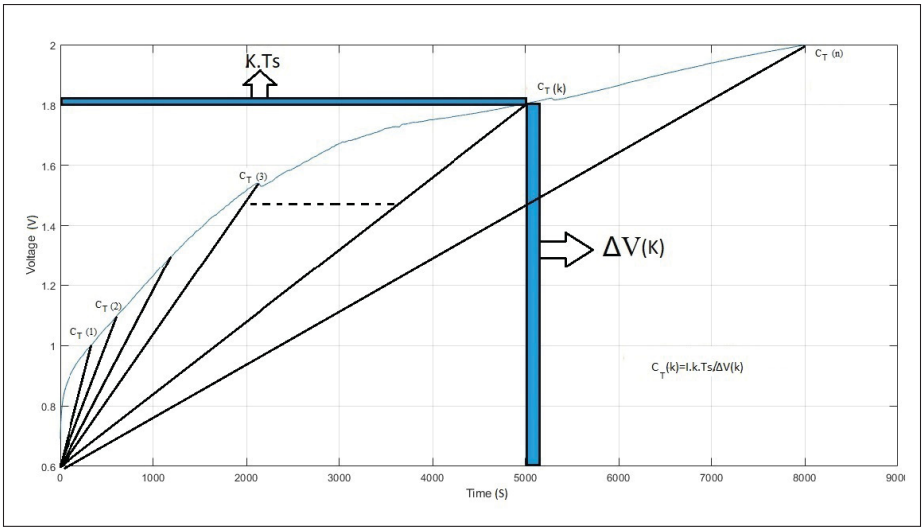

Figure 3.5 Traditional capacitance calculation

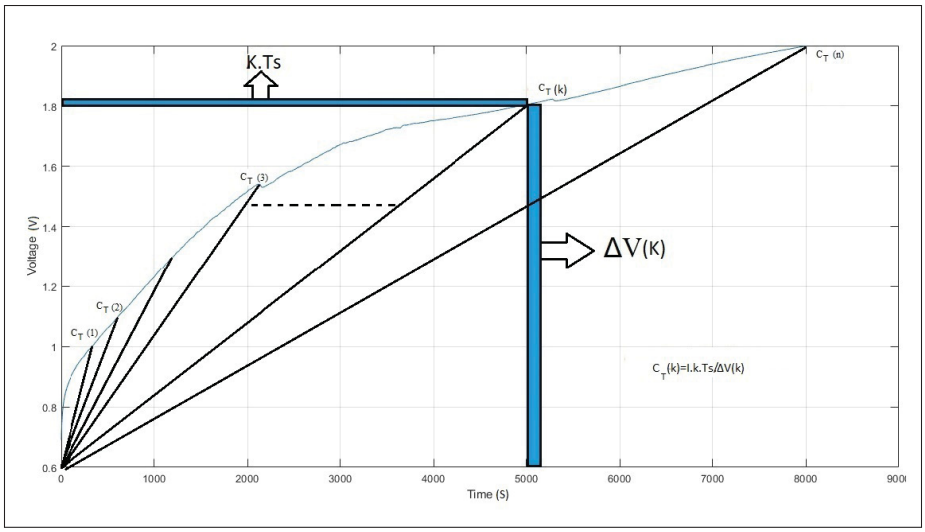

Figure 3.6 Traditional capacitance calculation

Figure 3.6 describes the identification of the parameters used in the calculation of this capacitance.

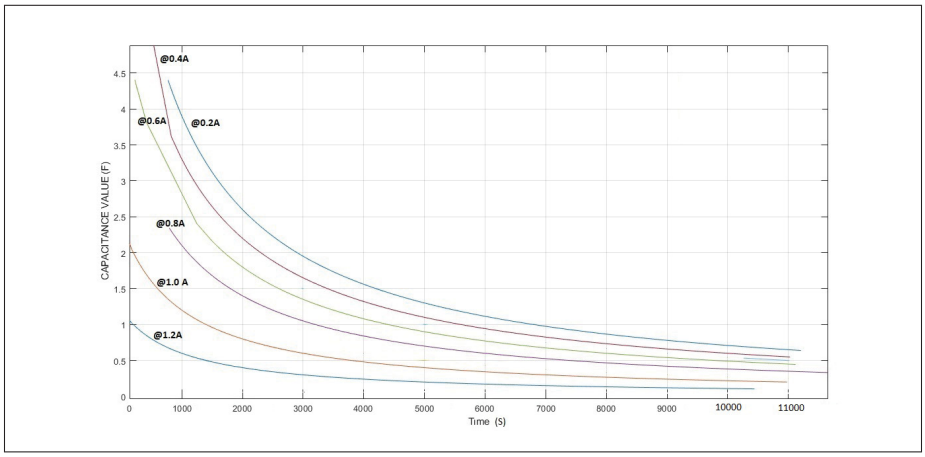

Figure 3.7 Traditional capacitance for the applied currents during the charging period

Figure 3.7 shows the evaluation curve of the traditional capacitance based on the cell applied charging current. As the voltage is increasing rapidly in the first charging periods due to the generation of the ions double layer, the value of this capacitance looks more important in the beginning of the charging phase. The higher charging current is applied, the lower the traditional

capacitance will behave, since the ions between the electrodes won't have the sufficient time to be adsorbed in the carbon porous.

3.4.1.2 Comparison between traditional and energetic capacitance

In Figure 3.8, the stored energy inside the cell by calculating the voltage and the current of the cell. Besides this curve, two curves are shown presenting the calculated energy based on the energetic capacitance and the traditional one. It shows the difference between the Traditional way calculating the energy (red line) and the energy balance way (green line).The average error between the experimental energy and one based on the energetic capacitance is about 2% compared to 47% based on the traditional one. Five main points could be made:

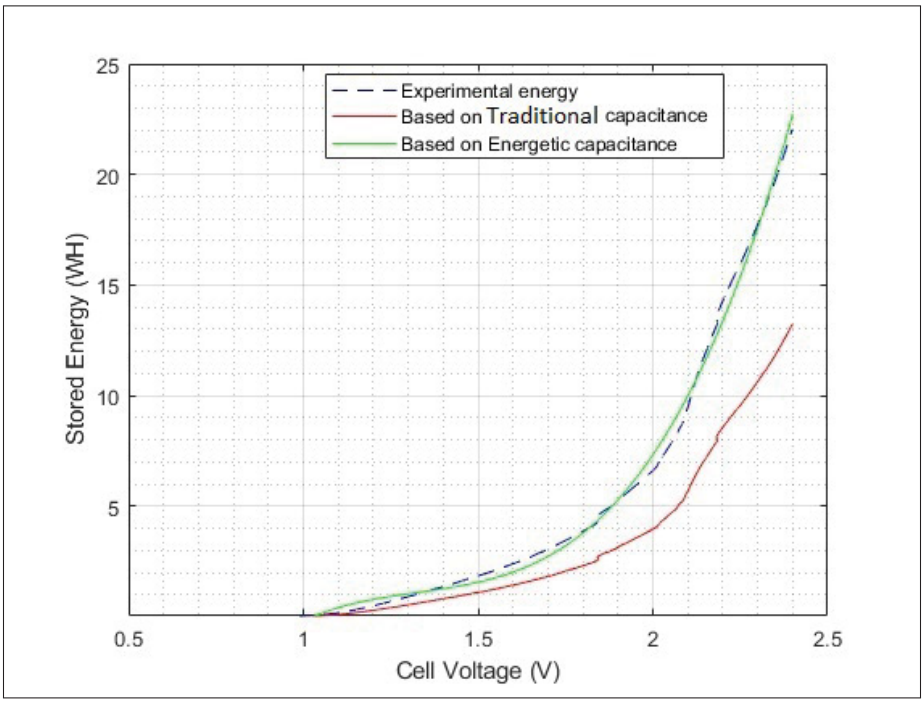

Figure 3.8 Stored energy comparison at 0.5A

- As the energetic curve calculated based on the traditional capacitance shows a deviated approach from the real measured energy, the MCDI could not be considered as a perfect capacitor and its electrical behavior should be treated as a combination of several parameters and components.

- The energy calculated curves and the real-data curve share the same quadratic trend of curves. The energy will show more important storage value on the highest voltage achieved.
- The calculated energy based on the traditional capacitance values shows more accurate presentation of the variation of the stored energy. The calculated model is able to reproduce the profile of the cell energy variation, however the amount of the stored energy cannot be estimated accurately through this capacitance. This model can be more beneficial to estimate the energy reaction of the cell in a simulation mode resulting different operational conditions. Thus, the use of this capacitance causes an underestimation of the stored energy.
- The calculated energy based on the energetic capacitance will show an interesting profile of the evolution of the stored energy inside the cell. Although that the model is not able to give a high precision on the variation of the stored energy inside the cell, it can give a very close estimation of the value of the charge inside the cell by measuring the terminal voltage.
- As the stored energy inside the cell depends on the quantity of ions retained by the electrodes, and as the energetic capacitance is able to give an accurate estimation of the stored energy, the C_E can be easily used to define the performance of the cell by defining the retained ions during the adsorption phase. The highest C_E we reach, the highest energetic performance the cell can achieve.

3.4.2 C_E as a performance indicator

In order to understand the reaction of the energetic parameter, especially C_E, inside the MCDI cell, the study will focus on two main electrical inputs of the cell : the current and the voltage. As many previous studies have shown the advantage of the application of a constant current versus a constant voltage applied on the cell (Zhao *et al.*, 2012a). The constant charging current will be adopted to calculate the EBM parameters, so it will be easier to compare them with other performance results in similar publications. Despite this advantage, the energetic parameters will be also calculated for a constant voltage, in order to show the impact on the cell performance. So it will be possible to conclude the best practice of voltage application on the cell. All the

following studies were conducted at a fix influent concentration of 50PPM, a flow of 0.25 L/min and a temperature of 12 °C.

3.4.3 Constant Current

The application of the constant current is presented in Figure 3.9). It shows that it will take a longer time to reach the saturation voltage for lower currents application. It also shows that the discharge period and the process cycle depend on the applied current on the cell. In the following comparison of the traditional standard performance indicator with the energetic capacitance, the test was realized with the application of 0.2A, 0.4A, 0.5A, 0.7A, 0.9A, 1.1A and 1.3A. During these tests, each current level is applied until the cell reaches its maximum allowable voltage on its terminal. Once it reaches its peak point, the discharge through the resistor until the voltage on the cell terminal reaches a minimum level of 0.08 V

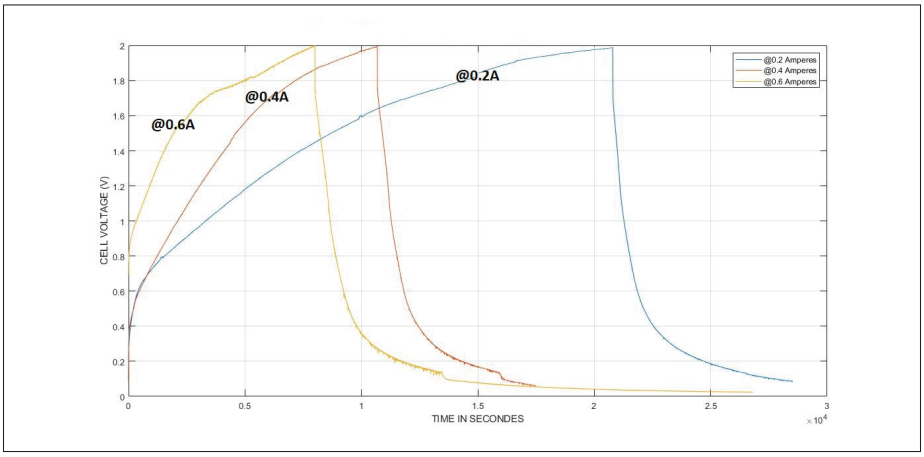

Figure 3.9 Application of different current level on the MCDI

3.4.3.1 Comparison of Water Recovery WR and capacitance C_E

The WR is a process rate that compares the treated water quantity versus the total water flows through the cell during the process cycle. It can be written as (Zhao *et al.*, 2013b) :

$$WR = \frac{\Phi.t_{ads}}{\Phi.t_{ads} + \Phi.t_{des}} \tag{3.18}$$

Where Φ is the constant water effluent flow-rate through the cell, t_{ads} is the adsorption period during the application of the current and t_{des} is the desorption period till reaching the zero voltage. The equation can be written as :

$$WR = \frac{\Phi.t_{ads}}{\Phi.(t_{ads} + t_{des})} = \frac{t_{ads}}{t_{cycle}} \tag{3.19}$$

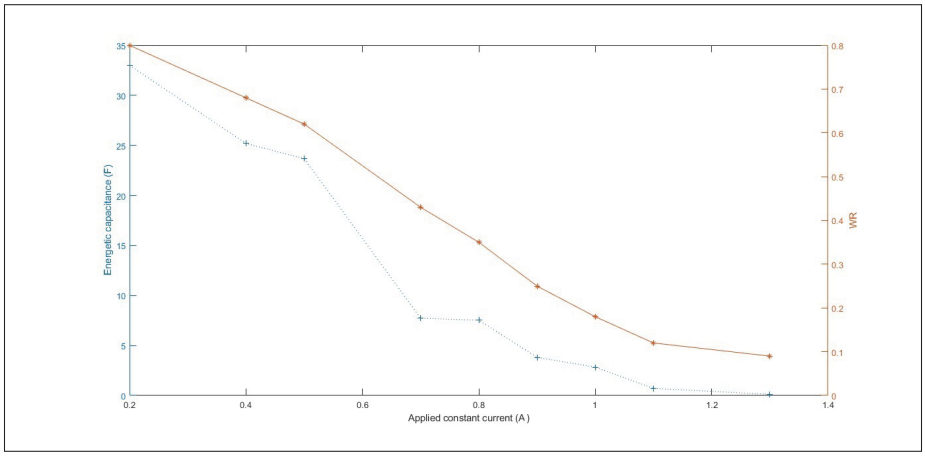

Figure 3.10 Comparison between the WR and the energetic capacitance

The comparison between the calculated energetic capacitance and the water recovery is shown in Figure 3.10). As per Zhao *et al.* (2013b) the WR is decreasing as the applied adsorption current is increasing. It can be observed as well that by varying the current during the adsorption the energetic capacitance will have a similar behavior of the WR. This is because that the increasing of the current will achieve the maximum target voltage rapidly which decreases the adsorption period t_{ads}. This decrease of the adsorption time will decrease the stored energy inside the cell which decreases consequently the energetic capacitance of the cell. Therefore, the link between the WR and C_E is obvious, it is possible to use theC_E as an equivalent replacement of the WR performance indicator due to the similarity between the two profiles.

3.4.3.2 Comparison of Average salt adsorption rate ASAR to Average energetic capacitance AC_E

The amount of salt adsorption rate (ASAR) is introduced as cell performance indicator since it was incontestable to have maximum of salt adsorption during the shorter time. This will be the optimal operation of the cell. Thus in order to describe this parameter, the ASAR was used as a substantial indicator which is the salt adsorption per cycle, per gram of total electrode mass divided by the cycle time. So it is mostly a rate dimension that describes the speed of the process itself as shown in the following equation (Chen *et al.*, 2018) :

$$ASAR = \frac{\Phi . \int_0^{t_{charge}} C_0 - C_{cha,ef}(t)\, dt}{n.m_{electrode}} \tag{3.20}$$

Where Φ is the water flow-rate, n=1 as one cell is used in our system, $m_{electrode}$ is the electrode mass, C_0 is the feed-water molar concentration, $C_{cha,ef}$(t) is the effluent salt molar concentration in charge cycle. As an equivalent of this parameter, the average energetic capacitance AC_E will be defined as the result of the division of the energetic capacitance by the cycle period. The idea is to have a rate process value that could be compared to the ASAR.

As a result of that, Figure 3.11 shows a similar ASAR behavior as described by Zhao *et al.* (2013b). Although these values depend on the specific characteristic of each MCDI construction materials, the ASAR curve shows a similar profile to the results shown in (Zhao *et al.*, 2013b), it starts small with a low current application and increase consequently to achieve its peak. The ASAR will decrease again to vanishes as the current was higher than normal operational conditions. Similarly, the average energetic capacitance shows a similar behavior of the ASAR. It increases as the adsorption current is increasing and decreases after reaching a maximum peak in its curve. It can be easily explained as the MCDI is a non-faradic process: the smaller applied current for charging the cell in the adsorption phase, the counter-ions will take smoothly their places inside the layer, so the stored energy will be higher and the cycle will take longer time. When a high current is applied, the retained ions quantity by the electrode is lower, so the stored energy is lower, the cycle will be shorter and the process will be quicker. Thus, the ASAR and

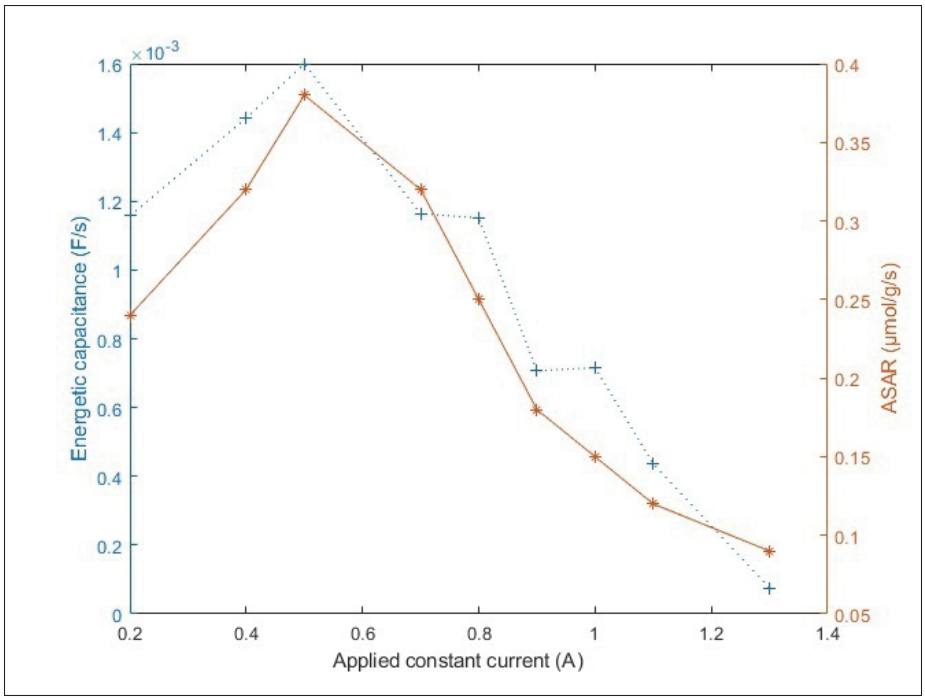

Figure 3.11 Comparison between the ASAR and the AC_E

AC_E show a similar behavior and the use of the AC_E seems to be the best alternative parameter to describe the ASAR performance indicator.

3.4.4 Constant Voltage

In order to understand the reaction of the MCDI cell following the application of a constant voltage, a different voltage level was applied, and the cell voltage evolution was registered. Figure 3.12 shows the application of 1.6V, 1.8V, 2.0V, 2.2V, 2.4V, 2.6V, 2.8V, 3.0V, 4.0V, 5.0V, 6.0V respectively on the cell. It shows the existence of two regions, one of low voltage application where the source voltage is lower than the nominal cell voltage V$\leq$ 1.8V, and one of high voltage application. In the low voltage application region, the cell voltage will never reach the cell maximal allowable voltage since the source is not able to provide it. In the high voltage region, the higher voltage is applied, the higher charging slope is observed due to the high current circulation due to the high difference potential between the source and the cell.

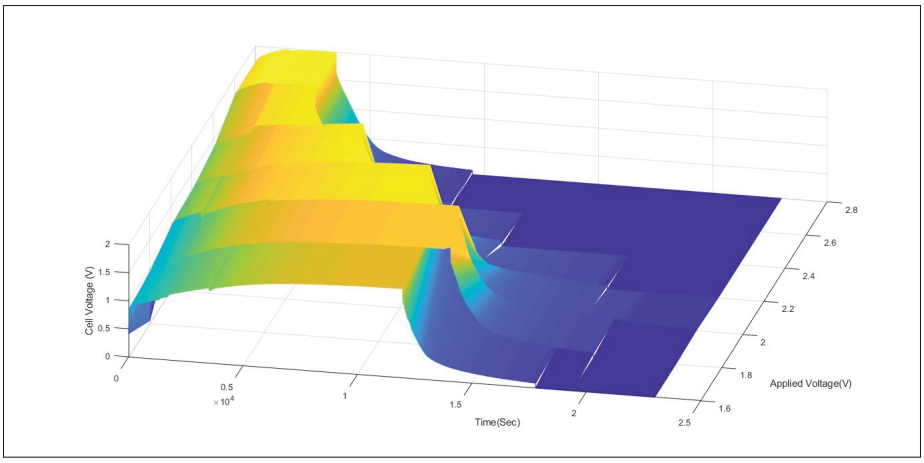

Figure 3.12 Application of different voltage levels on the MCDI

Despite that the cell was not able to reach the electrode saturation in the low voltage region, the stored energy and the energetic capacitance are also more interesting than the higher voltage region. The calculation of the energetic capacitance is shown in Figure 3.13. It is obvious that a maximum energetic value is obtained at 2V since it is the maximum allowed voltage that can be supported on the cell's terminal without the oxidation of the cell's carbon electrodes. Considering the energetic capacitance as a performance indicator, the low voltage application seems more beneficial for energy storage purpose than the higher one , for example for 1.6V, the capacitance is about 27 Farad, which is higher than the capacitance of the 2.6V, 2.8V, 3.0V, 4.0V, 5.0V, 6.0V application.

In brief, in a constant voltage, the application of a lower voltage level is more interesting than the higher one , in terms of energy storage and water recovery. With regards to the AC_E, the low voltage region doesn't show an interesting performance for water treatment. As show in Table 3.1, the peak of the salt removal performance was reached at 2.4V voltage application.

3.4.5 Various charging periods

In order to illustrate the impact of the charging period on the energetic profile of the MCDI cell, the system will be charged for different time periods at one constant charging current.. Figure

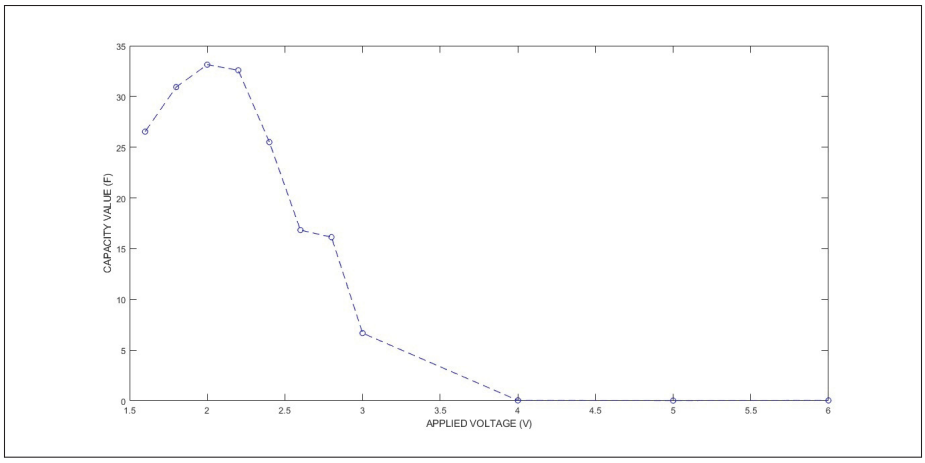

Figure 3.13 Evolution of the energy capacitance

Table 3.1 Average energetic capacitance with the constant voltage application

Source Voltage (V)	AC_E (F/S)x10^{-3}
1.6	2.45
1.8	2.46
2.0	2.83
2.2	3.14
2.4	3.33
2.6	2.83
2.8	2.76
3.0	2.4
4.0	1.05
5.0	0.62

3.14 shows the evolution of the voltage of the MCDI cell after the application of 0.5 A of 10 , 20 ,30 ,40 and 50 minutes respectively.

The purpose is to determine the way that the charging period is able to affect the value of the energetic capacitance and the cell behavior. Table 3.2 shows that the value of the capacitance C_E depends on the application period of the charging current. Therefore the longer this charging period, the higher the energetic capacitance is reached. The maximum allowed cell voltage

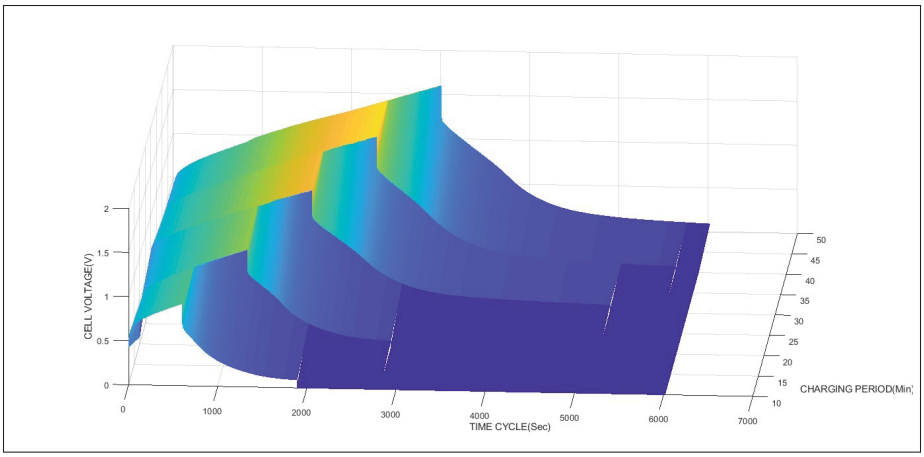

Figure 3.14 Limited time constant charging current

value will cap the adsorption period. As for the AC_E indicator, it shows close value regardless the applied charging period as shown also in Table 3.2.

Table 3.2 Periods

period (sec)	Energetic capacitance (F)	Average Energetic capacitance (mF/S)
600	3.04	1.77
1200	5.23	1.80
1800	7.56	1.75
2400	8.23	1.72
3000	10.11	1.78

In order to find a mathematical model of the energetic profile, the C_E curve can be associated to a slope equation based on period, the equation can be represented as :

$$C_{E(0.5A)}(t_{ads}) = 0,05.t_{ads} + 0.0714 \tag{3.21}$$

t_{ads} is the time in seconds of the actual applied charging period on the MCDI cell.

Equation 5.3 shows the impact of the charging time on the energetic capacitance. It demonstrates a linear proportional relation between the energetic capacitance and the applied period. However, and since the AC_E shows similar performance indicator for the charging periods, which period

can achieve the optimum energetic performance? To answer this question, let us assume the least common multiple between the C_E of two charging period. Based on that, if we calculated the required periods for the same stored energy, it will show us that the longest period applied, the faster we achieve our storage goal. Note that the measurements were taken with the same charging current(0.5 A), the same influent concentration(50 PPM), the same water flow (0.3 l/min) and the same temperature(12 °C).

3.4.6 One charging period

In this section, different current levels (0.2A, 0.4A, 0.6A and 0.8A) are applied for a fixed period of time of 15 minutes. Figure 3.15 represents the evolution of the MCDI voltage. As far as the charging current is higher, the evolution of the cell voltage is higher. The discharge period was determined by reaching a voltage level of 8 mV on the cell terminals. It is obvious that the higher discharge duration as the higher applied current, due to the fact that the MCDI cell has been charged with more counter-ions than the lower charging current.

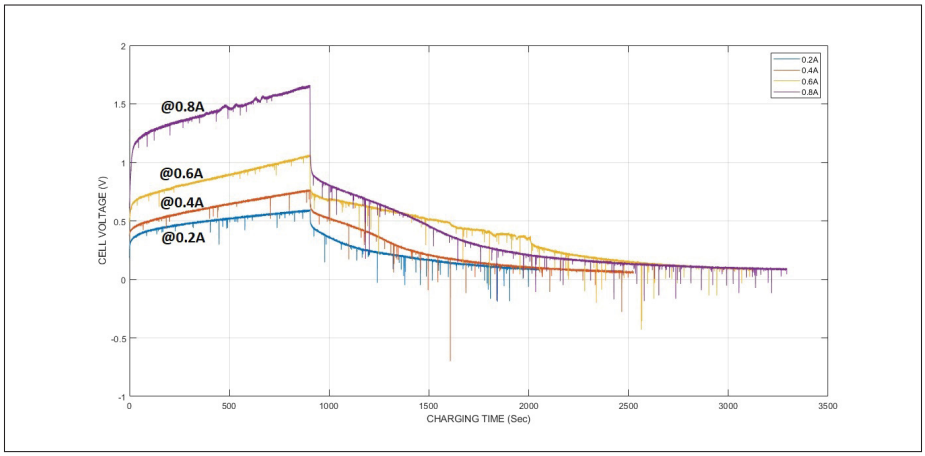

Figure 3.15 Fixed period charging current

Table 3.3 summarizes the discharge period corresponding to each applied current, it gives a comparison between the discharge duration of the cell as well as the calculated energetic capacitance. The result fully corresponds to the assumption that the energetic capacitance is

higher when the applied current is higher. However, it will take longer to discharge the higher applied charging current.

Table 3.3 Discharge periods

Current (A)	Maximum voltage (V)	Discharging period (S)	Energetic capacitance (F)
0.2	0.55	1000	9.46
0.4	0.76	1500	11.94
0.6	1.15	2000	14.48
0.8	1.68	2500	17.60

3.5 Industrial impact

Besides its advantages in identifying the stored energy inside the cell and the contribution to present a simple energetic model of the evolution of the energy inside, the energetic capacitance will impact the MCDI industries in several ways: the energetic based model will help to determine the amount of useful clean energy usable inside the MCDI plant. In addition to that, the fact of modeling the cell online will give the opportunity to compare the capacitance energetic reaction between the cells, which will make it easier to troubleshoot the defective cells, and save maintenance time and effort. On the other hand, the comparison of the energetic capacitance over the time will give a good idea of the cell aging, and whether the cell needs to be replaced or to be in order to renew the electrode and the membranes inside. Finally, identifying the cell's energetic capacitance will contribute in the plant design process, in order to determine the required power for the plant operation and draw a cleaner energy profile of the future MCDI water treatment plant.

3.6 Conclusions

Energetic model is a new approach of the MCDI cell seeking to represent cell's sustainable energetic behavior according to the operational electrical parameters (voltage, current,...). The energetic capacitance is also proven as a performance indicator for the water recovery and the

ASAR as well. The use of the energetic capacitance C_E requires the installation of current and voltage sensors for each cell, however the low price and the abundance of sensors supply in addition to the simplicity of cell maintenance afterwards justify such installation. Furthermore, another limitation can be added. This limitation lies in the calculation of the C_E which can only be accomplished at the end of the adsorption-desorption cycle. Despite this, the C_E is used as a performance indicator to judge the efficiency of the cell and not by an adjustment parameter. Waiting for the passage of a complete cycle (300s) cannot harm drawing conclusions on the performance of the process. The last limitation may concern the temporal characterization of the behavior of the cell using the C_E. As the interest is mainly for the energy behavior, redistribution phenomena, long-term internal leaks and instantaneous electrical profile have not been taken into account. The proposed model is based on an original method of characterization based solely on the use of real cycles for the energy identification of characteristics. In future work, a control system can be realized based on a validated energetic model targeting the best values of the C_E and AC_E during the operation of an MCDI cell.

Conflicts of interest

There are no conflicts to declare.

Acknowledgements

This work was supported by Current Water technologies , Research center.

CHAPTER 4

VOLTAGE CONTROL FOR MEMBRANE CAPACITIVE DE-IONIZATION CELL FOR HIGHER ENERGY EFFICIENCY IN SALT REMOVAL

Alaa Ghamrawi[1] , Maarouf Saad, Imad Mougharbel.

[1] Electrical Department, École de Technologie Supérieure,
1100 Notre-Dame Ouest, Montréal, Québec, Canada H3C 1K3

Paper published in « Cleaner Energy» in March 2023.

4.1 ABSTRACT

Membrane Capacitive DeIonization (MCDI) cells have proven to be advantageous in water desalination and ions removal. Therefore, the time has come to introduce an alternative water purification technique to reduce the global water shortage. MCDI is known to be environmentally friendly, energy efficient and economical. Besides its reduced energy footprint, recent applications underline the regenerated energy during the desorption phase, which makes the MCDI as a potential cleaner energy source. Thus, a large number of scientific publications addressing problems and enhancing the performance of an MCDI have been published. In this paper, we have developed a simple and inexpensive method to control the adsorption voltage of the cells. So, the ion adsorption/desorption mechanisms of the MCDI will be controlled by a variable charging voltage applied to the cell.The entire response of controlled MCDI integrated model was created and he simulated results were compared with the experimental ones in order to validate the results.

Accordingly, the controller parameters were tuned using the genetic algorithm optimization technique, based on the integral time absolute error criterion. Furthermore, the experimental results reveal that the control of the cell had increased the salt retention by 50%, the quantity of removed salt by the energy unit was improved by 10%, and the cell energy ratio from 28% to 32%.

Keywords: Control, MCDI,Energy,comparison,performance, closed-loop.

4.2 Introduction

As the shortage of freshwater becomes one of the essential threats of life on earth, the desalination had taken a capital importance as the most efficient solution to meet human freshwater requirements as for domestic, industrial and agriculture demands. A lot of desalination technologies were introduced to comply this need. These technologies were generally thermal or membrane technologies and they are classified according to operating parameters such as desalination capacity, energy recovery and demand, regeneration method, quality and efficiency of water production. In recent years, there has been a lot of water treatment research that has generated great interest in the Capacitive Deionization (CDI) technologies, especially in water desalination and specific ion removal (M., 2011) (Y., 2008). Although still in its infancy, the reduced consumed energy in the capacitive Deionization remains one of the most interesting aspects of this technology since it combines two main human resources to survive : water and energy (KK *et al.*, 2007) (MA *et al.*, 2010).The application of the MCDI had witnessed a lot of success in water softening, desalination, waste water treatment and recently the selectivity of adsorption like the phosphate (Miao *et al.*, 2021). The approximate expression for the ionic interaction, and the polarization of the ion was developed by Poisson-Boltzmann differential equation for the Electric Double Layer (EDL). Researches have proven that the Gouy-Chapman (Lim *et al.*, 2009) model of the double layer electrode is the most suitable for explaining the double layer phenomena on which CDI (CH *et al.*, 2012) (JC *et al.*, 1996), and especially MCDI (Biesheuvel & der Wal, 2010) cells are based. Therefore, the Gouy-Chapman model does not give the capacitance figure where the electrolyte is in motion.The movement of particles and ions inside the electrolyte solution will complicate the identification of the salt adsorption reaction of the electrodes inside the MCDI cell (Oh *et al.*, 2006).

MCDI cells commonly used in water treatment industries can be operated in adsoption phase by voltage application between 0.8V and 2.0 V in order to avoid water electrolysis between the carbon of the electrode and the produced hydrogen. Nowadays, MCDI in industrial application consists, after the saturation of the electrodes due to the adsorption of its maximum capacity of the solution ions, to short-circuit or reverse the applied voltage (BH *et al.*, 2011). In this

operational mode, the charging performance of the cell was not optimized, and so far for the applied desalination energy. On the other hand, as reported by Golub *et al.* (1987) the Capacitive Deionization process is affected by the influent water concentration (Ion solution in the aqueous electrolyte), the contact area between the carbon electrode, the solution concentration and the applied voltage to the cell. However, the fluctuation of the concentration for the same applied adsorption voltage will impact the quality of the produced water. This non-stability of the cell water quality effluent will impact the large-scale water plants final product. Water flow can also be a major factor beside the mentioned factors, as it can affect the adsorption process and the migration of ions to the charged poles. It can also increase or decrease the quantity of ions between the electrodes. Hence, since there are many contributory factors to water quality, this study will focus on the applied voltage for its ease of being electrically controlled, in addition to its major influence on the process inside MCDI cells. To the best of our knowledge, there have been no published papers showing results of the closed-loop control application on the MCDI cell charging performance, as well as the energy efficiency and the close relation between them. In this paper, a new concept of cell operation based on a closed-loop control system will be introduced. The idea is to develop a concentration oriented MCDI where the water ions concentration obtained on the cell output is predefined, this being one of the biggest advantages of the electrical controlled application. The developed control will be targeted on a fix effluent concentration setpoint. The controller will measure the difference between the actual effluent and the desired setpoint, so it can calculate the error input. The controller will then react on the charging voltage and consequently the applied current on the MCDI terminals. The controller will try to maintain a fixed and steady output conductivity value and the MCDI will ensure a stable water quality production against a fluctuating and unstable quality of uncontrolled ones.

4.2.1 Main contribution

Although optimizing the operation, the MCDI cell attracts great interest from researchers, most studies have used the conventional open-loop operation of the cell with a direct supply. As this control is able to operate the cell by an applied constant voltage or current, the output

concentration shows fluctuation and instability. The need for a stable and consistent product becomes more important in order to control the product quality of a large-scale MCDI water desalination plant.

On other hand, as the energetic footprint is one of the utmost criteria in the water treatment industry, the need to maximize salt retention in the cell for each consumed energy unit is crucial. Energy reduction will contribute in a cell cleaner energy system in consumption and higher efficiency during the regeneration phase. The paper was the first to adopt the closed-loop control and develop the state matrix for the cell control and operation. The study also shows the application of the Genetic Algorithm to tune to PID controller methodology for the MCDI application. Finally, the control had successfully demonstrated the possibility to stabilize the product concentration of the cell and increase the efficiency of the consumed energy for a maximum salt removal.

4.3 State of the art

The most recent publications focus on the physicochemical properties of MCDI processes by enhancing the performance of the membrane or the synthesis of novel carbon materials. As MCDI technology becomes more widespread, the operational aspect of the MCDI should become more predominant in order to optimize the operation of the MCDI cells. Zhao *et al.* (2012a) were one of the first to work on the electrical operational mode of the cell based on a constant voltage or constant current application. Quismondo *et al.* (2015) also worked on the energy efficiency aspect of the cell by varying the charging and discharging current and the advantage of applying a concentrated brine stream during the desorption period. Hassanvand *et al.* (2016) compared theoretically and experimentally the variation of the desorption time based on the flushing concentration and the effect on the water productivity and the total water recovery. And recently, the improvement of the cell performance was the subject of several studies as the application of a pulse power supply for a higher hardness removal rate (Wang *et al.*, 2021). The open-loop application presented thus far deals with prototypes operating in stable and fixed conditions of water flowrate, water temperature, and influent concentration. To

illustrate this problem of operation , if the input concentration, for example, is increased by 10%, it will raise the output effluent by 7% as per our observation. The cell energetic efficiency is also considered one of the main points to be improved. The aim is not to reduce the consumed energy during the adsorption phase but rather to increase the quantity of salt removed per applied energy unit.

In the field of water desalination, higher feed water production with the less energy wasted during the adsorption is the optimal energetic application of the cell. Yet more research is needed to improve the operational design aspect of the MCDI. As many input parameters can affect the cell operation, such as water flow, process temperature, influent concentration, . . . This study will focus specifically on the electrical parameters of the cell and more specifically on the control of the applied voltage during the adsorption phase. The selection of voltage is considered based on the practicality of the voltage and consequently the current control by a simple electronic rectifier and the fast response of the electrical domain. The cell fast response is an important complement to control the MCDI as for maintaining a stable production and a smooth operation of the cells. In this paper, the theoretical model will be based on the model defined by Biesheuvel *et al.* (2009). Their model is on adaptation of the Donnan theory of the electrode double layer (EDL) system. The concept will also use an experimental technique to validate the results of the theoretical model. It is important to note that the application of the theoretical model is based on various simplified assumptions and parameters calculated based on the experimental results of the cell.These assumptions and experimental results are detailed in section 4.4.

Finally, the approach proposed in this work for the operation of the MCDI cell ensures:

- a concentration-oriented way of controlling the cell,
- a dynamic way to guarantee the product quality,
- a method to optimize the water production according to the available source of energy specifically when the source is a fluctuating renewable energy source like wind and solar.

4.4 MCDI simulation Model

4.4.1 Modeling theory

The dynamic model adopted in our study is the model proposed by Biesheuvel *et al.* (2009) and further improved by Hassanvand *et al.* (2016). In these models, Deionization is based on Donnan's theory of the electrical double layer (EDL), where the water flow is completely homogeneous and stirred. Therefore, the value of the output concentration C and its variation with time dC/dt is written as (Biesheuvel *et al.*, 2009):

$$V.\frac{dC}{dt} = F.(C_{in} - C) - \phi_{salt} \tag{4.1}$$

Where F (ml/s) is the volumetric water flow rate through the cell, C_{in} (mM) is the water concentration of the influent, V (ml) is the actual volume of the cell and ϕ_{salt} (mmol/s) is the amount of ions removed per time unit from the solution during the adsorption period. As ϕ_{salt} could be obtained as the amount of the charge which had successfully retained ions from the solution, so it could be represented by the expression 5.2 where A (m^2) is the effective contact surface between the electrode layer and the water solution, λ is the efficiency coefficient and J_{charge} (mmol/s.m^2) is the applied density of current.

$$\phi_{salt} = A.J_{charge}.\lambda \tag{4.2}$$

The value of the differential charge efficiency is given by Biesheuvel *et al.* (2009) as follows :

$$\lambda = \frac{J_{salt}}{J_{charge}} = \frac{d\Gamma_{salt}}{d\sigma} = tanh\frac{\Delta\phi_d}{2} \tag{4.3}$$

Where J_{salt} (mmol/s.m^2) is the effective density of current representing the rate of salt removal, J_{charge} (mmol/s.m^2) is the density of current representing the rate of applied electrical charge on the electrode, Γ_{salt} (mmol/m^2) is the total amount of ions removed from the solution, σ (mmol/m^2) is the surface charge density of the diffusion layer and $\Delta\phi_d$ is the normalized electrical

potential difference over the diffuse part of the double layer. As the salt adsorption per cycle is calculated as follows:

$$\Gamma_{salt} = \frac{F.\int_0^{t_{ads}} C_{in} - C(t)\, dt}{M_{carbon}} \tag{4.4}$$

where M_{carbon} (m) is the total mass of the carbon of the electrode and t_{ads} is the adsorption cycle. The electrical charge balance during the adsorption-desorption cycle is calculated by the formula:

$$\sigma = \int_0^{t_{ads/des}} I_e(t)\, dt \tag{4.5}$$

Where $I_e(t)$ (A) is the actual current of the cell during the adsorption period t_{ads} and the desorption one t_{des}

Thus, knowing the salt removed amount ratio $d\Gamma_{salt}$ and the surface charge density σ based on the applied current $I_e(t)$, the differential charge efficiency λ in equation 5.3 can be easily deduced.

Finally, to resume the model of the control , the state-space model defined as $\dot{X}$=A.X+B.U+D.Cin can be written:

$$\begin{pmatrix} \dot{C} \\ \dot{\Gamma}_{salt} \\ \dot{V}_{cell} \end{pmatrix} = \begin{pmatrix} -F/V & 0 & 0 \\ -F/M & 0 & 0 \\ 0 & 0 & 1/\tau \end{pmatrix} . \begin{pmatrix} C \\ \Gamma_{salt} \\ V_{cell} \end{pmatrix} + \begin{pmatrix} -A.\lambda & 0 \\ 0 & 0 \\ 0 & -1/\tau \end{pmatrix} . \begin{pmatrix} J_{charge} \\ V_{source} \end{pmatrix} + \begin{pmatrix} +F/V \\ +F/M \\ 0 \end{pmatrix} . \begin{pmatrix} C_{in} \end{pmatrix} \tag{4.6}$$

Where τ is the electrical characteristic of the capacitive behavior of the cell. τ is noted as result of the product of the cell Resistance (R_{cell} in Ohms(Ω)) and its capacitance (Cap_{cell} in Farad (F)).

$$\tau = R_{cell}.Cap_{cell} \tag{4.7}$$

and the output equation will be presented as Y=E.X :

$$Y = \begin{pmatrix} 1 & 0 & 0 \end{pmatrix} \cdot \begin{pmatrix} C \\ \Gamma_{salt} \\ V_{cell} \end{pmatrix} \tag{4.8}$$

4.4.2 Model validation

The calculation of the parameters for the cell behavior simulation is based on the cell physical and operational values. The algorithm is presented in Appendix A in Algorithm 4.1. The model is based on two sets of data: constant one such the dimension and the volume of the cell itself and operating variables such as the cells applied voltage and the influent water flowrate. Equilibrium adsorption and desorption experiments of MCDI were first conducted at four feed concentrations ranging from 450 ppm (8 mM) to 580 ppm (10 mM) to validate the mathematical model. The outcome of the validated model was then compared to the performance of the MCDI unit under the same operating conditions. Figure 4.1 shows the typical concentration change in the recycle reservoir during one full cycle adsorption mode. This data was used to determine the MCDI cell specification as the characteristic of the carbon electrode and the effective surface of the electrode itself.

The charge efficiency of the MCDI treating a feed of 500 ppm of NaCl in single-pass mode has been experimentally measured at 92.3%. Considering that the co-ion flux is negligible, the charge efficiency below 100% is attributed to other factors such as faradaic reactions due to carbon surface oxidation, and electromigration of hydronium and hydroxyl ions (Hassanvand *et al.*, 2016). It is worth mentioning that these factors have not been considered in the MCDI theory employed in this work. Figure 4.1 shows the reproduction of the concentration output experimental values versus the calculated one based on the given model with the same environmental condition (Water Temperature =15 °C, Water flow rate = 400 ml/min, and influent concentration of 10

mM. Note that the concentration signal noise is generated by the sensor high sensitivity and the curves are presented without any low-pass filter application.

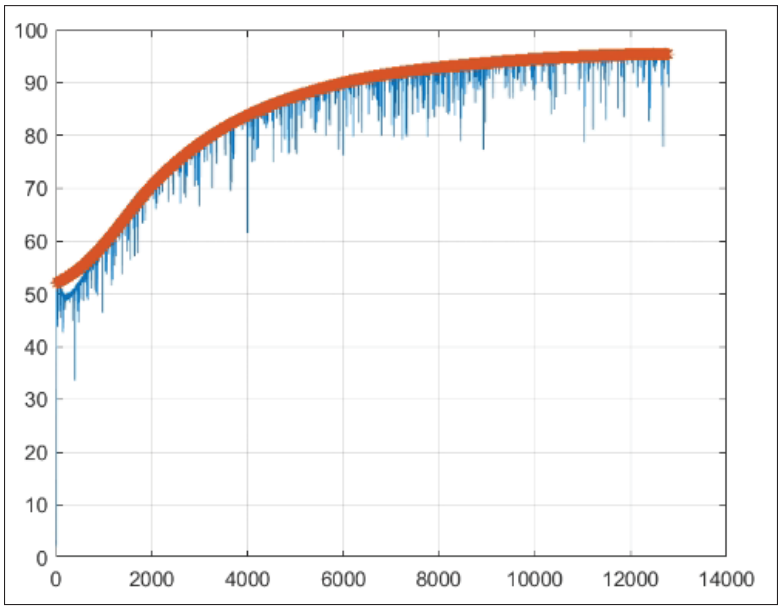

Figure 4.1 Model validation results

4.5 The MCDI in closed loop

4.5.1 Control design

After Modeling the MCDI charging dynamics, the work was proceeded to present a control system to complete the entire layout of the active charging unit. A dynamic model has been used in the result simulation and also to determine the effectiveness of applying a closed loop control on the effluent concentration of the MCDI cell.

The influent concentration changes the behavior of the MCDI cell and affects the quality of the product water. Ensuring a stable effluent concentration despite changing operating conditions has been reported as a critical challenge and it is considered as essential for the successful integration of the industrial MCDI cell. Many studies have been reported on this subject (Kang *et al.*, 2014) (Jande *et al.*, 2013) (Saleem *et al.*, 2016) (Zhao *et al.*, 2012a) (Zhao *et al.*, 2012b)

(Porada *et al.*, 2013b) in their researches. Some of these studies are based on a constant voltage application on the cell terminals, while others focus on the application of a constant current. For a proper operation of the cell at a desired concentration output, a controller is required as increasing the concentration output is unavoidable if the input concentration increases, or if the current supply drops, or if an increase in the flow steam crossing the cell. The nominal output concentration of the cell should be kept constant to prevent high salinity in the product line or high-power consumption for less productivity. The proposed controller in this study will try to keep the effluent concentration at nominal level by changing the cell supply voltage against changing of the cell working conditions.

4.5.2 MCDI Charge Controller

Using conventional operational control, the voltage source is directly applied to the cell terminal in order to attain the differential potential on the inner carbon electrode of the cell. No feedback is required in such operation and no control is performed during the process.

The PID controller shown in Figure4.2 was chosen for its simplicity, performance, robustness and domination in industrial application. As it is known, this controller was operated on the basis of the error calculation represented in equation 4.9, in which the error signal e(t) is stated as the difference between the concentration reference input (C_{ri}) and the MCDI output concentration (C) :

$$e(t) = C_{ri} - C \tag{4.9}$$

Figure 4.2 shows the closed-loop controlled application on the MCDI Cell. The applied voltage on the cell is adjusted constantly by a PID controller. The controller will take the error calculated by the difference between the setpoint and the actual effluent output. This error will be then used to find the voltage to ensure a constant output concentration. If the error is negative, the controller tries to decrease the voltage and if it is positive it will try to increase the applied voltage on the cell.

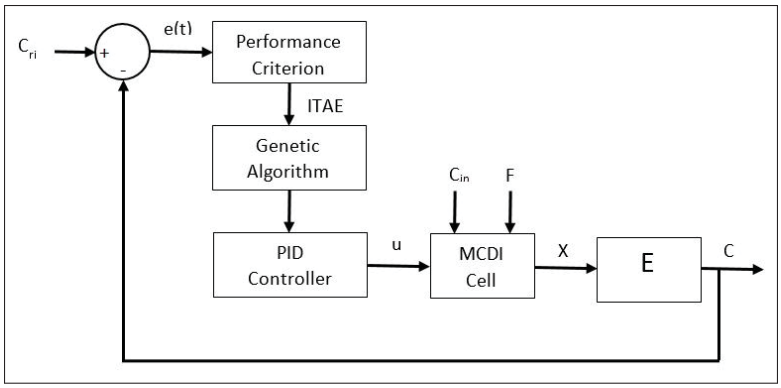

Figure 4.2 Closed-loop MCDI control block diagram

4.5.3 Genetic algorithm (GA) parameter tuning for the PID controller

In the current study, the use of the traditional Zeigler Nichols tuning scheme was not optimal (Laily *et al.*, 2016): the proportional controller reduces the rise time of the system response during the transient period. However the concentration output will be fluctuating as shown in Figure 4.8. Genetic algorithm had proven a lot of success in water processing industries. Kim *et al.* (2008) had used it to optimize the PID gains in reversed osmosis process. The objective function of the above-mentioned technique is formulated using the best-suited error criterion method, which is termed as ITAE (Rao *et al.*, 2020) to design the optimal PID controller:

$$ITAE = \int_0^\infty t.|e(t)|.dt \tag{4.10}$$

where t is the time and e(t) is the difference between the reference input and the controlled variable. The objective function for this optimization technique was formulated considering the combination of various performances operating conditions like the water temperature, the inlet concentration and the maximum voltage for the MCDI cell. The GA is applied from the Matlab global optimization toolbox using the function 'ga'.

The lower and upper bounds for various PID controller parameters are mentioned in Table 4.1. Similarly, the table list also gives the GA operational parameters values.

Table 4.1 Genetic algorithm operational parameters with PID controller lower and upper bounds

Parameters	Values
Population size	100
Generation	200
Fitness scaling	Rank
Crossover fraction	0.75
Mutation approach	Uniform
Generation gap	0.95
Lower bounds	[0,0,0]
Upper bounds	[100,100,100]

Based on the optimization of GA, the gain parameters of PID controller K_p, K_i and K_d were obtained optimally for the above performance objective using Matlab/simulink functions. The corresponding controller gains are listed in Table 4.2 :

Table 4.2 PID controller parameter gain values using the Genetic algorithm

Controller terms	Description	GA-optimized PID
K_p	Proportional	0.6453
K_i	Integral	4.362
K_d	Derivative	9.74 x10^{-4}

The entire GA working structure to optimize the PID controller parameters results are clearly illustrated in Figure 4.8, and Figures 4.9(a,b,c and d) which show a smoother control and a stable output by the application of the optimized PID gains.

4.6 Experimental Application

4.6.1 Materials and setup

The test bench (figure 5.1A) is based on two MCDI in order to validate the results on two separate units. The used MCDI units are originally from Enpar company, known as current water technologies[b]. The used MCDI units are the ESD400 model with 4-pole connection, two for the positive pole and two for the negative one. In the cell, several layers of membrane separate the carbon electrodes. The use of the two cells is to validate the result of the first cell on the second one.

The cell is connected through a power resistor R of 1 ohm. The R resistor has a double function in the system setup, the first one is to contribute in charging current and validate the current measurement by a simple reading of the voltage on it, the second function is to provide a discharge load able to release the energy inside the charge cell in a regulated way through that resistance. Finally, the system will switch from the charging phase to the discharging phase based on the controlled position of the switch SW1. In position s1, a variable controlled voltage power supply will supply the cells with the needed energy to maintain the process. Moving to the second position s2, the power supply is removed from the circuit and a short-circuit is providing the connection between the charged cell and the dissipating power resistor.

The test bench includes, in addition to the electrical connection, a process setup: the influent tank is connected to a peristaltic pump feeding the two MCDI units through two adjustable valves (figure 5.1 C). Valve 1 is connected to MCDI cell 1, and valve 2 to the second cell.Both cells will push their product into an effluent tank equipped with a conductivity measurement probe. Through these probes, a concentration output feedback is connected to an arduino controller. A closed loop configuration is programmed in the controller to adjust the applied voltage on the terminal of the MCDI cell.

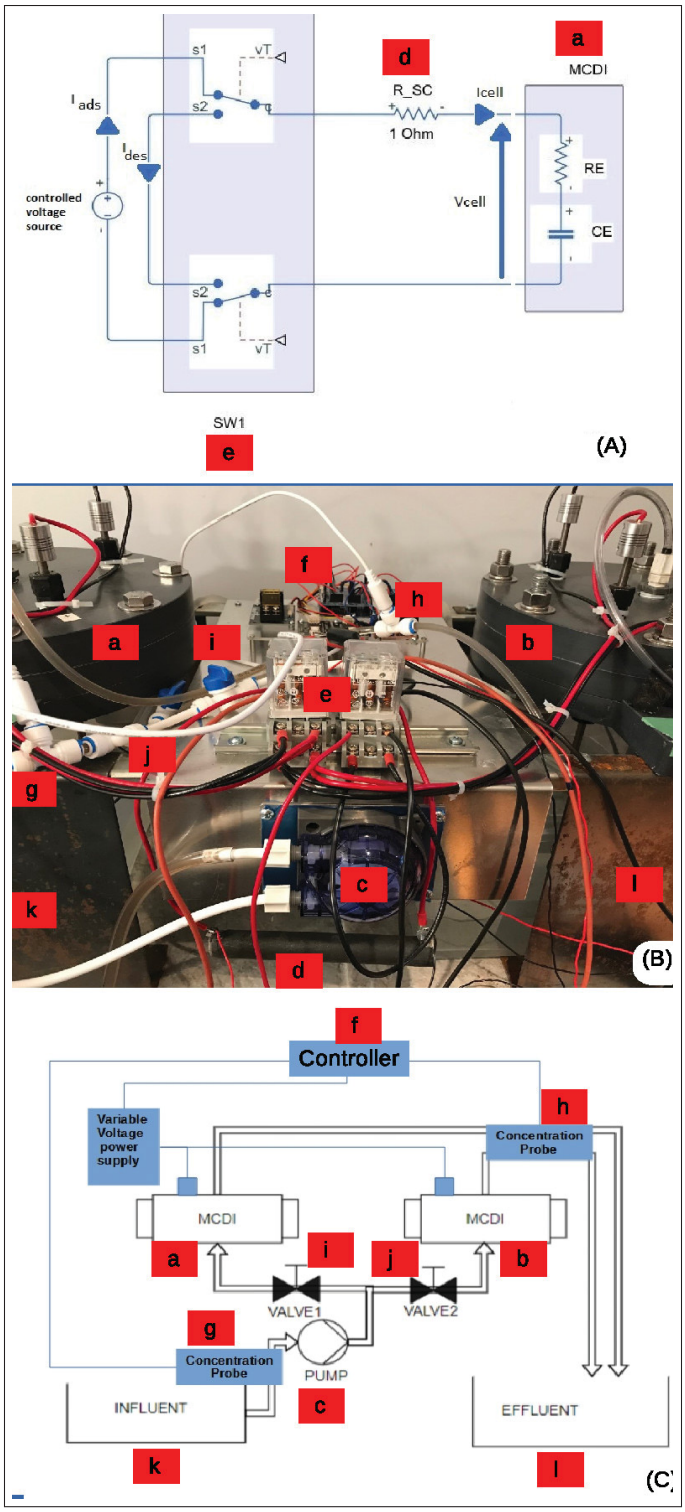

Figure 4.3 MCDI installation : (A) Electrical wiring diagram, (B) Experimental workbench, (C) Flow diagram : (a) MCDI unit1 , (b) MCDI unit 2 for results confirmation, (c)12v peristaltic pump, (d) 1 ohm electrical resistor, (e) electrical controlled 2 SPDT switch, (f) processing controller, (g) influent concentration probe, (h) effluent concentration probe, (i) Unit1 manual valve, (j) Unit2 manual valve, (k) influent water tank, (l) effluent product tank

4.6.2 Experimental procedure

When the experimental setup was designed, it was essential as the first step to replicate the results of other publications. This step is essential to validate the capability of the mounted assembly to reproduce the same behavior. The setup is also used to verify the simulated results and to ensure that the developed model on MATLAB is a real life replication. This experimental approach should be able to control also the MCDI cell charging voltage and current beside reading the concentration of the water input and output. For these reasons, the system was built based on a constant voltage source able to go till 25V DC and a constant current source for a maximum of 6 Amperes. The setup used an ANATEK power source supply manually adjusted for this reason. However, when it comes to the control, An AC/DC converter from COTEK is used. The PID loop is programmed inside an Arduino controller, it has mainly one analog input for the output concentration based on TDS meter card V1.0 from KEYSTUDIO. The metering cards were calibrated and tested on different water samples with a validation probe factory calibrated. The controller is equipped also with an analog output from 0-10 V to control the AC/DC converter which will generate the adapted voltage and a current up to 160 Amperes. Monitoring the system is based on DT9812 from ECON series. The Source and cell voltage, the circulating current and the input/output concentration are connected to the data acquisition card so all the cell parameters could be monitored.

4.7 Results and discussions

Many operation modes have been the subject of several studies. Those modes were initially identified by Zhao *et al.* (2012a) (Zhao *et al.*, 2012b), and summarized in table 4.3.

The CVA and CCA adsorption mode operation will be detailed in the operations mode section. And since the paper treat the voltage control in adsorption phase,the desorption phase as aZVD or RVD will not be considered. RVD mode is applicable when by the end of the adsoprtion phase a reversed voltage is applied on the terminals of the cell. A ZVD is considered when the

Table 4.3 Traditional operational modes

Abbrev.	Description
CVA	Constant Voltage Adsorption
CCA	Constant Current Adsorption
ZVD	Zero Voltage Desorption
RVD	Reversed Voltage Desorption

cell terminals are electrically short-circuited. The ZVD is adopted in the current paper work due to its simplicity.

4.7.1 Operations mode

4.7.1.1 CVA mode

The most common industrial application of the MCDI is based on CVA-ZVD (Liu *et al.*, 2020). On the application of a constant voltage on the cell terminal, the effluent salt concentration reaches a maximum. In the beginning, the salt removal is the fastest and slowly increases back to the influent concentration as the removal rate slows down (Figure 4.4). This phenomenon is due to the increase of the counter-ions EDL voltage (Porada *et al.*, 2013b) (Zhao *et al.*, 2012b).

As the source voltage is constant, the voltage of the cell is increasing as for the capacitor voltage during the charging phase and the current is increasing accordingly due to the increase of the differential potential between the source the cell. The increased current will reduce the circulated electrons in the electrode and the output concentration will start increasing. The result is consistent with Zhao *et al.* (2012a) observation in their paper.

4.7.1.2 CCA mode

The constant current application on the MCDI was initially introduced by Zhao *et al.* (2012a,b) as shown in Figure 4.5. Under the CCA, a more stable concentration is obtained due to the direct

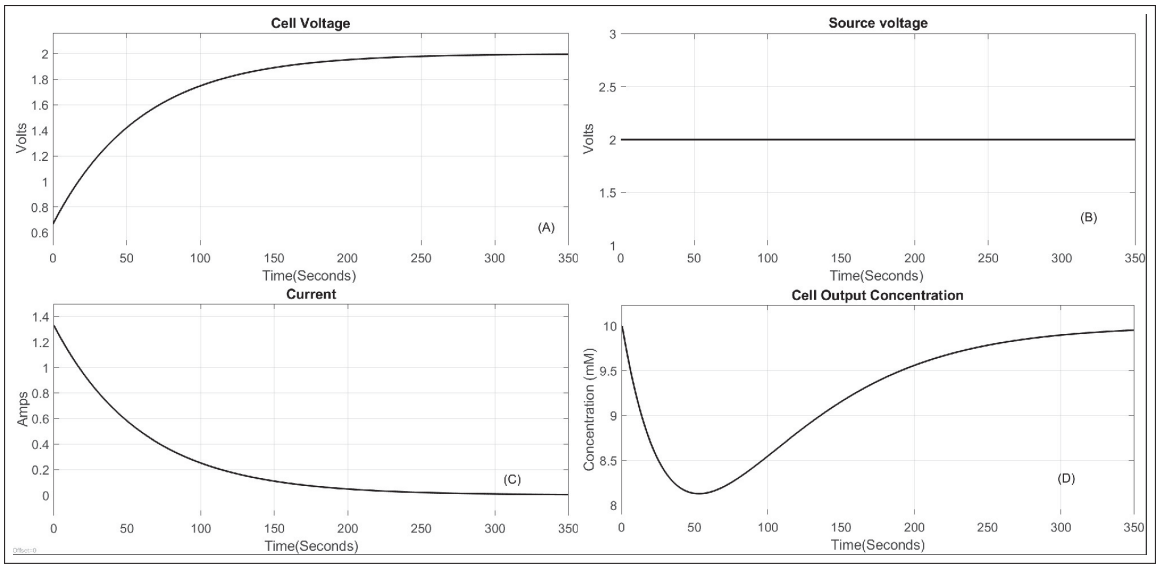

Figure 4.4 Constant Voltage application:(A) Cell Voltage , (B) Source applied voltage, (C)Measured current, (D) Effluent output concentration

correlation of the constant applied current and constant ionic current. That will lead to more stable salt removal rate from the bulk solution and therefore, a more constant salt concentration in the cell effluent (Saleem *et al.*, 2016) (Zhao *et al.*, 2012a).

As the current is constant , the applied voltage would steadily increase due to the increase of the counter-ions EDL voltage and the lower electrolyte concentration (Zhao *et al.*, 2012a). The end of the CCA period is determined when the voltage reaches its maximum allowed values as 1.4V, 1.6V, 2.0V (Kang *et al.*, 2014) (Jande & Kim, 2013).

Porada *et al.* (2013b) however had limited the application of the CCA mode to the use of the Ion Exchange Membranes (IEM) incorporated into the cell architecture. Since the counter-ion adsorption flux and the co-ions expulsion flux constitute the ionic current, and since the rejection of the IEM minimizes the co-ions expulsions, the constant ionic current will only result in a constant counter-ion adsorption flux. Thus, without the use of the IEM, the constant ionic current cannot fully translate into constant counter-ions adsorption flux. As a result, both counter-ion and co-ion will be driven by the ionic current and the effluent concentration cannot quickly reach

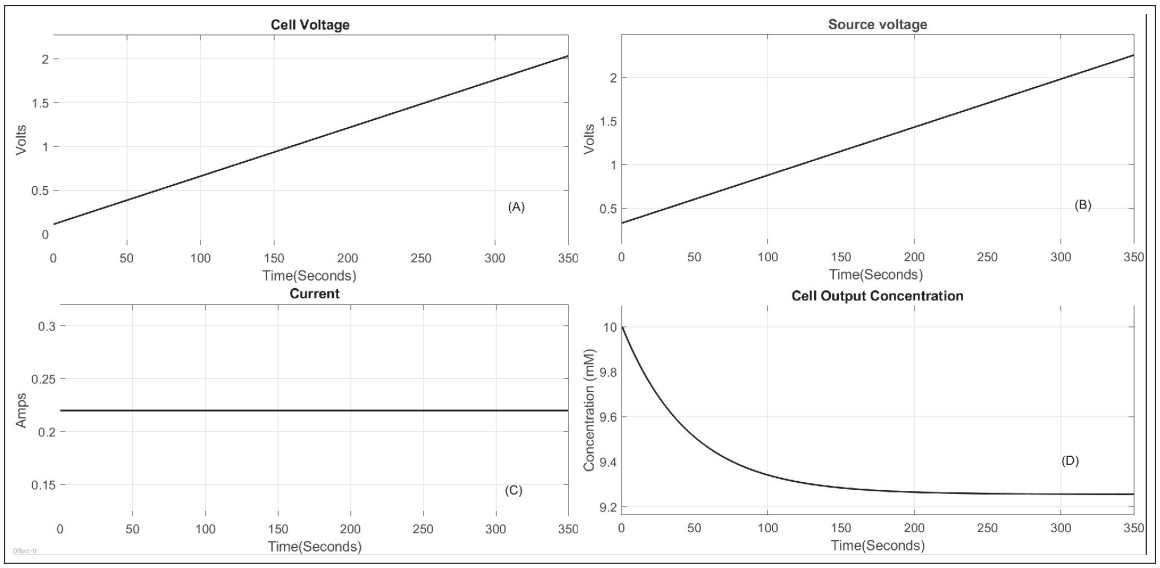

Figure 4.5 Constant Current application:(A) Cell Voltage , (B) Source applied voltage, (C)Measured current, (D) Effluent output concentration

the desired "Low plateau" value under constant current operation (Liu *et al.*, 2020) (Porada *et al.*, 2013b). This phenomenon is shown in Figure 4.5 D because the cell reacts slowly to the application of the constant current to reach its stability only when the duration of the adsorption period has expired.

4.7.1.3 CVCA mode

An hybrid operation mode was recently introduced by Saleem *et al.* (2016). In the hybrid mode represented in Figure 4.6, the CVA and the CCA operating processes were combined as constant Voltage and then Current Adsorption (CVCA). It consists in applying a constant voltage to a short time of the adsorption cycle. This first voltage application is called the power mode. The goal is to push the cell effluent concentration in a very short time to its lowest point in the CVA mode. In order to avoid the increase of the effluent concentration again, the mode starts the application of a CCA when the concentration value of the CVA is equal to that of the operating CCA. One of the biggest difficulties of this mode is to find the optimal application of the voltage on the cell and then of the current, in order to reach the adsorption period of the other mode.

Many combinations seem possible, however the 1.2 V for the power mode and 0.18 amps for the current mode had been chosen.

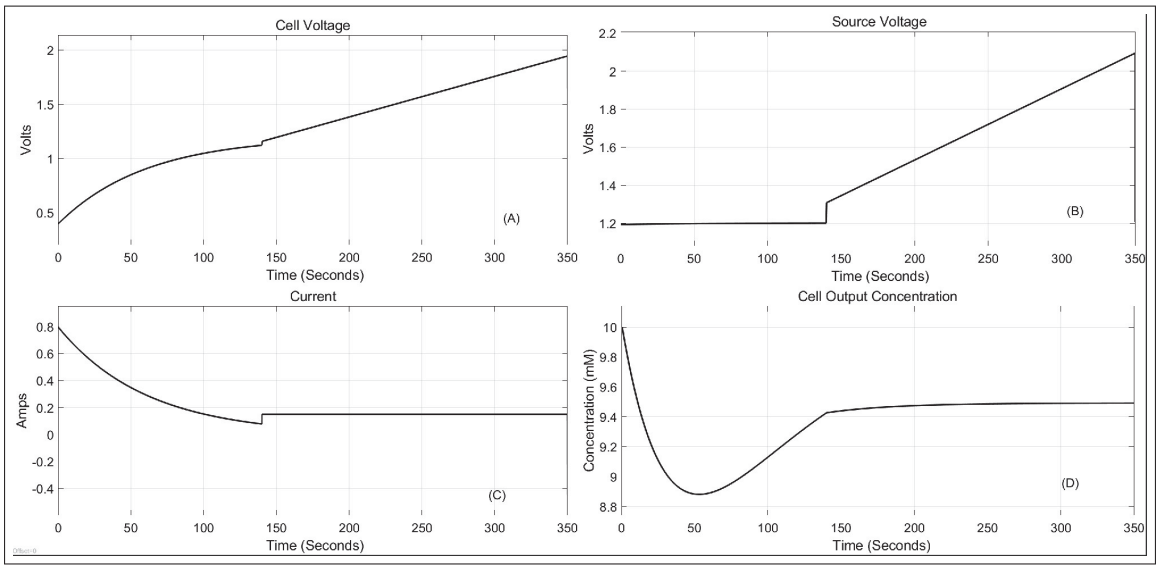

Figure 4.6 Hybrid application: (A) Cell Voltage , (B) Source applied voltage, (C)Measured current, (D) Effluent output concentration

4.7.1.4 Closed-loop mode

Figure 4.7 shows the result of applying of a closed-loop control to the MCDI cell. The applied voltage source is adjusted to maintain the concentration output on a determined level of 8.5 mM. It is noticeable that the presented design allows the source to switch to negative voltage to readjust the concentration once it gets below the setpoint. It also reacts like a constant current at the end of the pre-regulation phase allowing to benefits from the advantage of CCA mode with the adapted current value applied.

4.7.2 Open vs Closed loop

Figure 4.8 shows a comparison of the behavior of the cell effluent concentration following the application of a conventional open versus a closed-loop control. The simulation was carried

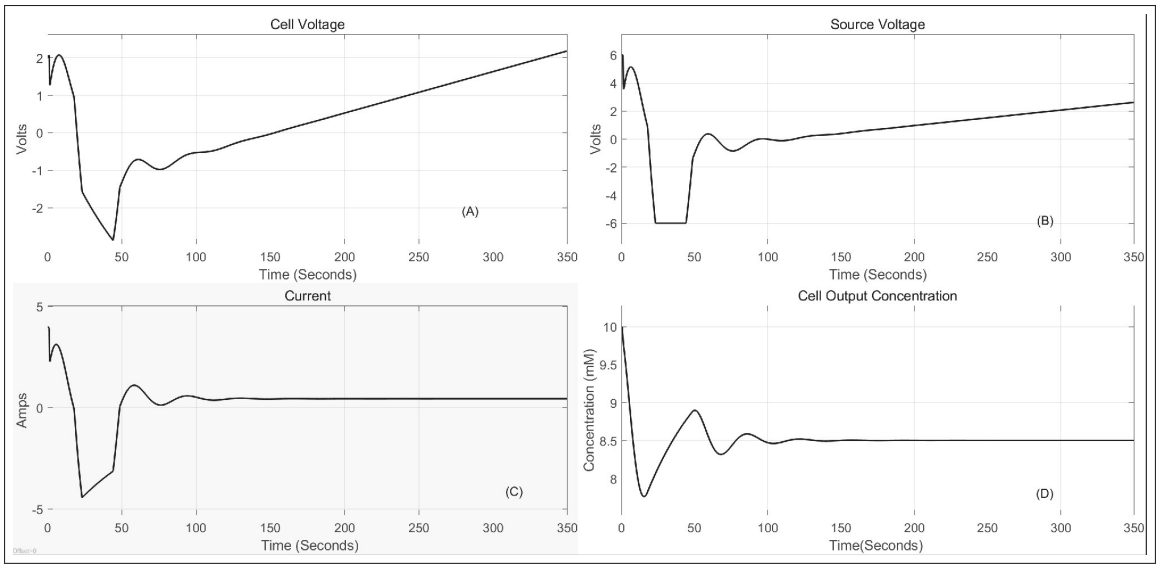

Figure 4.7 PID Control application:(A) Cell Voltage , (B) Source applied voltage, (C)Measured current, (D) Effluent output concentration

out for the same water influent quality and under the same operational conditions of water temperature, the cell flow rate . . .

Two major points had to be observed when operating the cell :

1- The maximum cell voltage:the maximum voltage that can be handled by the cell is considered 2 volts in order to avoid the faradaic reactions due to the carbon surface oxidation, and electromigration of hydronium and hydroxyl ions. Therefore, the operating conditions (applied voltage value in CVA mode, applied current value in CCA mode,..) were adjusted in order to obtain the maximum voltage at the end of the same adsorption period.

2- The effluent setpoint: The setpoint of the desired output effluent should be chosen within the actual operating range of the cell itself. In the example of Figure 4.8, the concentration in the open-loop oscillates between 10 and 8.2 mM, so the desired value was set at 8.5 mM relative to the operational concentration limit of the cell.

The comparison is held principally between the constant voltage and the closed-loop application in the Matlab simulator without any adsorption period restriction using the same source of voltage supply for both modes.

Figure 4.8 shows that the closed-loop control handles the adsorption phase for a longer period, which means that a controlled cell could cycle less and avoid unnecessary wasting operational time in the desorption phase.

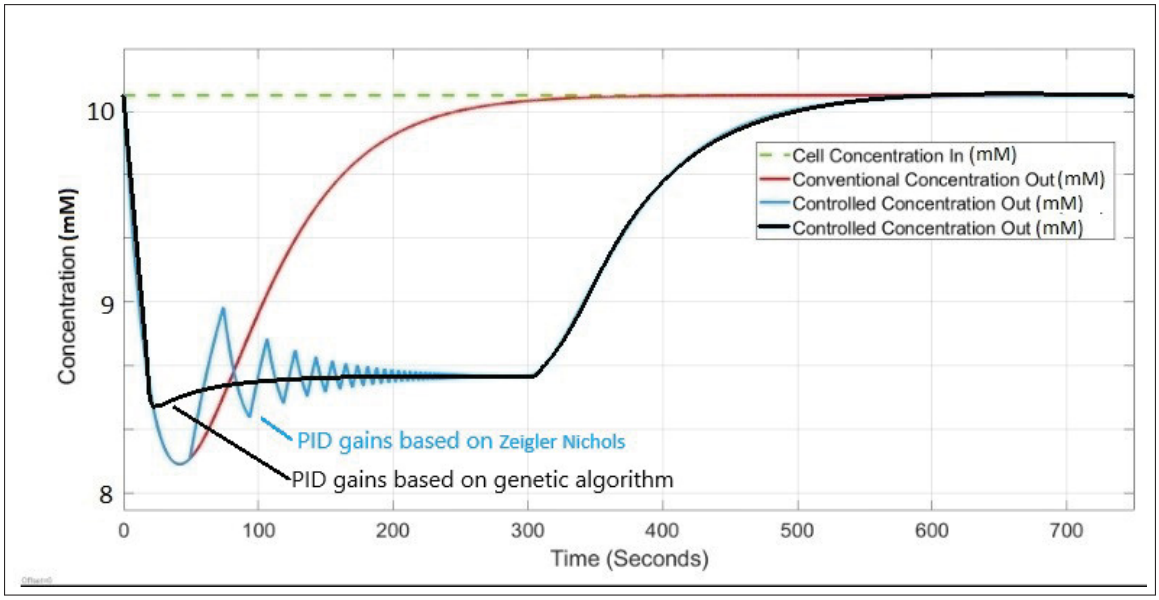

Figure 4.8 Simulated concentration output comparison between the open-loop, the closed-loop with Ziegler Nichols gains parametes, and Closed loop based on GA gains parameters

4.7.2.1 Energetic Capacitance

In a recent study, Ghamrawi *et al.* (2022)defined the energetic capacitance as a the ratio between the consumed energy during the adsorption phase and the one generated during the desorption phase. The Energetic capacitance CE as well as Average Energetic capacitance ACE were presented as a performance indicator of the cell behavior for energetic efficiency. Table 4.4 shows a comparison between the different control modes of the cell , it shows that the MCDI in a closed-loop control marks the highest energetic behavior than the other ones.

Table 4.4 Energetic Capacitance indicators comparison

Control Mode	Energetic capacitance (F)	Average Energetic capacitance (mF/S)
CVA	12.5	2.5
CCA	13.7	3.01
CVCA	13.9	3.2
Controled	14.68	3.77

4.7.2.2 Salt removal Ratio

Figure 4.9(a) shows a higher salt removal performance of the cell in the controlled application. The difference between the two approaches is explained by the ion's distribution on the carbon electrode.

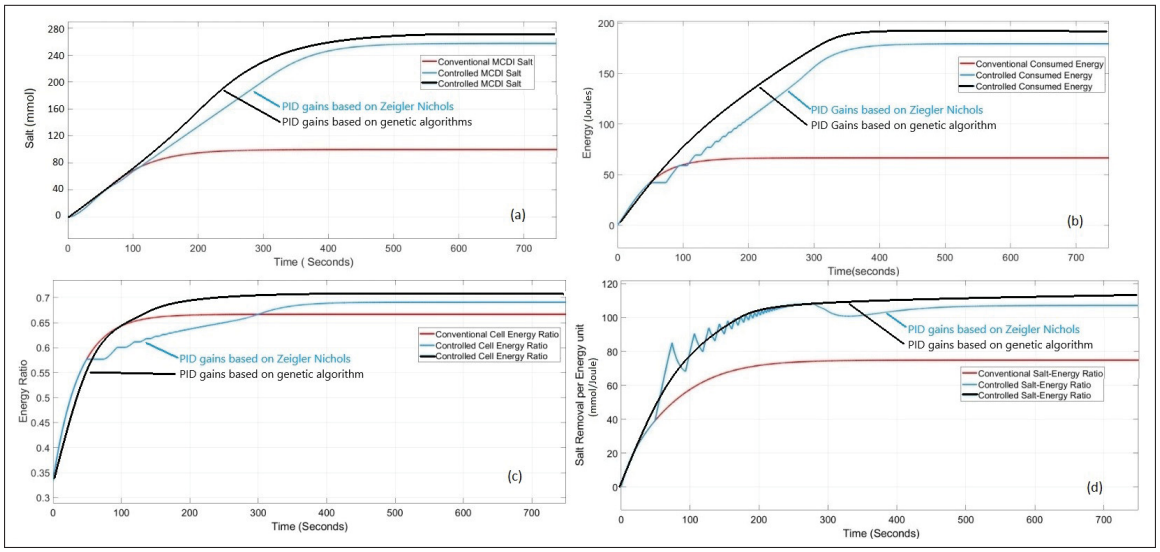

Figure 4.9 Simulation results of the controlled cell based on Ziegle Nichols gains parameters and GA gains parameters, (a) the quantity of removed salt, (b) the consumed energy, (c) the energy ratio, (d) The quantity of removed salt per energy unit

4.7.2.3 Energy consumption

The energy consumption per charging cycle has increased significantly since the total amount of adsorbed salt has been increased compared to the conventional open-loop and the controlled closed-loop application as shown in Figure 4.9(b). At start-up, the two applications share the same curve until second 50, when the cell output concentration reaches its setpoint. Thus, the charging behavior starts to change in order to maintain the salt effluent concentration in the closed-loop. As the conventional setup is saturated in 100 seconds, the controlled MCDI continues to consume energy from the source for the adsorption purposes until second 300, when the controlled system reaches saturation. As explained, it will be obvious that the quantity of energy absorbed by the controlled MCDI reaches a higher level than the conventional one.

4.7.2.4 Cell Energy ratio

When dealing with a high efficiency desalination process, one of the important issues is to verify the efficiency of the cell performance by the application of the closed-loop. In this work, we aimed to investigate whether or not there is an impact of such application on the cell energy profile. This information is vital for effective MCDI control design. Stabilizing the performance of the MCDI and maintaining a fixed output concentration should not have any impact on the cell consumed energy. Figure 4.9(c) shows the Cell Energy Ratio (CER) of the cell calculated for a given time (i) as:

$$\begin{aligned} CER(i) &= \frac{\text{cell consumed energy}}{\text{Source supplied energy}} \\ &= \frac{\sum_{n=0}^{i} |V(n)_{cell}.I(n)_{cell}\Delta t|}{\sum_{n=0}^{i} |V(n)_{source}.I(n)_{cell}\Delta t|} \end{aligned} \tag{4.11}$$

It is clear the cell energy ratio of the conventional one presents a similar behavior to that of the controlled one. However, it is noticed that during the reaction, the controlled cell shows a small energy ratio decrease of 57% to 65% between the 50th and the 300th. This can be explained by considering the absolute value in the calculation of the consumed energy by the cell without

taking into consideration the energetic values of the reversed current during the relax time of the control modulation. Furthermore, at the end of the process, Figure 4.9 shows that the overall energetic performance of the controlled cell is slightly advantageous compared to the conventional one. Similarly, for the concentration profile, when the cell reaches its maximum saturation values, the consumed energy in the controlled cell will have more margin to fill in due to the equal and uniform distribution of the ions on the surface of the electrodes. This margin explains this slight increase of the consumed energy of the controlled cell at the end of the adsorption phase.

4.7.2.5 Salt-Energy ratio

Comparison of the removed salt quantity during the adsorption period has shown a noticeable advantage of the closed-loop application. As the controlled cell consumes more energy than the conventional one, the question raised is how to determine if the controlled MCDI is more efficient in salt removal for a given limited energy applied. To answer this question, the amount of the removed salt by an energy unit should be calculated. A Salt-Energy ratio (SER) is defined as:

$$\begin{aligned} SER(i) &= \frac{\text{Salt removed amount}}{\text{Cell consumed energy}} \\ &= \frac{\sum_{n=0}^{i}(C(n)_{in} - C(n)_{out}.F.\Delta t|}{\sum_{n=0}^{i}|V(n)_{cell}.I(n)_{cell}\Delta t|} \end{aligned} \tag{4.12}$$

The calculated SER is shown in Figure 4.9(d). It clearly shows the superiority of the controlled cell over the conventional in terms of the amount of salt removal per unit of energy in the cell. As for comparison at 300s, one watt-second can remove 62 mg of salt in conventional application compared to 106 mg of salt in the controlled one.

4.7.3 All modes comparison

As the advantage of the closed-loop control in the behavior of the MCDI cell performance has been demonstrated, let us extend the comparison for all the four existing control mode of the MCDI known to date. Figure 4.10 shows the quantity of the removed salt for the same adsorption period for the four operating modes. It is obvious that the removed salt part using the closed-loop method shows the highest amount. This application of the closed-loop controlled loop shows a slightly higher quantity in the early stages of the application since it reacts like the conventional mode. As the ions are uniformly distributed as explained in section 4.7.2.2, the closed-loop will try to apply a constant current which results in a higher salt removed quantity achieved by the end of the process.

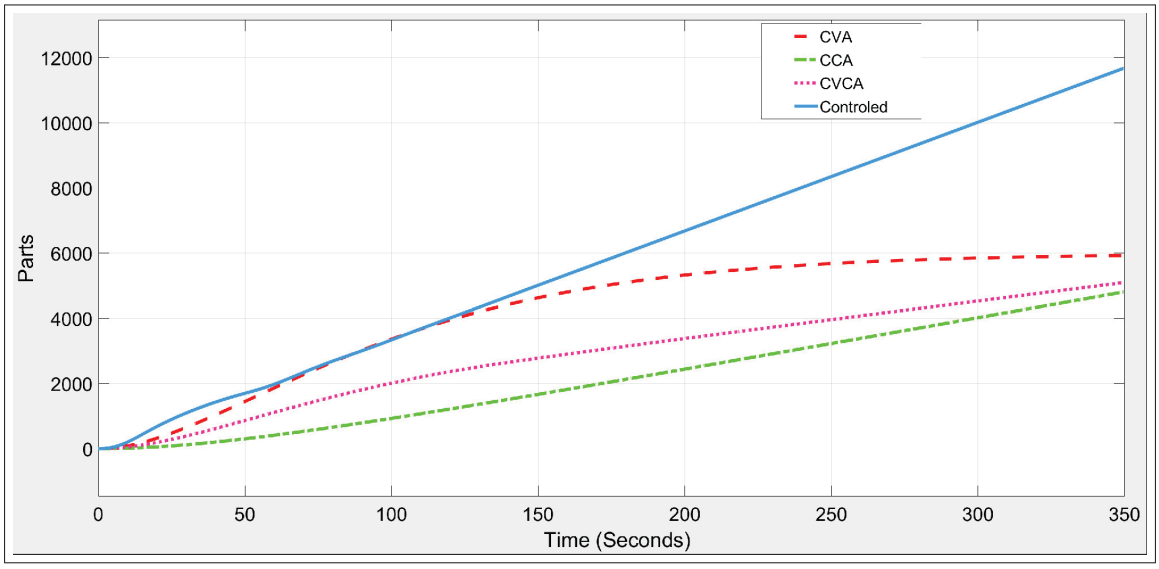

Figure 4.10 Quantity of removed Cell

The quantity of removed salt per energy unit (SER) is presented in Figure 4.11. It is fair to say that the CCA application has the best ratio at the beginning of adsorption process, however, as more of salt quantity is retained on the electrodes surface, the CCA mode loses its advantage to the closed-loop control. Note that the CVCA mode can achieve a similar result to the CCA if the adapted voltage and current have been chosen to optimize the control of the cell. In all cases,

the closed-loop control remains slightly higher with its ratio of 80 parts per joules at the end of the adsorption period.

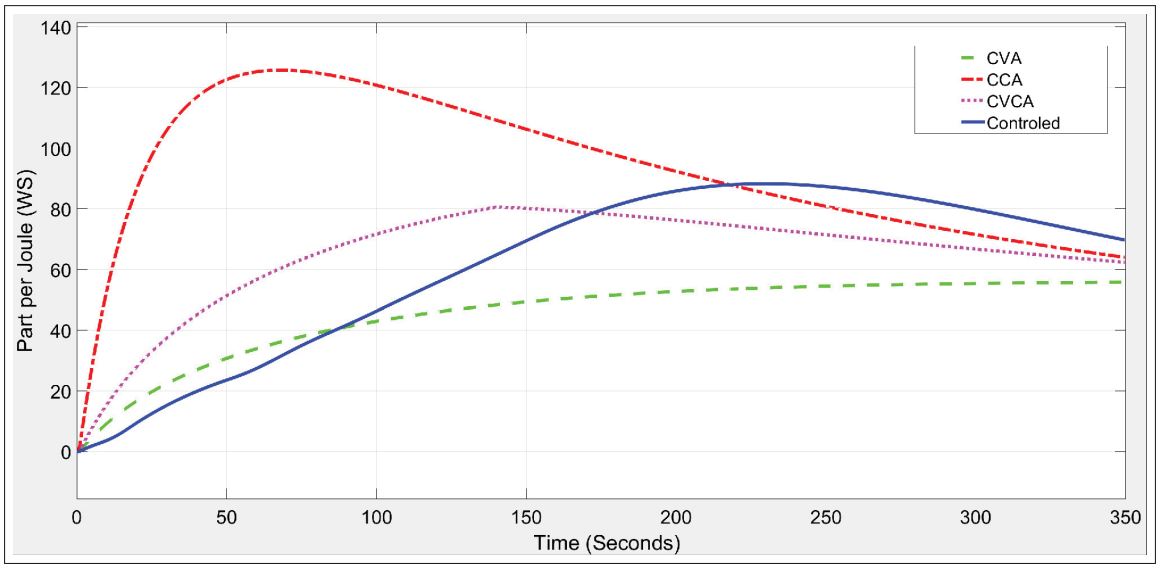

Figure 4.11 Quantity of removed salt per Energy unit

4.7.4 Experimental Results

The experimental results come to confirm the simulation ones. Figure 4.12 shows the output effluent of the MCDI cell by the application of the four operating modes, in addition to the simulated one. All four experiments were conducted with the same operating conditions with a constant input concentration of 10mM, a constant flow of 0.38 L/min and stable water temperature of 15°C. The conventional control mode as the CVA, the CCA and the CVCA presents an unstable output concentration of the product. The voltage shows the highest increase slope, beside the CVCA that presents a combination of the CVA and the CCA aspects. The controlled closed-loop shows stable effluent concentration, with a small fluctuation related to the speed of the correction of the MCDI cell.

The resulting curves shown in Figure 4.12 give a better understanding of the process and the regulation and reveal many interesting observations:

A. Between the simulated and the experimental concentration curves :

- The similarity of the response time between the simulated and the experimental results is clear, the two curves take less than 10 seconds to achieve the stability of the output concentration.
- The last 300 seconds of the adsorption phase reveal a slight increase of the output concentration compared to the stable simulated one. That is due mainly to the distribution of the charge on the electrode. As in the developed model, it was considered a uniform distribution on the surface of the electrode. However in reality, the electrodes charges are unequally located on the surface which reduces the performance of the salt retaining in some spots at the end of the adsorption process.
- The amount of released ions during the desorption phase does not show the same profile in simulation and experimental, and this is due to current regeneration during this phase. We strongly believe that the cell resistance during the adsorption is different from the one in desorption phase, in addition the value of this resistance is not constant during the whole phase. Experimental curve shows an important variation in the second 2200 and the second 2600 in the cleaning phase. Further investigation of this variation could be achieved in future works aiming a control of the desorption phase of the cell.

B. Between the controlled and non-controlled curves:

- The response time to reach the reference concentration is clearly faster in the closed-loop control, it takes around 10 seconds compared to 300 seconds for other modes.
- All the non-controlled curves present an important overshoot of the output concentration that can reach 0.5 mM (about 40%) of the set value. The overshoot can fluctuate the final product concentration during an extended continuous production.
- By the end of the adsorption phase, the produced water quality tumbles down using the traditional CVA , CCA and even CVCA application. The end of that phase is also marked with an output concentration of 9.75 mM for the CVA, a 9.5 mM for the CCA/CVCA compared to 8.8mM for the close-loop application. As described before, the excess ions retention of the electrodes in the beginning of the desalination process will cause an earlier saturation by the end. This saturation will limit the capability to retain more ions by the time.

- The desorption phase is a phenomenon due to the electrodes time requirement to release all the retained charges. it is clear that the mode with the highest amount of retained salt shows the highest desorption profile. Efficiency of the process is evaluated based on the amount of consumed charges versus the amount of removed salt as shown in Figure 4.11

C. Dynamic response of the cell :

- The control had also proven a fast time response in achieving the reference concentration. This fast response is due to a high voltage application in the beginning of the phase. In order to decrease the response time, a higher starting voltage is required. However such design will oversize the supply system and the cost of the materials. In the current model, the transition time is about 0.5% of the total period of the desalination process, which make a faster response has been no big advantage.
- No overshooting in the output concentration which will confirm again that the suitability of the obtained gains in the genetic algorithm.
- Finally the stability of the produced water quality with a fluctuation of less than 1%(8.8-8.75/8.75) compared to the reference concentration will give high advantage of the controller in the future MCDI industrial application.

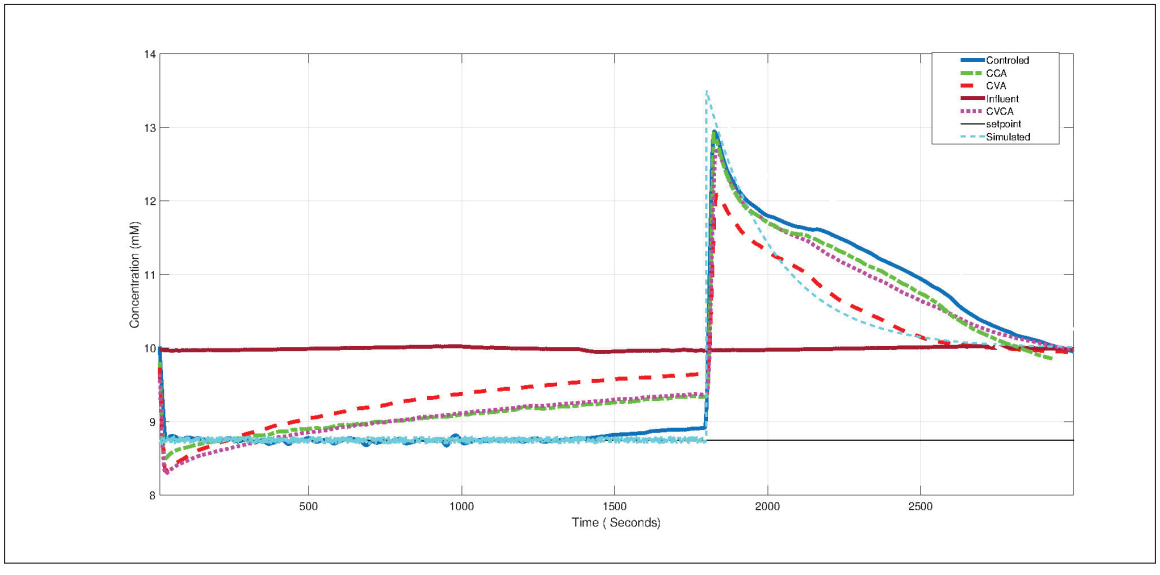

Figure 4.12 Experimental and the simulated control concentration output

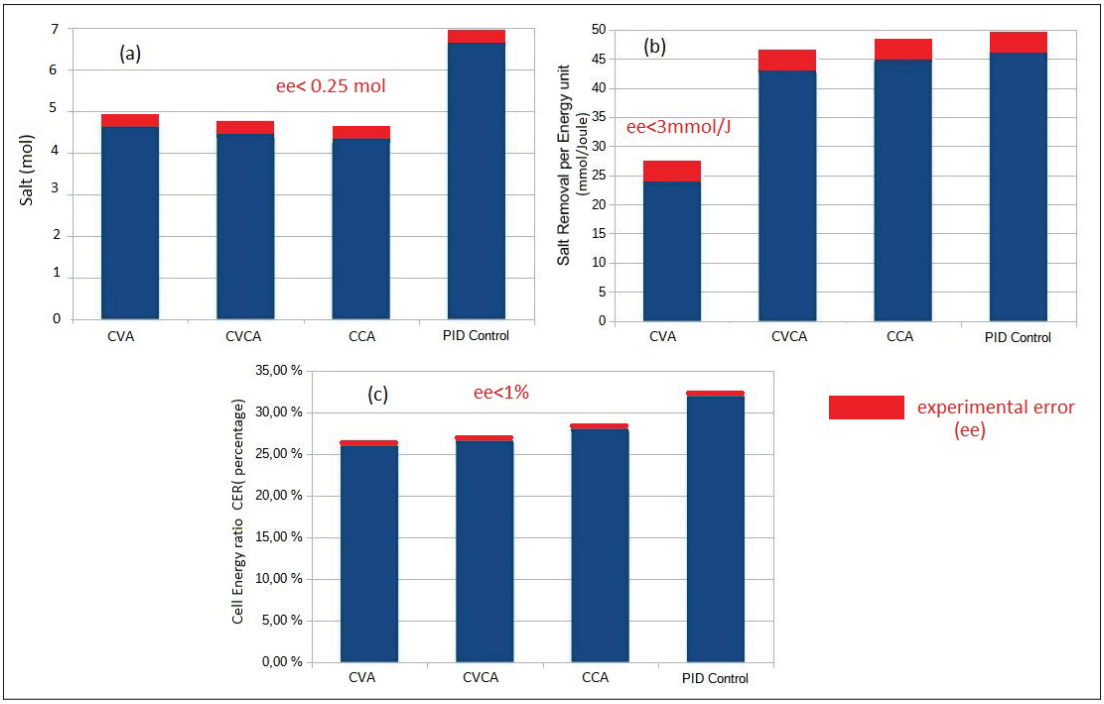

Figure 4.13 Comparison between the Experimental of all applied mode : (a) Quantity of removed salt, (b) Quantity of removed salt per energy unit, (c) Percentage of Energy performance CER

Figure 4.13(a) shows a comparison of the experimental quantity of salt removed from the cell. The quantity of removed salt inside the cell is determined by the difference between the concentration and the quantity of water passing through the cell. In Figure 4.12, from the 300 seconds till the end of the phase, the controlled mode presents the lowest concentration which means the highest performance in salt removal and the highest quantity of the salt.

On the other hand, Figure 4.13(b) also shows the slight energetic advantage of the closed-loop for the quantity of salt removed by energy unit of one joule (Watt Second).The biggest period of energy consumption is in the last period when the controller is trying to maintain the output concentration. Despite that, the energy joule in the close-loop was able to retain more salt for a longer adsorption period.

The Cell Energy Ratio CER shown in Figure 4.13 (c) is not only a performance indicator but it is more representing the energetic loss inside the cell during the adsorption process. The

controlled use of the energy with respect to the concentration performance will avoid the over consumption of energy for unnecessary water quality. About 5% of the energy is saved from the CCA and CVCA mode and 10% from the CVA mode.

It is worth to mention in the end that the cost of the implementation of the current source CCA and CVCA application) for the MCDI is the most expensive in component and installation, which can go up to 345$ in some electronic design, the voltage source CVA application is the less expensive with the simple buck-booster converter about 10$. However the PID controller will not exceed the 20$ including the TDS sensor. As value for price, the PID controller still the best and cheapest solution.

4.8 Conclusions

The voltage regulation of the cell terminals during the adsorption phase announce a new era of a controlled output concentration, a cleaner energetic footprint and a higher performance in salt removing. To address the non-stability of MCDI water product quality , a model-driven control strategy was constructed in this paper and then applied to a typical experimental cell.

Using the closed-loop control framework, the optimization of the quantity of removed salt by energy unit was achieved in addition to a stable effluent concentration was guaranteed at the desired setting point. As the controller adjustment is based on the cell parameters, the optimization of the control will be limited consequently to a close identification of the physical arrangement of the cell, the construction materials of the electrodes and the membranes besides the external operational conditions as the water temperature. Another limitation of the application is related to the effluent concentration: A high input concentration could saturate quickly the electrode and prevent the voltage control to take place. Controlling the water passing flowrate through the MCDi could be a solution prior to future studies. Finally, the development of such a closed-loop controller with the respect of the cell upper bounds of concentration and voltage has proved to be effective to accomplish continuous process optimization and a reduced energetic footprint.

Conflicts of interest

There are no conflicts to declare.

Acknowledgements

This work was supported by Current Water technologies[b], Research center.

[0] [b] *70 Southgate Drive, Unit 4, Guelph, ON, Canada, N1G 4P5 https://www.currentwatertechnologies.com/.*

4.9 Algorithms in annexes

4.9.1 Modeling algoritm

Modeling algorithm: The model is determined by introducing the cell physical dimension as the volume, the full water capacity, the water flow and applied voltage on the cell. The output concentration is calculated based on σ, λ and ϕ_{salt}.

Algorithm 4.1 Calculating experimental bench parameters algorithm

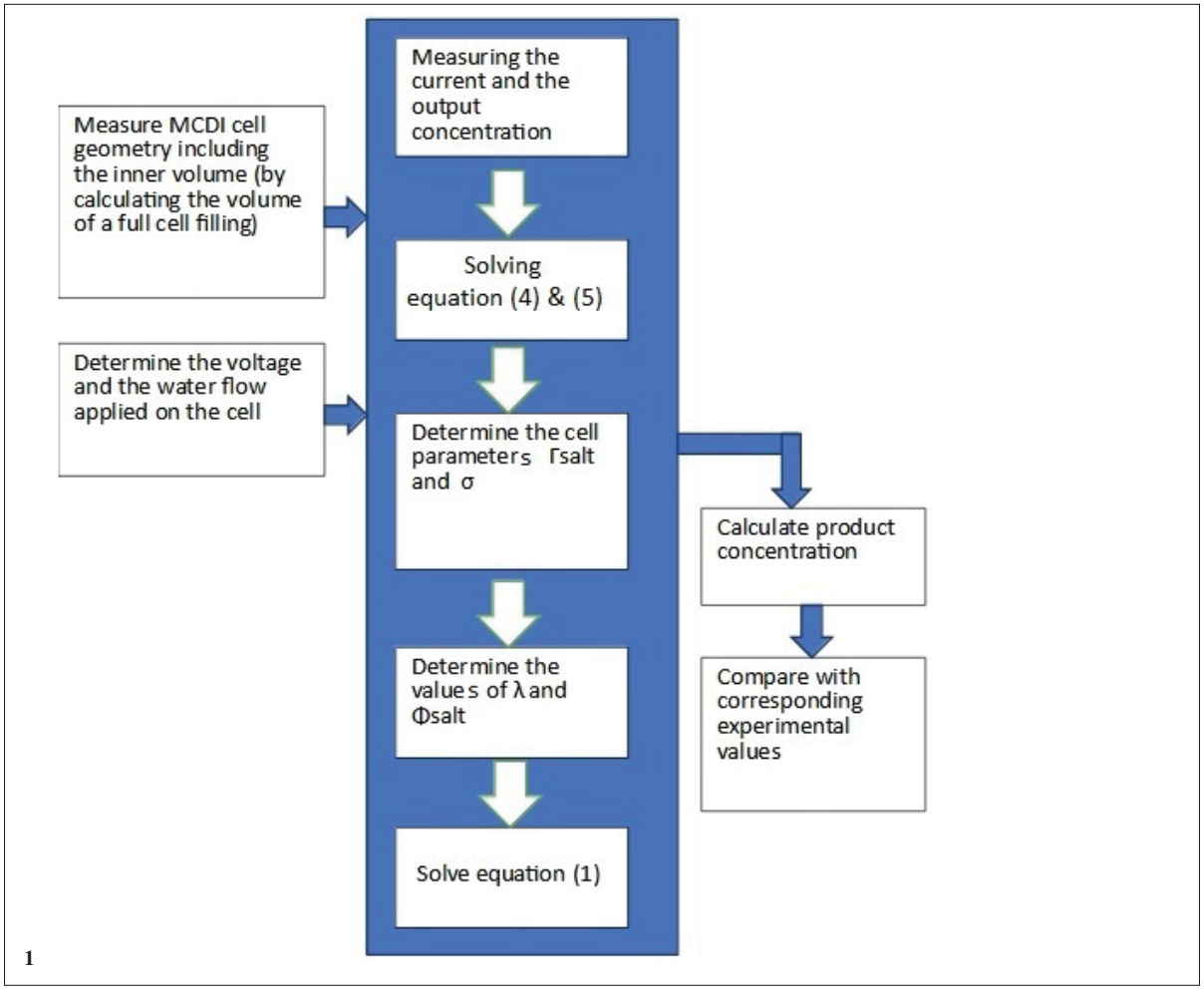

1

4.9.2 Optimizing algoritm

Optimization of proportional integral derivative controller using genetic algorithm: The algorithm start with a random generation of the initial chromosome population. The chromosomes are the gains obtained by Zeigler and Nichols as the first candidate solution for the PID gains. Afterwards, the best gains parameters are chosen based on the fitness of each individual. The crossover and the mutation are applied to the "elite" chosen population in order to improve the next generation solution. Crossover is the operation that recombines the two parents chromosomes parameters solution to produce offspring. Mutation is however the operation that creates variation into the chromosomes and change the entire value of it. Using the mutation operation, the gains are integrated into the model to explore the better solutions. If the solution is optimal than the gains are retained , otherwise the process continue until the population converge toward a better solution or another stop criterion is achieved.

Algorithm 4.2 Genetic Algorithm

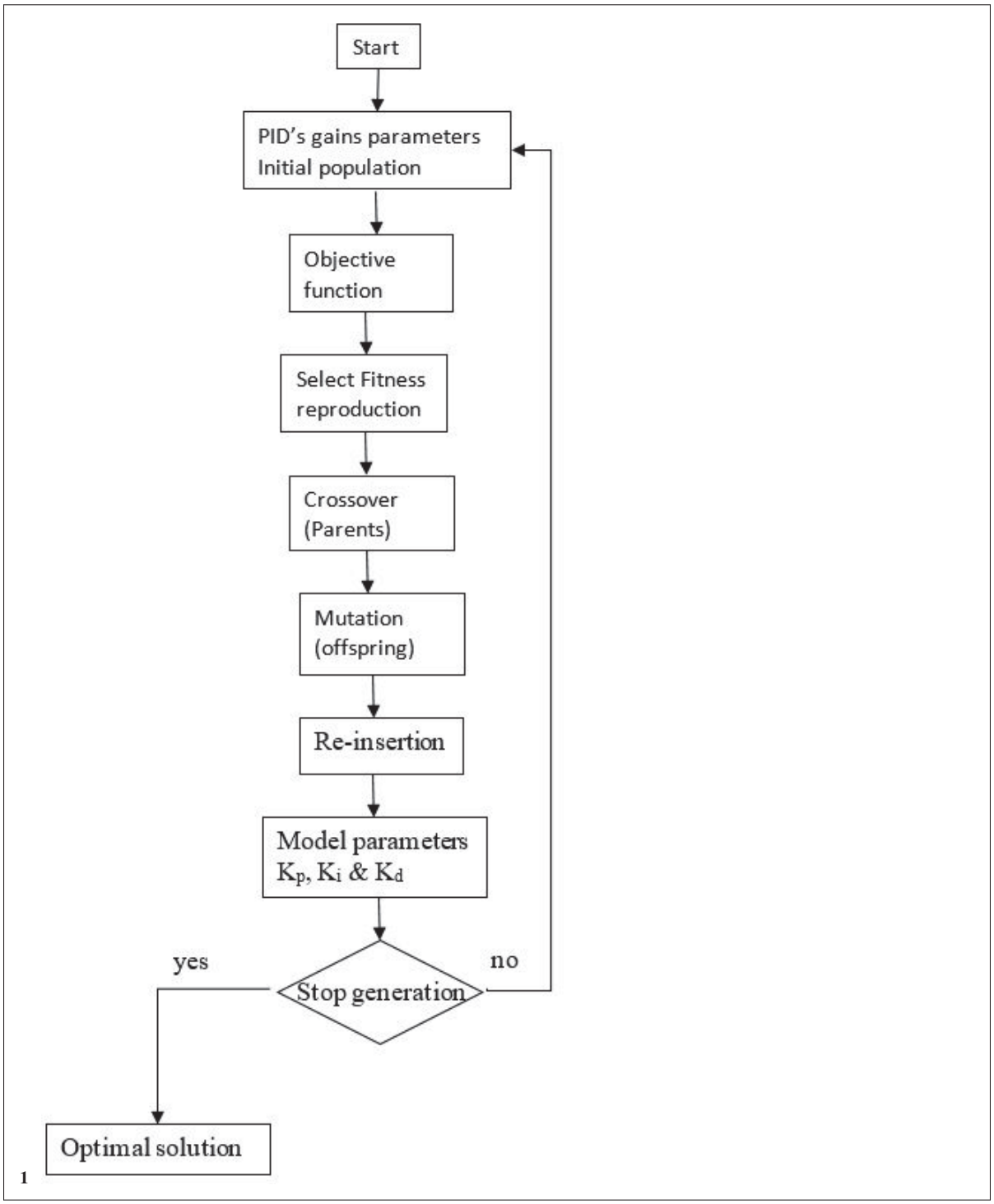

1

CHAPTER 5

MAXIMUM SALT ADSORPTION TRACKING IN CAPACITIVE DEIONIZATION CELL POWERED BY PHOTOVOLTAIC SOLAR PANEL

Alaa Ghamrawi[1] , Maarouf Saad, Imad Mougharbel.

[1] Electrical Department, École de Technologie Supérieure,
1100 Notre-Dame Ouest, Montréal, Québec, Canada H3C 1K3

Paper to be published in « Desalination» in November 2023.

5.1 ABSTRACT

Photovoltaic (PV) systems are considered as a support unit and eco-friendly energy source for the desalination system. If the surface of the desalination plant is covered by PV cells, it is possible to produce self energized desalination plants. Capacitive deionization (CDI) is a water purification technology known for it reduced energetic footprint. The cells are supplied with DC voltage power which makes the application of the PV panels logically intuitive. Conventional existing PV maximum power point trackers (MPPT) are similar to each other in hardware as electrically DC modulated and operated, but different in software. Through different algorithms, existing PV power trackers aims battery charging or grid-tie exportation as application. In this study, a new power tracking using the water flow control is presented as an adapted solution for water desalination using the solar power. The developed algorithm is based on Maximum Salt Adsorption Tracking (MSAT). The proposed algorithm shows a comparative performance as other tracking algorithms under varying radiations. Besides, MSAT brings considerable lower costs by eliminating the need of batteries or any storage unit in between. The developed controller is described in detail and comparative simulated/experimental analysis and performance evaluation are presented.

Keywords:MSAT, CDI, Photovoltaic,Model,Performance, Flow, Control.

sectionIntroduction

Nowadays, a number of studies have been carried out on using clean energy for desalination purpose. Solar panels are expected to take place on desalination plants as an electrical support unit with the advantage of their environmental benefits. Substantial amount of electrical energy can be obtained and stored into the battery in case of integrating solar panels onto the conventional desalination plants facilities. The MPP is the operating point where it is possible to obtain maximum power from solar panels. MPP varies continuously with environmental factors, i.e., solar irradiance and ambient temperature. Hence, maximum power tracking controller consists of both hardware and software components. The physical components are typically equipped with a dc–dc converter, sensors, and a control unit. The control unit has embedded software which runs a specific algorithm to perform MPP tracking. Several different MPP tracking algorithms are developed by many researches, they were classified by Esram *et al.* (2007) into 12 categories, Kamarzaman *et al.* (2014) resume them to four classes as follows:

- The Hill Climbing (Xiao *et al.*, 2004) algorithm that uses a perturbation in the duty ratio of the power converter, it can be applied for open circuit voltage and short circuit current as well.
- The conventional one that includes: the P&O involves the perturbation in the operating voltage of the PV panel (Jain *et al.*, 2004; Tafticht *et al.*, 2004; Femia *et al.*, 2005; D'Souza *et al.*, 2005) , besides the P&O, incremental conductance is a method that uses the slope of the PV panel power curve, it will be zero at the MPP, positive on the left of the MPP and negative on the right (Kim *et al.*, 2001; Husain *et al.*, 2017; Kobayashi *et al.*, 2003).
- The ripple correlation current adopts the switching action of the power converter connected to the PV array to impose the voltage and the current ripple(Midya *et al.*, 1996).
- The stochastic based MPPT algorithms include the swarm optimization (Mohandes, 2012), fuzzy logic controller (Senjyu *et al.*, 1994; Patcharaprakiti *et al.*, 2002; Khaehintung *et al.*, 2004), artificial neural network(Zhang *et al.*, 2002), and differential evolution(Firmanza *et al.*, 2020).

All of the above mentioned studies are related to algorithms for standard PV structures or improved versions of these applications mainly the battery charging or grid tie connection. On

the other hand, performance assessments of existing algorithms should be evaluated distinctly for desalination systems, like Reverse Osmosis, Electro-dialysis, since the performance is evaluated based on the quantity of removed salt and not the produced power. The application of conventional MPP algorithm to desalination process requires the implementation of storage units or batteries. This energy storage will limit the desalination operation to the batteries capacities. It is due to the waste energy when the batteries are fully charged. Oversizing the storage bank will have an important financial impact on the project. As for the grid application, the solution will be useless in grid shortage condition. So far the need of an adapted DC load based on the maximum produced energy. Traditional desalination technique as the Reverse Osmosis (RO) and Electrodiyasis (ED) could not offer an adapted controlled DC load. Their high energy footprint, environmental impact and other fooling problem(Zou *et al.*, 2008a,b; Xu *et al.*, 2008), have pushed researchers to work on a new desalination process which is more adapted to nowadays technologies.

Capacitive deionization (CDI) is a desalination technology that starts to take its place as an efficient energy and environmental technology (Ryoo *et al.*, 2003; Lim *et al.*, 2009; Welgemoed *et al.*, 2005b). The CDI function is based on potential-induced capacitive adsorption process of ions on the surface of a charge carbon electrode. The process is composed mainly of two phases:

- The adsorption took place when an electrical voltage is applied on the electrodes through cell terminals. The effluent charged ions will migrate to the opposite electrode and will be held in the electric double layer (EDL), a phenomenon modelled by Guoy-Chapman, the adsorption will take place until the electrical potential on the cell terminal reaches its maximal allowable limit. This limit is considered between 0.8V and 2.0V once exceeded hydrogen is produced due to water electrolysis on the carbon electrode(CH *et al.*, 2012; JC *et al.*, 1996).
- The desorption phase starts upon reaching the potential limit. The voltage is removed from the terminal and the retained ions on the EDL are quickly released to the bulk solution (Ying *et al.*, 2002). This phase is marked by a reversed current from the cell that can be exploited in other applications, as charging another cell (Álvarez González *et al.*, 2016).

Upon the application of the electrical potential, the counter-ions are adsorbed on the electrode and at the same time the co-ions are expelled from it. This migration occurs simultaneously and seriously reduces the desalination efficiency (Jeon *et al.*, 2013). Lee *et al.* (2009a) introduced the first ion-exchange membranes between the electrodes in the CDI cell. These membranes capacitive deionization (MCDI) had shown a salt removal efficiency of 49.2 % (Li *et al.*, 2008b). Despite the advantage of the MCDI in water desalination and ion removal (Biesheuvel & der Wal, 2010), the MCDI has another interesting aspect of flow influence on the cell operation and performance (Zhao *et al.*, 2012a). As the water influent increases as the quantities of ions brought to the cell is increased, so the more the salt removal per cycle is achieved.

MCDI technology had gained increasing importance especially in specific ions removal(M., 2011; Y., 2008) due to the improvement in carbon materials of the electrodes. The cells are normally operated between 0.8V and 2.0 V in order to avoid water electrolysis and hydrogen production. Nowadays, the most popular application of the MCDI consists of doing a short circuit or applying a reverse voltage on the electrodes when the maximum concentration on ions is reached during adsorption(BH *et al.*, 2011). In this phase the adsorbed ions are disorbed or discharged. However, the stored energy inside the cell is lost. On the other hand, and as reported by KY *et al.* (2009), the capacitive deionization process is not only affected by the influent water concentration (Ion solution in the aqueous electrolyte), the contact surface area between the carbon electrode and the solution and the voltage applied on the cell but also by the water flow rate. As it can affect the adsorption process and the migration of the ions to the charged poles, it can increase or decrease the quantity of the ions between the electrodes. This interesting aspect of the flow influence on the cell operation(Zhao *et al.*, 2012a) lead us to the Photo-MCDI: An MCDI cell equipped with a PV panel that use the flow rate as a control parameter. The variation of the flow rate will be an essential factor to adapt the MCDI cell impedance and eventually the load applied on the PV panel. So the study will present a new developed MSAT algorithm that control the flow inside the cell to an adapted level to optimize the power produced by the PV panel and benefit a maximum period for salt removal . The study will be ended by a comparison of the advantage of the MSAT application versus the existing technology in the market.

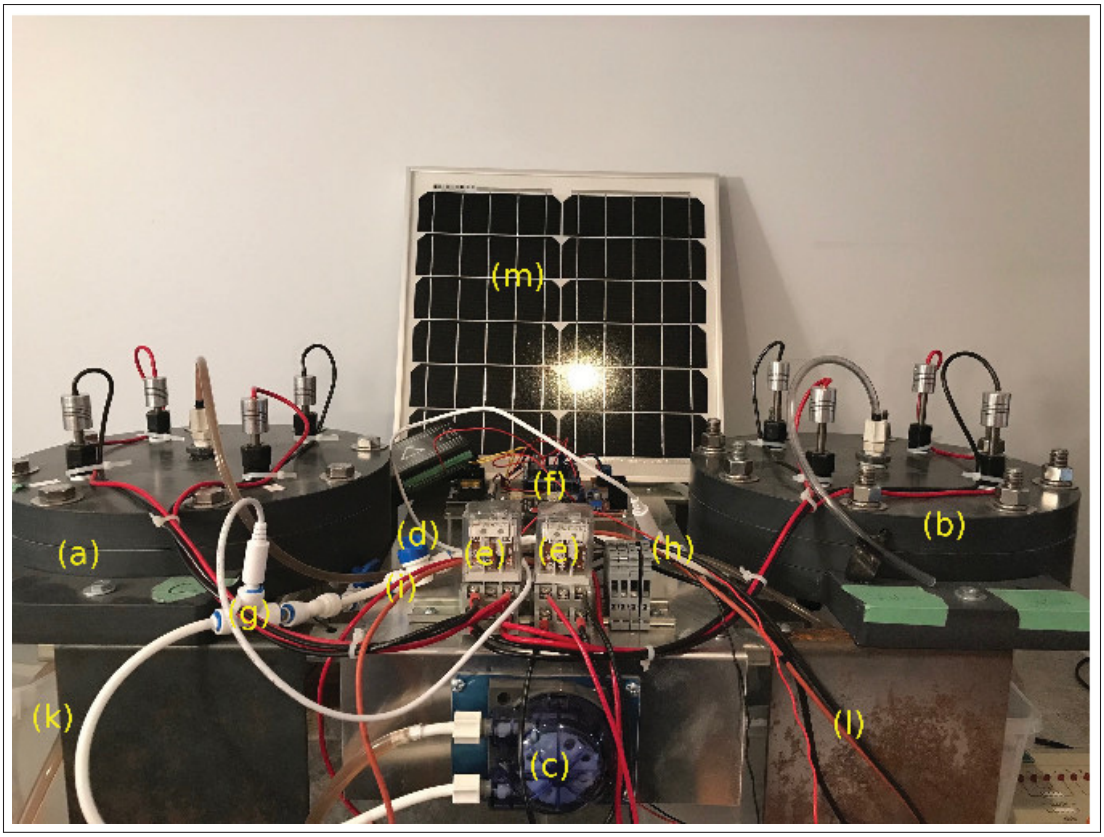

Figure 5.1 MCDI Experimental workbench including : (a) MCDI unit1 , (b) MCDI unit 2 , (c)12v peristaltic pump, (d) 1 ohm electrical resistor, (e) electrical controlled 2 SPDT switch, (f) processing controller, (g) influent concentration probe, (h) effluent concentration probe, (i) Unit1 manual valve, (j) Unit 2 manual valve, (k) influent water tank, (l) effluent product tank, (m) Solar Panel

5.2 Methodology

5.2.1 Photo-MCDI Modeling

The electric circuit model of the photovoltaic panel consists of photo generated current source in parallel with a diode and shunt resistor with a series one. The PV is supplying directly the MCDI which is represented by a capacitor in series with a cell resistor as mounted in Figure 5.1 and schematically represented in Figure 5.2.

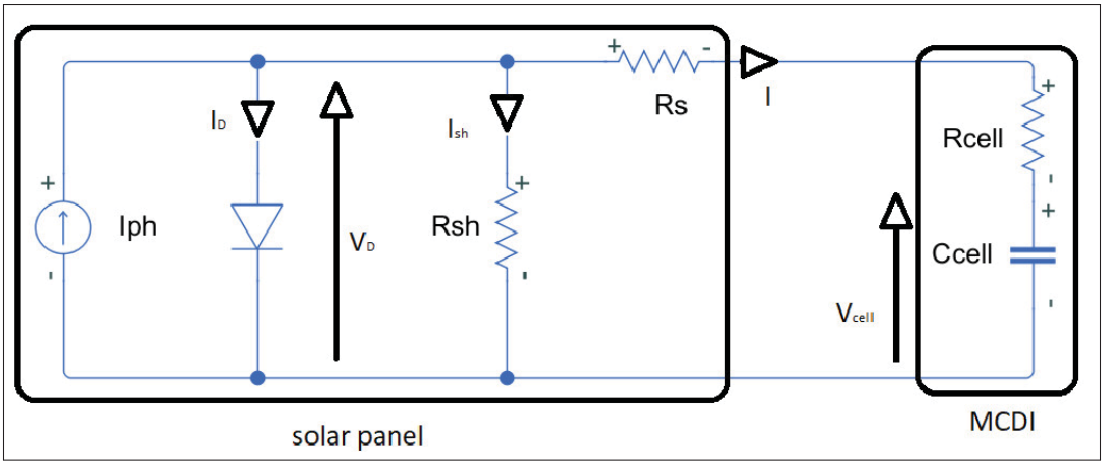

Figure 5.2 Schematic model

Considering that Rsh≫ (Rs+Rcell) which means that Ish≪ I and applying kirchhoff's current and voltage laws to the above circuit , we will have the following equations:

$$I_D + I = I_{ph} \tag{5.1}$$

$$(R_S + R_{cell})I + V_{cell} = V_D \tag{5.2}$$

where I_{ph} is the photogenerated current source, I_0 is the reverse saturation current, I_D is the diode current, I is the charging MCDI cell current,V_D is the diode voltage, R_S is the panel serial resistance, R_{cell} is the MCDI cell serial resistance, C_{cell} is the equivalent capacitance of the MCDI cell. So we obtain the following first order differential equations:

$$\frac{dI_D}{dt} + \frac{dI}{dt} = \frac{dI_{ph}}{dt} \tag{5.3}$$

$$(R_S + R_{cell}).\frac{dI}{dt} + \frac{dV_{cell}}{dt} = \frac{dV_D}{dt} \tag{5.4}$$

As for the diode characteristic, the current can be written as :

$$I_D = I_0.(e^{\frac{V_D}{A.V_T}} - 1) \tag{5.5}$$

As the voltage can be presented :

$$V_D = V_T.ln(\frac{I_D + I_0}{I_0}) \tag{5.6}$$

As for the MCDI cell, the voltage is mainly maintained by the capacitor component of the MCDI model :

$$\frac{dV_{cell}}{dt} = \frac{I}{C_{cell}} \tag{5.7}$$

As for the Diode, using equation 5.1 in 5.6, the voltage will be :

$$V_D = V_T.ln(\frac{I_{ph} - I + I_0}{I_0}) \tag{5.8}$$

Deriving equation 5.8 will give :

$$\frac{dV_D}{dt} = -V_T.\frac{\frac{dI}{dt}}{I_{ph} - I + I_0} \tag{5.9}$$

$$(R_S + R_{cell} + \frac{V_T}{I_{ph} - I + I_0})\frac{dI}{dt} + \frac{I}{C_{cell}} = 0 \tag{5.10}$$

$$(R_S + R_{cell})\frac{dI}{dt} + \frac{V_T}{I_{ph} - I + I_0}\frac{dI}{dt} + \frac{I}{C_{cell}} = 0 \tag{5.11}$$

In order to obtain the current expression, let us integrate the equation 5.11:

$$\int C_{cell}.(R_S + R_{cell})\frac{dI}{I} + \int \frac{C_{cell}.V_T}{I_{ph} - I + I_0}\frac{dI}{I} + \int dt = K \tag{5.12}$$

$$\begin{aligned} &C_{cell}.(R_S + R_{cell})lnI + \frac{C_{cell}.V_T}{I_{ph} + I_0}lnI \\ &-\frac{C_{cell}.V_T}{I_{ph} + I_0}ln(I_{ph} - I + I_0) + t = K \end{aligned} \tag{5.13}$$

As the MCDI cell resistor R_{cell} and the serial resistor R_S are so small to affect the current of charging the cell , so they will be neglected in the calculation . The value of K is obtained from the initial conditions defined as $I_{t=0} = I_{ph}$, so the I(t) will be written as :

$$I_{cell}(t) = I = \frac{I_{ph} + I_0}{1 + \frac{I_0}{I_{ph}}.e^{t.\frac{I_{ph}+I_0}{C_{cell}.V_T}}} \tag{5.14}$$

and the voltage of the MCDI cell can be written as :

$$V_{cell}(t) = V_T ln(\frac{I_{ph} + I_0}{I_0}.(1 - \frac{I_{ph}}{I_{ph} + I_0.e^{t.\frac{I_{ph}+I_0}{C_{cell}.V_T}}})) \tag{5.15}$$

5.2.2 MCDI Cell capacitance

As shown in equations 5.14 and 5.17, the solar operating point depends on the MCDI capacitance, so it is obvious that a successful control to this capacitance will lead to an optimized energy for the cell operation. So let's first define the main parameters in MCDI operation.

5.2.2.1 Flow and concentration

The approximate expression for the ionic interaction, and the polarization of the ion was developed by Poisson-Boltzmann differential equation for the electric double layer, research

has proven that the Gouy-Chapman model of the double layer electrode is the most suitable for explaining the double layer phenomena that the CDI cells rely on (CH *et al.*, 2012; JC *et al.*, 1996) and especially the MCDI ones(Biesheuvel & der Wal, 2010). Therefore the given model of Gouy-Chapman doesn't give the capacitance figure where the electrolyte is in motion.The movement of the particles and the ions inside the electrolyte solution will complicate the identification of the capacitance reaction of the electrodes inside the MCDI cell(Jeon *et al.*, 2013).Variation of the output concentration is directly related to the water flow passing across the MCDI cell(Zhao *et al.*, 2012a) as:

$$V.\frac{dC}{dt} = F.(C_{in} - C) - \phi_{salt} \tag{5.16}$$

Where F (ml/s) is the volumetric water flow rate through the cell, C_{in} (mM) is the water concentration of the influent, V (ml) is the actual volume of the cell and ϕ_{salt} (mmol/s) is the amount of ions removed per time unit from the solution during the adsorption period. Under the same operating conditions , increasing the water flow rate will result on increasing the outlet concentration. It is due to electrode retaining ions capacity for a given applied charging current. It is also noticeable that the cell desalination/adsorption period will be longer with a lower water flow, since the MCDI electrode is not yet saturated with the ions due to the limit amount of ions in the effluent. It will take more time to achieve the voltage charged level on the cell terminal.

Figure 5.3 shows the impact of the water flow rate through the MCDI cell. The figure shows the voltage variation on the cell terminal working under the same operating condition as the source voltage and input concentration. It shows clearly that the cell voltage is closely related to the flow rate in the adsorption period: as the flow increase the voltage charging slope increase,controversially for the desorption phase, the flow rate has no noticeable effect on the discharging voltage.

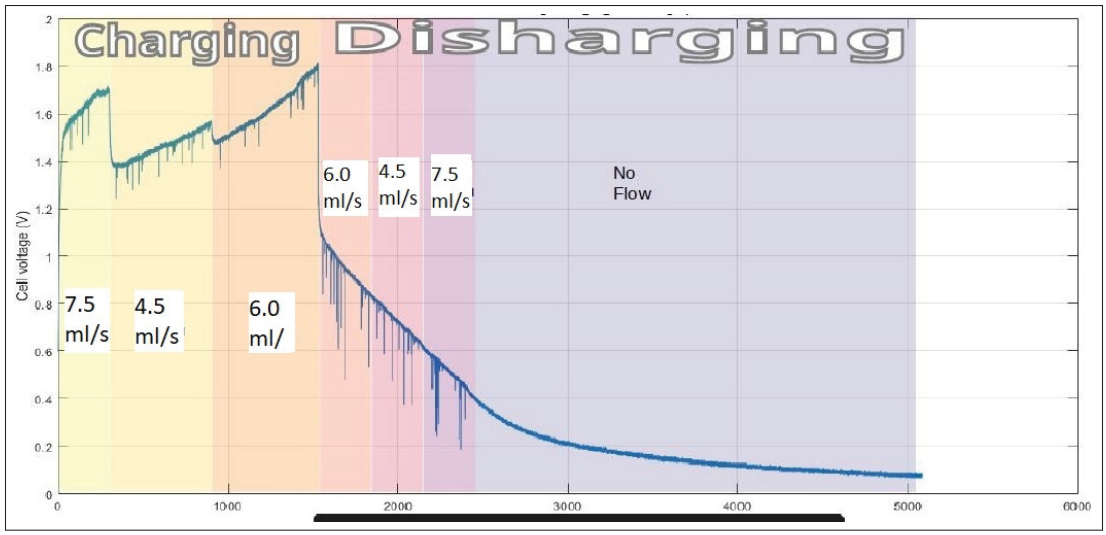

Figure 5.3 MCDI voltage variation based on water flow rate

5.2.2.2 Adapting and controling the flow

In order to maintain a fixed output product concentration, for a variable applied voltage on the MCDI cell, the flow is controlled accordingly. The aim is to monitor the cell reaction and to conclude about the relation between the flow and the voltage of the cell. Table 5.1 shows the adapted flow rate of different voltage to maintain the same average output of 300PPM as the cell working under the same operating conditions of input concentration and temperature. The voltage application is closely related to the passing effluent of the MCDI cell. So as the

Table 5.1 Adapted water Flow variation
for different voltage applications

Applied Flow (mL/s)	Applied voltage (V)	Average output concentration (PPM)
9.0	5.0	300.9
7.5	4.2	302.7
6.0	3.4	301.4
4.5	2.2	294.4
3.0	1.75	298.6

voltage/current increase, the electrodes are able to retain more ions and so a higher flow rate will bring more ions in between and stabilize the output concentration.

5.2.2.3 Water flow and cell capacitance

Since the electrical charging curve is affected by the flow variation, the electrical capacitance of the cell will be closely related. The capacitance is an important characteristic that describes the electrical behavior of the cell as well as for electrical load estimation. The capacitance is calculated based on the slope as described by Álvarez González *et al.* (2016) as :

$$Cap = \frac{I}{tan(\alpha)} \tag{5.17}$$

Where I is the charging current and α is the slope of the voltage. Figure 5.4 shows the variation of the capacitance of the cell based on the flow rate. That inversely proportional relation between the flow and the capacitance is due to the time that takes the cell to saturate their electrodes during different flow applications.

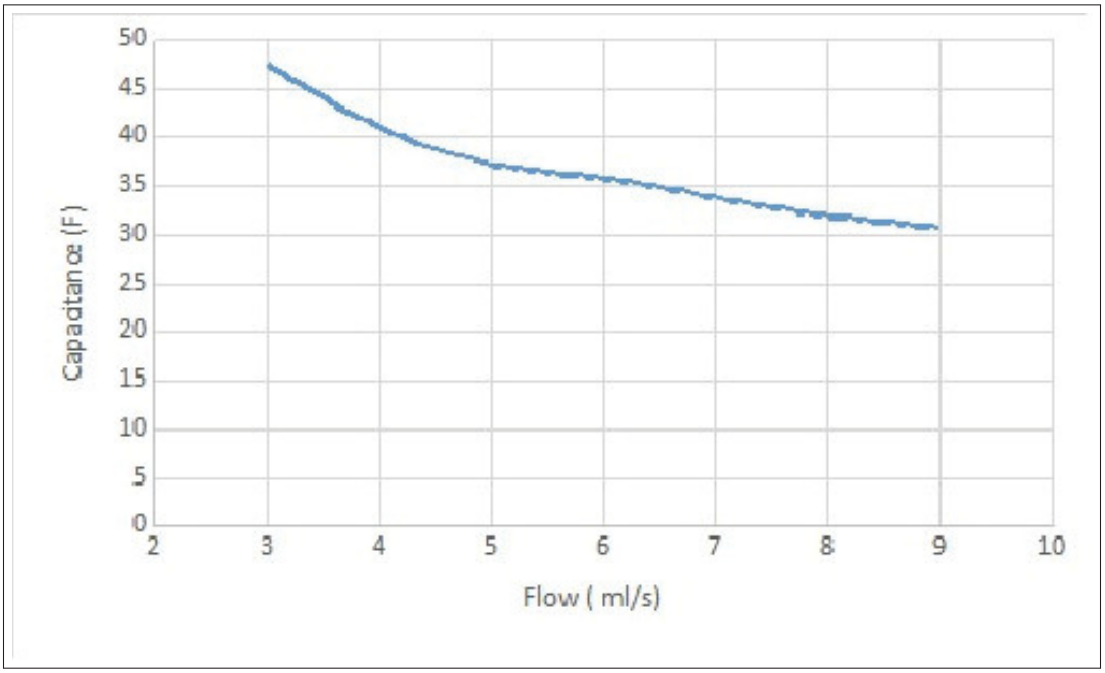

Figure 5.4 MCDI voltage variation based on water flow rate

Note that at the end of the desalination phase, the amount of salt removed by the solution will be the same for each flow rate since the quantity of adsorption is related to the electrode capacity on ions and not to the applied flow rate.

5.2.3 MSAT Algorithm

Among all the used technique in solar power tracking, the perturb and observe (Kim *et al.*, 2001; Husain *et al.*, 2017; Kobayashi *et al.*, 2003) was chosen for its popularity, practicality and simplicity in application. Standard P&O algorithm is based on voltage perturbation of the PV panel: thank to a DC-DC converter, perturbing the duty ratio of the power converter perturbs the PV panel current and consequently perturbs the PV panel voltage. Since the electrical parameters, especially the capacitance of the MCDI, are affected by the flow rate crossing the membrane as proved in paragraph 2.2, and since the solar charging current and voltage are affected by the load applied on the PV panel, varying the load capacitance will result on changing the electrical operating point (voltage and current) of the PV panel. Conversely to the voltage perturbation, MSAT algorithm is introduced based on the perturbation in the flow rate of the MCDI cell feed by the PV panel. The algorithm will monitor the variation of the two parameters : the output concentration and the consumed power as shown in Table 5.2. Controling the flow rate will adjust the capacitance of the cell and consequently the impedance load on PV panels. The load variation will result voltage and current variation, and so the power. Finally,the flow is controlled based on the panel power operating point in order to shift it toward its maximum power operation. Therefore, if there is an increase in power, the subsequent perturbation should be kept the same to reach the MPP and if there is a decrease in power, the perturbation should be reversed. This algorithm is summarized in Table 5.2 and it should be applied as the output concentration is not affected. If the output concentration is decreasing, the system will continue operating on the flow to optimize the produced power from the PV panel. As soon as the output effluent concentration will increase, the controller will try to maintain it by decreasing the flow and increasing the capacitance so decreasing the load on the solar panel. The process is repeated periodically until the MPP is reached. The system then oscillates around the MPP. The

oscillation can be minimized by reducing the perturbation flow step size. However, a smaller perturbation size slows down the MSAT. Therefore a variable step method will be investigated in a future study.

Table 5.2 Variable Flow and voltage

Flow perturbation	Change of Output Concentration	Power Change	Next Flow perturbation
positive	negative	positive	positive
positive	negative	negative	negative
negative	negative	positive	negative
negative	negative	negative	positive
positive	positive	—	negative
negative	positive	—	negative

The flowchart of the MSAT is shown in Figure 5.1.

5.2.4 Operation process

As the algorithm of the photo-MCDI flow control is defined, the system operation needs to be identified in order to optimize the cell production during the sun lighted day. As the adsorption phase period is slightly longer than the desorption phase, it is considered that both phases will take the same time, and equal period of adsorption/desorption is adopted in the operation design.

Figure5.5 shows the different phases of the photo-MCDI operation, starting with the initial phase when the first cell starts the desalination. The second phase will take place when the MCDI Cell#1 is fully charged which allows Cell#2 to go in the adsorption mode while the MCDI Cell#1 is in desorption mode. Upon the end of the adsorption of Cell#2 marked by the full charge of the cell, the cycle will take over and starts with the adsorption of the MCDI Cell#1.

Algorithm 5.1 MSAT control Flowchart

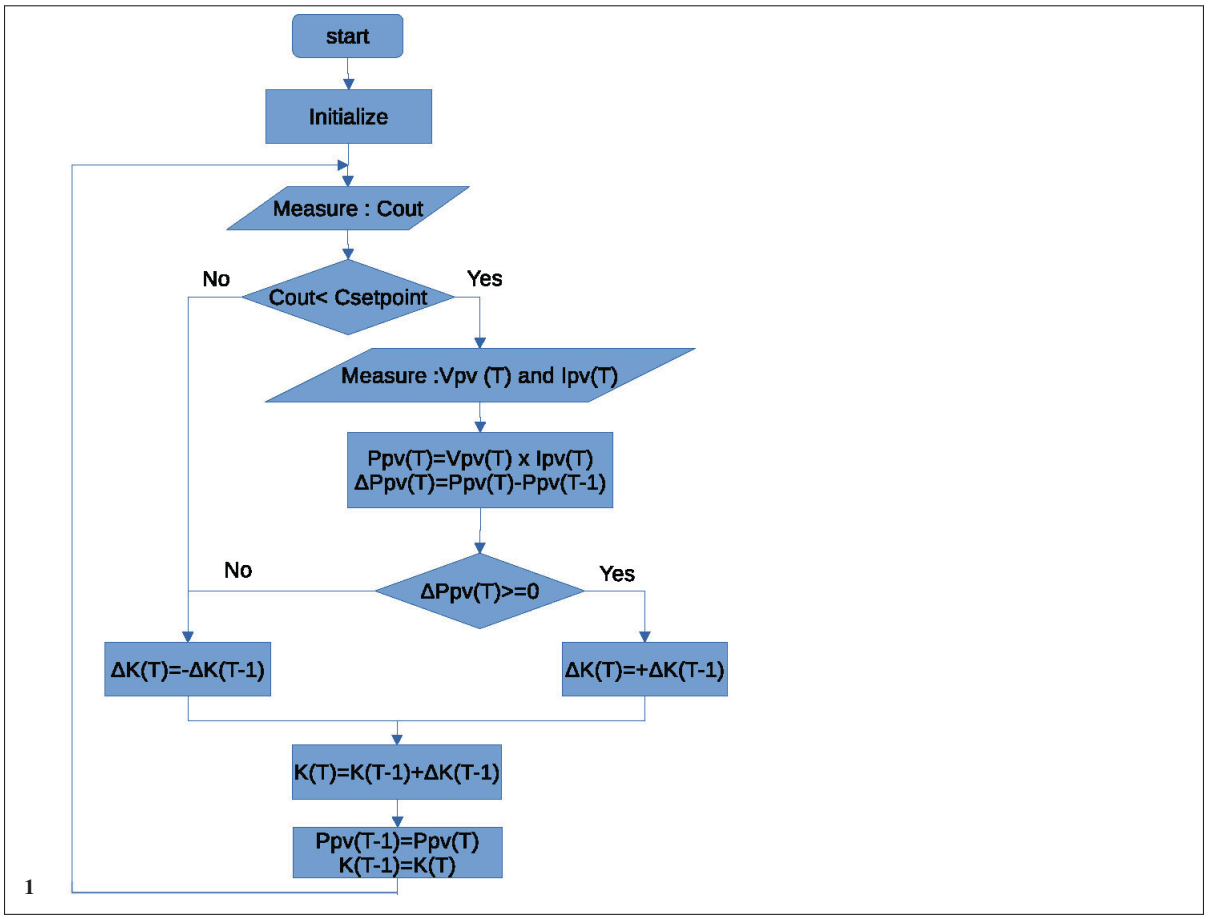

5.3 Experimental setup

5.3.1 Hardware

The test bench (Figure 5.1) is based on two MCDI to maintain a continuous operation of the Photo-MCDI. The used MCDI cells are originally the ESD400 model from Enpar company, known as current water technologies[b]. With 4-pole connection, two for the positive termination and two for the negative one, the terminals are connected to carbon electrodes separated with several membranes layers.The use of the two cells is explained in section 5.2.4. The test bench includes, in addition to the electrical connection, a process setup: the influent tank is connected to a peristaltic pump feeding the two MCDI units through two adjustable valves (Figure 5.1) .

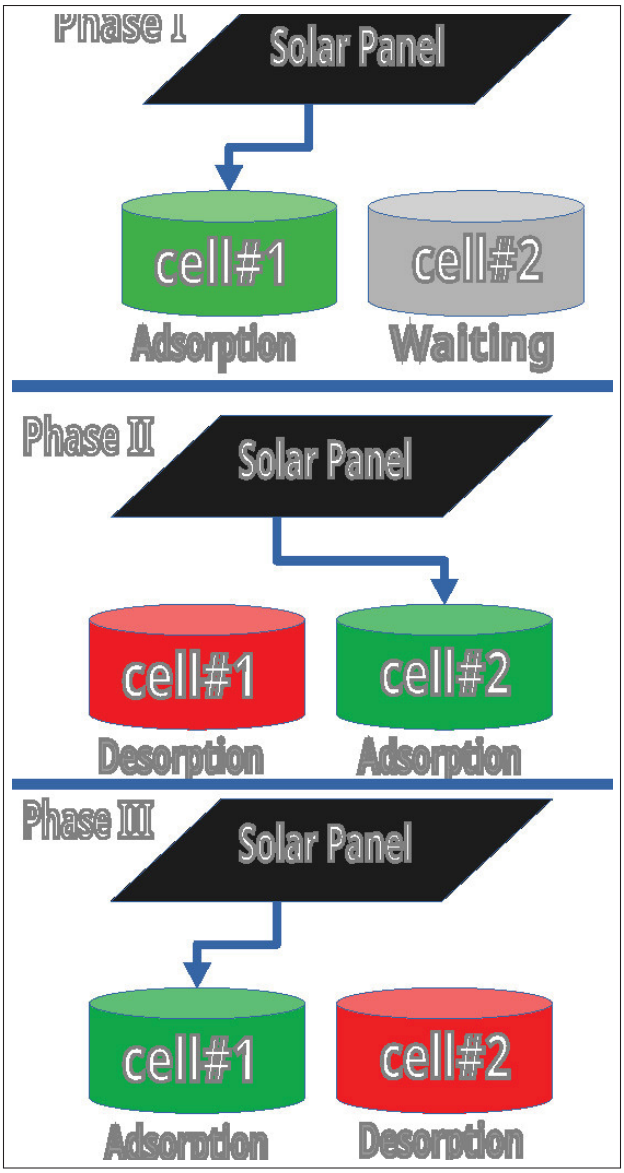

Figure 5.5 Photo-MCDI operation process

Valve 1 is connected to MCDI cell#1, and valve 2 to the second cell. Both cells will push their product into an effluent tank equipped with a conductivity measurement probe connected to the system controller. The peristaltic pump is equipped with a DC motor controlled by the voltage variation through the controller(figure 5.6).

A closed loop configuration is programmed in the controller to adjust the speed of the pump and consequently the passing flow rate across the MCDI cell. Figure 5.7 shows the closed-loop

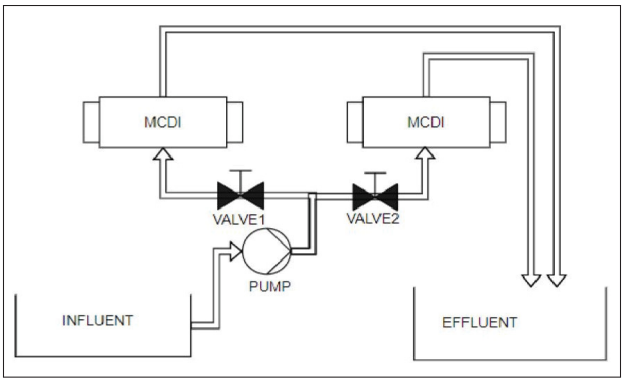

Figure 5.6 Flow control Schematic

controlled application on the MCDI Cell. The applied flow rate crossing the cell is adjusted constantly by the system controller. The controller will take the error calculated by the difference between the setpoint and the actual effluent output. This error will be then used to adapt the operational condition to ensure a constant output concentration. If the error is negative, the controller tries to decrease the flow rate and if it is positive it will try to increase the applied voltage to the cell.

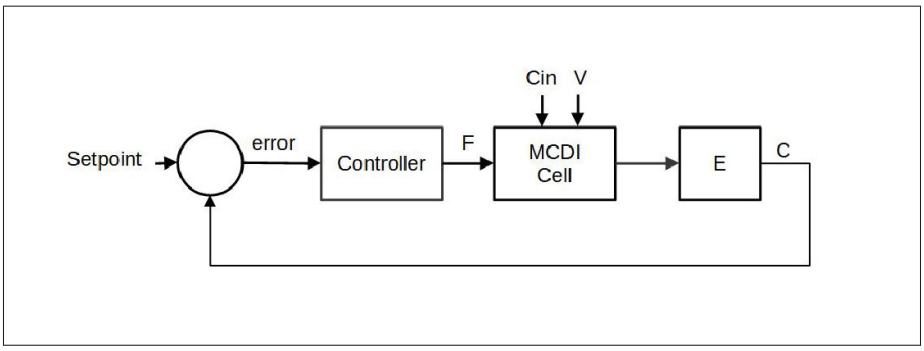

Figure 5.7 MCDI cell flow control diagram

Figure 5.8 shows the electrical connection of the photo-MCDI. The cell is connected to the solar PV panel through a resistor R of 1 ohm. An electromechanical relay was installed on each cell. If the relay CR1 is energized, the solar power will be applied on the terminal of the cell#1 and it will go in the adsorption phase. Once the CR1 is de-energized, a short -circuit is applied on the cell terminal, and the cell go in the desorption/cleaning mode. The same functionality is

foreseen for cell#2 through the contact of the relay CR2. Finally, the system will interlock the switching between the two relays in order to be sure that only one MCDI is in adsorption phase and the other one in desorption phase.

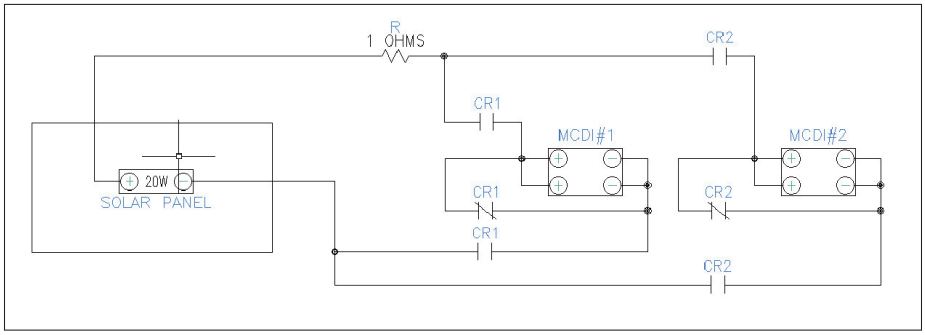

Figure 5.8 Electrical testing bench connection

5.4 Results and discussions

All the following studies were conducted at a fix influent concentration of 100PPM and a temperature of 12 °C.

5.4.1 Model validation

In order to validate the model of the solar current and the MCDI cell voltage, a simple PV panel is mounted on a MCDI cell. The assembly is operated under the same condition of temperature, water concentration and solar irradiance. Equilibrium adsorption and desorption experiments of MCDI were first conducted after on different water flow rate. Each experiment was able to determine the equivalent capacitance of the MCDI cell. Figure 4.1 shows the experimental PV generated current and the cell voltage at a fix flow rate of 9ml/s. They were used to determine the value of the cell capacitance at this operating point. The calculated value was after that included in equation 5.14 to simulate the current and in equation 5.17 to draw the voltage behavior. Both curves are also presented in Figure 5.9. The figure confirms the similarity between the experimental and the simulated behaviors of the voltage and the current as well.

Noises that are noticed on signals are due to the high sensitivity of the electrical measurement equipment. A low-pass filter is not used in order to avoid its effect on the response time.

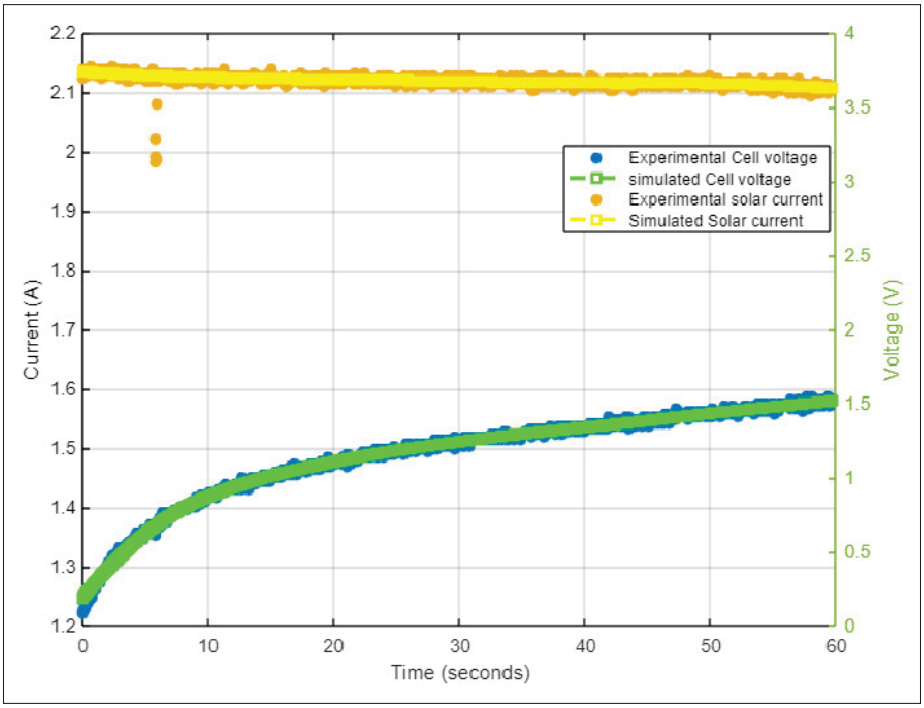

Figure 5.9 Model Validation Results

5.4.2 Power Tracking through flow control

Figure 5.10 shows the evolution of the photo-MCDI cell voltage, the charging current and the solar voltage applied following 7.5ml/s of water flow during the charge and the discharging phase. Figure 5.11 shows the same photo-MCDI with the same solar irradiance with the application of a higher passing flow rate of 9.0ml/s. The output concentration is maintained to the same level in both applications as shown in Figure 5.12. It is obvious that increasing the flow into the Photo-MCDI using the MSAT algorithm required more energy from the PV panel to maintain the same concentration output. When the amount of ions introduced by high flow exceeds the power generated by PV panel, the concentration of the output starts to increase due to a shortage on retaining current. The variation of the voltage for different flow rate is explained by the variation of applied charge and especially the cell capacitance as shown in Table 5.1.

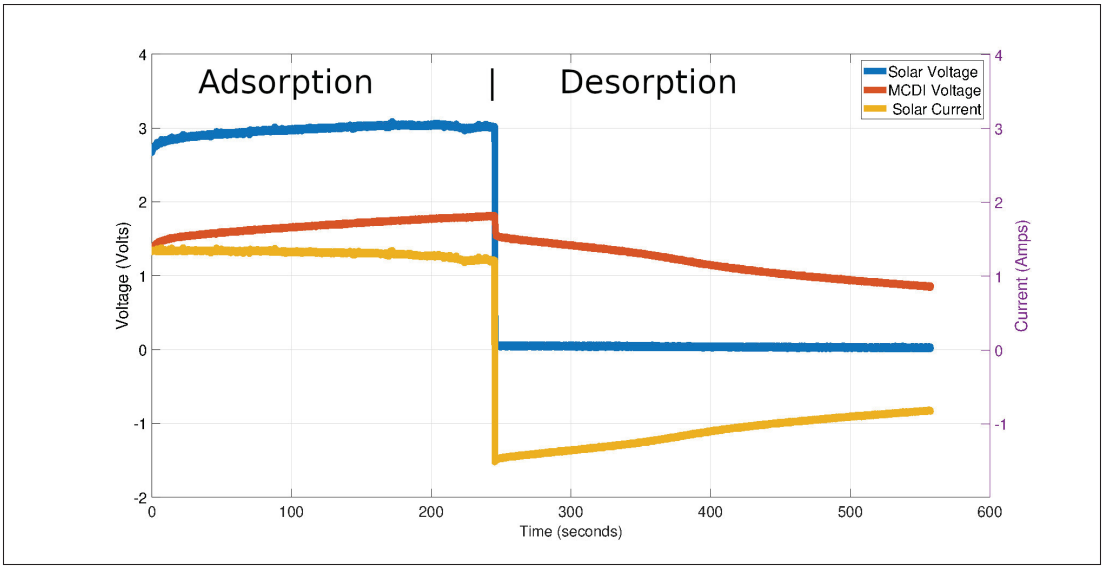

Figure 5.10 PHOTO-MCDI at 7.5 ml/s flow

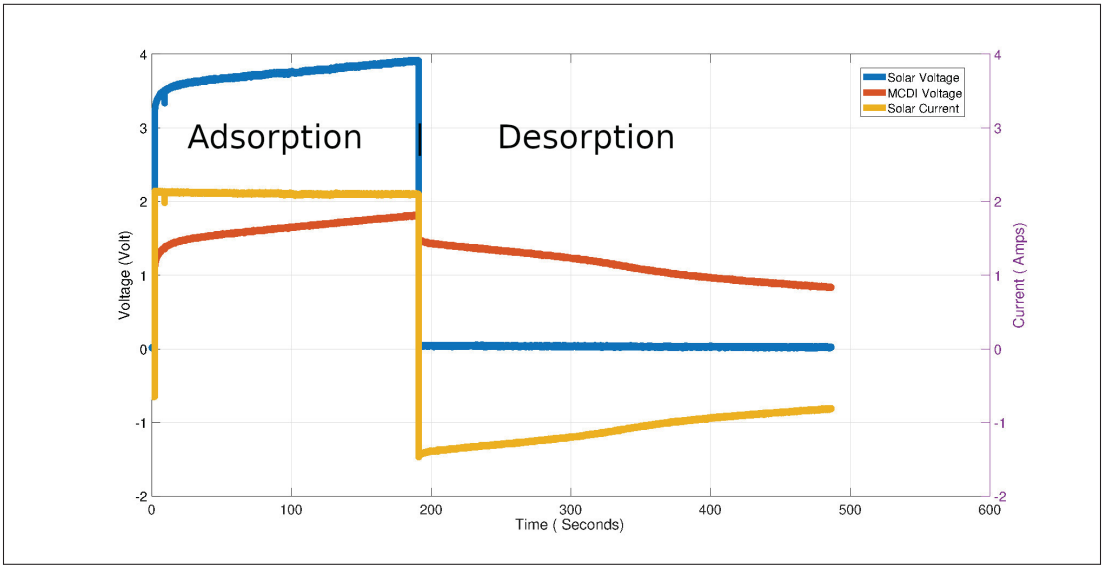

Figure 5.11 PHOTO-MCDI at 9.0 ml/s flow

Furthermore, Figure 5.13 shows an average irradiance profile during a typical summer day. The MSAT controling the MCDI presents an adapted and similar profile for the flow rate passing through the cell. Hence, as a result, the generated power profile shows an optimal profile based on the PV panel performance for the variable applied load. Therefore, it is obvious that when

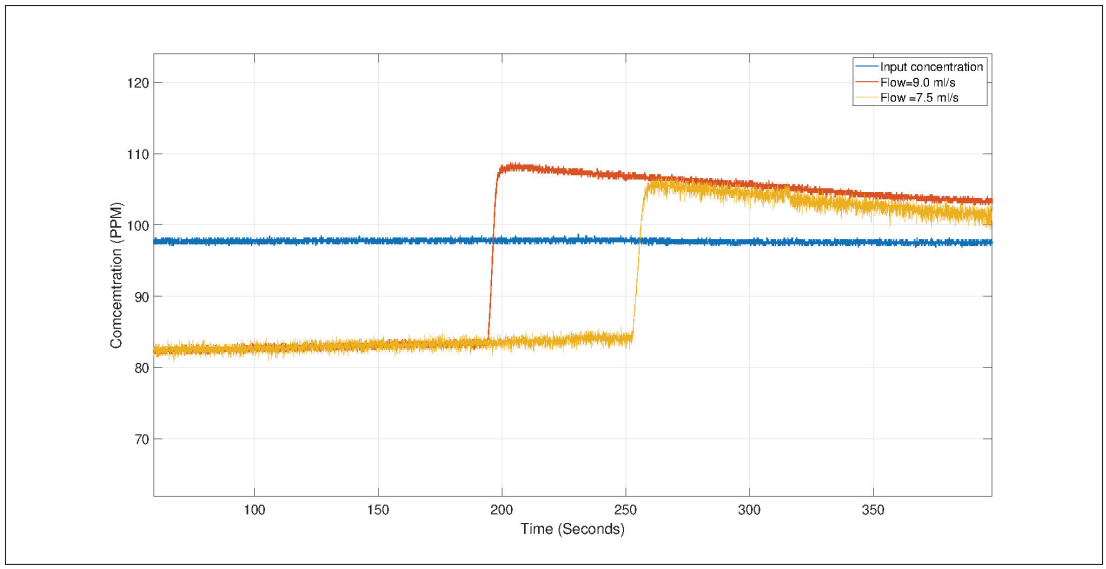

Figure 5.12 Output concentration for different flow rate application

the irradiance reaches its maximum, the MSAT applies the highest flow extracting the maximum power from the PV panel, and purifying maximum water during the day.

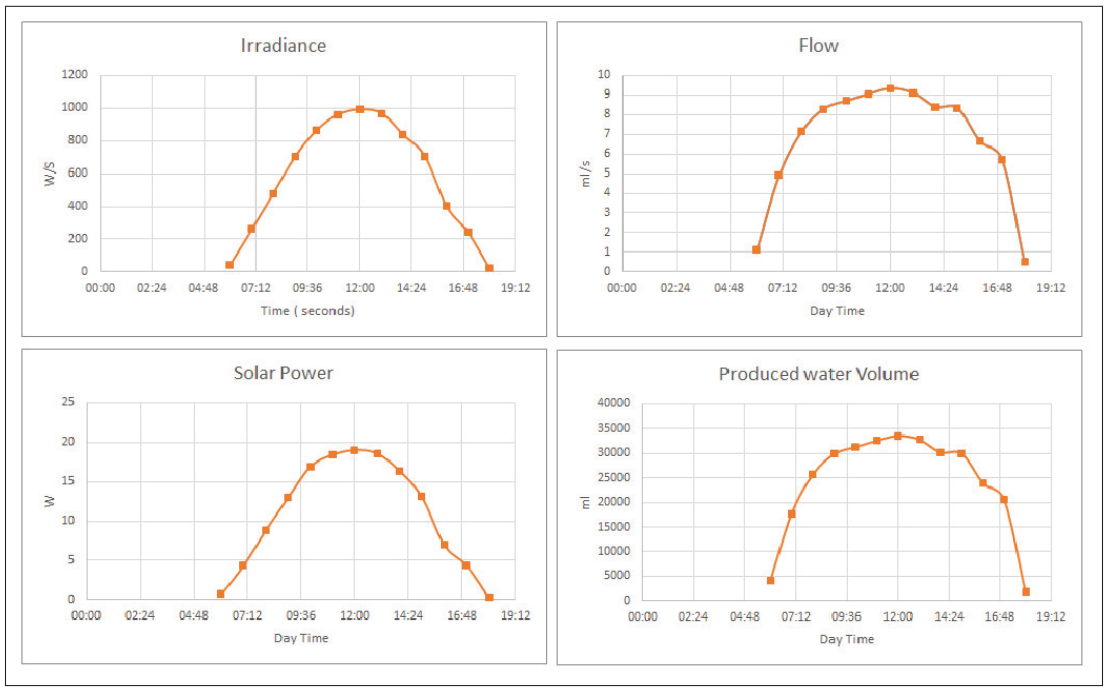

Figure 5.13 Water quantity during a typical summer day

5.4.3 Comparison with conventional plant:

Tan *et al.* (2018) in their paper on the integration of PV panels with the MCDI were among the first approaches of such integration. However, their approach is based on a conventional solar application using a buffer battery . As they identify the capacity of water production, the quantity of removed ions is determined and consequently the applied charge needed for the system. That load will allow to calculate the needed battery system and the adequate PV panel to be installed on the system.

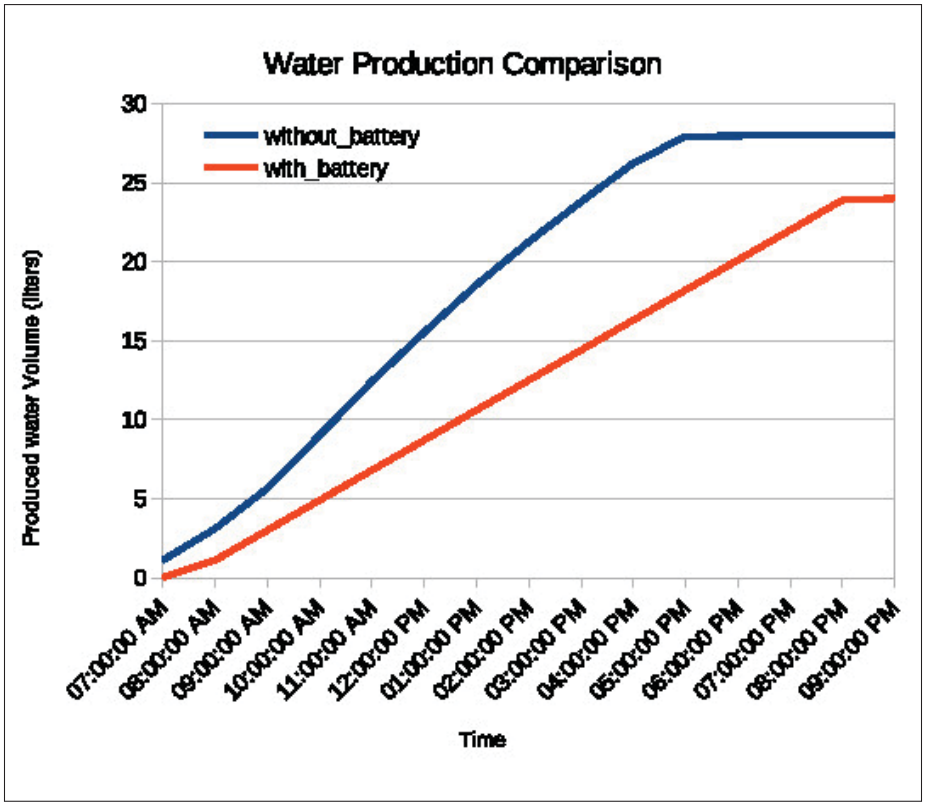

Figure 5.14 Solar conventional MCDI vs Photo-MCDI operation

Figure 5.14 shows a comparison between the conventional solar PV panel application on the MCDI and the new proposed Photo-MCDI based on MSAT algorithm. Many advantages of the Photo-MCDI can be deducted as follows :

- **Easier design and modular application:** The concept of the photo-MCDI is based on the individual cell operation and not the full plant scale. So designing such system will not require a different aspect of the solar, electrical and process expertise. Since each photo-MCDI will have its own control, designer can structure them in the final product and capacity required.
- **Low maintenance and simple operation:** Less equipment in the production line means simpler operation and lower maintenance cost due to less possibility of failure. Batteries, DC-DC converters are removed from the production line, so the operator will not be affected by their maintenance and troubleshooting.
- **Operation conditions fluctuation:** As the conventional system is built based on the number of ions to be retained inside the cell by the end of the day. Any fluctuation in operating conditions will cause a fluctuation in the quality of the produced water. Photo-MCDI is based on two major feedbacks, the power of the solar system and the output concentration. As far as the concentration input will increase, the feedback from the output concentration will be higher and the control will try to limit and decrease the water flow passing across the cell. As a result, the Photo-MCDI will maintain the design output concentration based on the operation conditions and the solar irradiance as well.
- **Energy losses:** In comparison between the conventional MPPT and the MSAT controllers, the conventional ones require the installation of energy storage system, which yields more energy losses during the charging, storage and discharging phase. Figure 5.15 shows a comparison of the losses between the conventional and the photo-MCDI. It summarizes the different aspects of these losses. It is obvious that reducing the components between the solar panel production and the consumption (MCDI) will increase the system operational efficiency.

5.4.4 MSAT limitation

Table 5.3 shows the efficiency of the controllers based on the power generated by the PV panel on the terminals of the PV

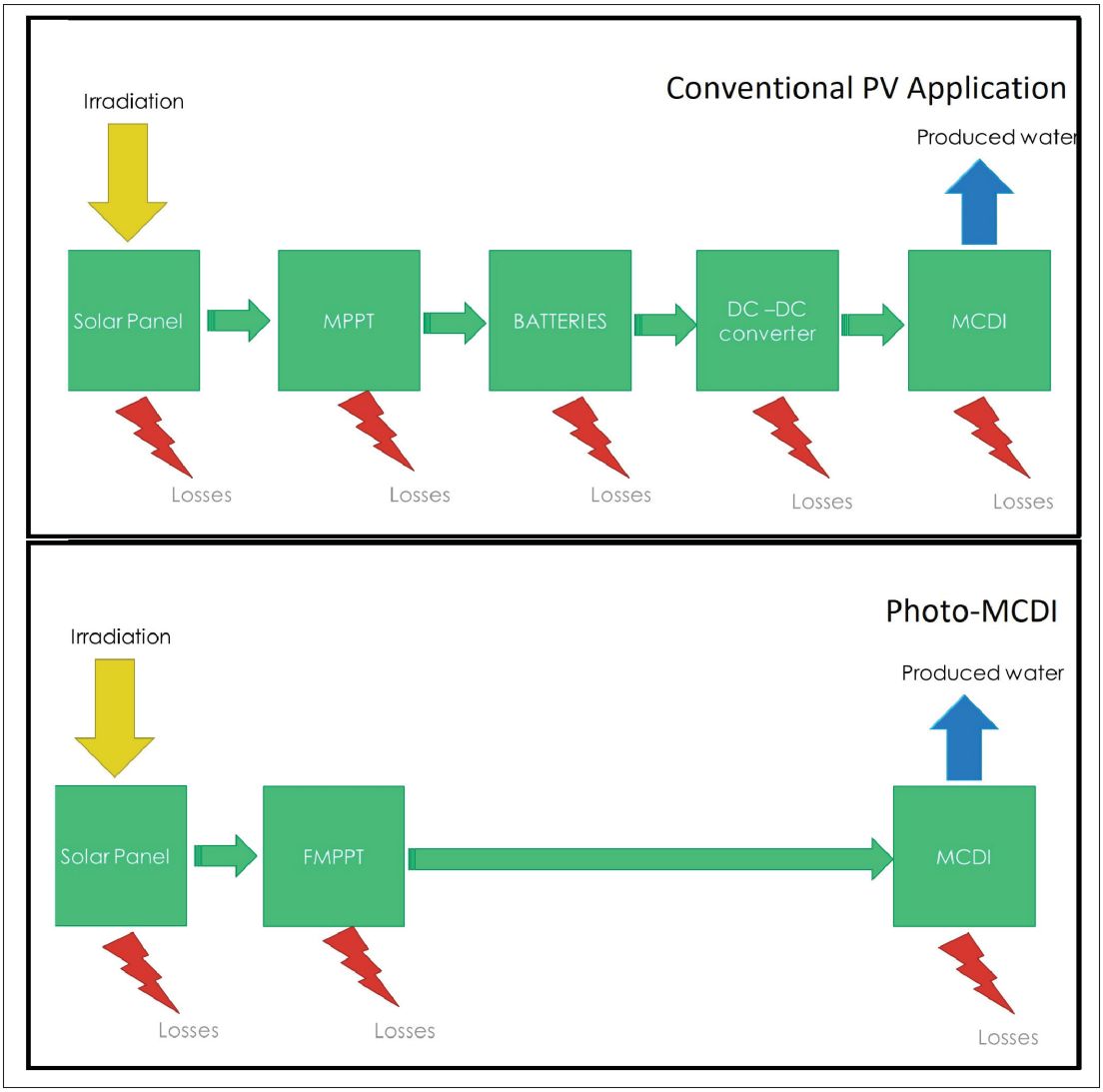

Figure 5.15 Losses comparison between conventional and photo-MCDI

Although the cited advantages of the MSAT in water desalination and salt removal, the conventional MPPT shows a superlative efficiency when it comes to the generated power from the PV. The lost varies from 1% to 3% which is negligible compared to the retained advantages of the MSAT. Many factors impact this lost , as the maturity of the conventional algorithms, the electrical application of the conventional compared to the electro-chemical aspect of the MSAT, and finally the time response of the pump and the flow inside the cell.

Table 5.3 Controllers effciency comparison

Power (W)	Conventional MPPT	MSAT
20	99.8%	98.6%
18	99.44%	97.4%
15	98.5%	96.98%
10	95.8%	92.64%
5	89.3%	87.79%

5.4.5 Economic Considerations

The ultimate target of this study is to propose an optimized solution for water desalination to balance the trade-off between performance and cost. It is of interest to discuss and compare the system cost and energy with its counterparts. The flow perturbation method is proposed for saving system cost, especially considering the price of the batteries, the DC-DC converters, which requires much more maintenance as well. The MSAT controller can be realized using a low controller. However, the major drawback of the conventional method is that they were not oriented to desalination solution. This is where our MSAT comes in to solve this problem by customized design mainly for the desalination systems based on Capacitance Deionization. Besides, they also require more costly MPPT controllers for a high performance. The battery cost for each CDI cell is about 200 dollars as for 200AH battery. To that cost, it should be considered the cost of the controller which is approximately around 10 dollars; and the MPPT micro-controller cost more than 20 dollars. Table 5.3 shows using low-cost controller reports that the MSAT tracking efficiency is 98.6%, which is comparable with the conventional MPPT.

5.5 Conclusions

A new technique called MSAT has been proposed for maximum power use for water desalination. The system used a controlled flow approach to supply water to the capacitance deionization cells in order to adapt the load to the solar irradiance and the produced power of the PV panels. The paper also proposed a simplified algorithm based on direct flow controller which eliminated

the requirement of energy storage and complex tracking circuits. An experimental prototype is developed to verify the operation of the system. Without considering the maintenance cost of the conventional system installation and the troubleshooting expenses, the photo-MCDI was able to produce more desalinated water volume (about 28 liters in a sunny summer day) than the conventional solar MCDI application (about 24 liters in a sunny summer day) with a reduced energy footprint. This leads to the advantage of increasing the water desalination production volume for the same solar irradiance received on the solar panel.

Conflicts of interest

There are no conflicts to declare.

Acknowledgements

This work was supported by Current Water technologies[b], Research center.

[0] [b] *70 Southgate Drive, Unit 4, Guelph, ON, Canada, N1G 4P5 https://www.currentwatertechnologies.com/.*

BIBLIOGRAPHY

Abarca, A., Gómez-Sal, P., Martín, A., Mena, M., Poblet, J. M. & Yélamos, C. (2000). Ammonolysis of mono(pentamethylcyclopentadienyl) titanium(IV) derivatives. *Inorg. Chem.*, 39(4), 642–651.

Alkuran, M. & Orabi, M. (2008). Utilization of a buck boost converter and the method of segmented capacitors in a CDI water purification system. *2008 12th International Middle-East Power System Conference*, 470-474.

Anderson, J. (1994). The Debye-Falkenhagen effectexperimental fact or friction? *Journal of Non-Crystalline Solids*, 1190–1194.

Andres, G. L., Mizugami, T. & Yoshihara, Y. (2008). Simulation of an electric behavior of the MCDI system. *Elsevier*, 011, 9164/2017.

Avraham, E., Bouhadana, Y., Soffer, A. & Aurbach, D. (2009). Limitations of Charge Efficiency in Capacitive Deionization: II. On the Behavior of CDI Cells Comprising Two Activated Carbon Electrodes. *J. Electrochem. Soc.*, (156), 95-99.

Avraham, E., Noked, M., Cohen, I., Soffer, A. & Aurbach, D. (2011a). Enhanced Charge Efficiency in Capacitive Deionization Achieved by Surface-Treated Electrodes and by Means of a Third Electrode. *J. Electrochem. Soc.*, (158), 168-173.

Avraham, E., Noked, M., Soffer, A. & Aurbach, D. (2011b). The feasibility of boron removal from water by capacitive deionization. *Electrochim. Acta*, (56), 6312–6317.

Badescu, V. (2006). Single Optimization Procedure for Silicon-Based Solar Cell Interconnection in a Series-Parallel PV Module. *Energy Conversion and Management*, 47(9), 1146 - 1158.

Bai, Y., Huang, Z.-H., Yu, X.-L. & Kang, F. (2014). Graphene oxide-embedded porous carbon nanofiber webs by electrospinning for capacitive deionization. *Colloids Surf.*, (444), 153–158.

Barrade, P. (2002). Series connection of supercapacitors : Comparative study of solutions for the active equalization of the voltages. *Proceedings of 7th International Conference on Modeling and Simulation of Electric Machines, Converters and Systems*, 4–5.

BH, P., YJ, K., JS, P. & J., C. (2011). Capacitive deionization using a carbon electrode prepared with water-soluble poly(vinyl alcohol) binder. *J Ind Eng Chem*, 17, 717-22.

Bian, Y., Liang, P., Yang, X., Jiang, Y., Zhang, C. & Huang, X. (2016). Using activated carbon fiber separators to enhance the desalination rate of membrane capacitive deionization. *Desalination*, 381(1-3), 95–96.

Biesheuvel, P. & der Wal, A. V. (2010). Membrane capacitive deionization. *J. Membr. Sci.*, 346, 256–262.

Biesheuvel, P. M., van Limpt, B. & van der Wal, A. (2009). Dynamic Adsorption/Desorption Process Model for Capacitive Deionization. *The Journal of Physical Chemistry C*, 113(14), 5636-5640.

Biesheuvel, P. M., Fu, Y. & Bazant, M. Z. (2011a). Diffuse charge and Faradaic reactions in porous electrodes. *Phys. Rev. E*, 83, 061507.

Biesheuvel, P. M., Porada, S., Levi, M. & Bazant, M. Z. (2014). Attractive forces in microporous carbon electrodes for capacitive deionization. *J. Solid State Electrochem.*, (18), 1365–1376.

Biesheuvel, P., Zhao, R., Porada, S. & van der Wal, A. (2011b). Theory of membrane capacitive deionization including the effect of the electrode pore space. *Journal of Colloid and Interface Science*, 360(1), 239-248.

Biesheuvel, P., Y.Fu & M.Z.Bazant. (2012). Electrochemistry and capacitive charging of porous electrodes in asymmetric multicomponent electrolytes. *Russ. J. Electrochem*, 48(6), 580–592.

Blair, J. & Murphy, G. W. (1960a). Electrochemical demineralization of water with porous electrodes of large surface area. *Adv. Chem. Ser.*, (27), 206.

Blair, J. & Murphy, G. W. (1960b). Saline water conversion. *American Chemical Society*, (2), 206–223.

Bouhadana, Y., Avraham, E., Soffer, A. & Aurbach, D. (2010). Several basic and practical aspects related to electrochemical deionization of water. *IChE J.*, (56), 779–789.

Bouhadana, Y., Avraham, E., Noked, M., Ben-Tzion, M., Soffer, A. & Aurbach, D. (2011). Capacitive deionization of NaCl solutions at non-steady-state conditions: inversion functionality of the carbon electrodes. *J. Phys. Chem. C*, (115), 16567–16573.

Brunini, V. E., Chiang, Y.-M. & Carter, W. C. (2012). Modeling the hydrodynamic and electrochemical efficiency of semi-solid flow batteries. *Electrochim. Acta*, (69), 301-843.

Béguin, F., Presser, V., Balducci, A. & Frackowiak, E. (2014). Carbons and electrolytes for advanced supercapacitors. *Adv. Mater.*, (26), 2219-2251.

Camara, M. B., Gualous, H., Gustin, F., Berthon, A. & Dakyo, B. (2007). DC/DC converter design for supercapacitor and battery power management in hybrid vehicle applications—Polynomial control strategy. *IEEE Trans. Ind. Electron.*, 57(2), 587–597.

Ceraolo, M. (2000). New dynamical models of lead-acid batteries. *IEEE Transactions on Power Systems*, 15(4), 1184-1190.

CH, H., JF, H., HK, L. & BY., W. (2012). Preparation of activated carbon sheet electrode assisted electrosorption process. *J Taiwan Inst Chem Eng*, 43, 473-9.

Chen, L., Yin, X., Zhu, L. & Qiu, Y. (2018). Energy recovery and electrode regeneration under different charge/discharge conditions in membrane capacitive deionization. *Desalination*, 439, 93-101.

Chen, Y., Peng, L., Zeng, Q., Yang, Y., Lei, M., Song, H., Chai, L. & Gu, J. (2014). Removal of trace As (V) from water with the titanium dioxide/ACF composite electrode. *Clean Technol. Environ. Policy*, (2), 1-9.

Chuang, Y.-C. & Ke, Y.-L. (2007). A novel high-efficiency battery charger with a buck zero-voltage-switching resonant converter. *IEEE Trans. Energy Convers.*, 22(4), 848–854.

Cohen, I., Avraham, E., Noked, M., Soffer, A. & Aurbach, D. (2011). Enhanced charge efficiency in capacitive deionization achieved by surface-treated electrodes and by means of a third electrode. *J. Phys. Chem. C*, (115), 19856-1863.

Curto, D., Franzitta, V. & Guercio, A. (2021). A Review of the Water Desalination Technologies. *Applied Sciences*, 11, 670.

Dlugolecki, P. & van der Wal, A. (2013). Energy recovery in membrane capacitive deionization. *Environ. Sci. Technol.*, (47), 4904–4910.

D'Souza, N., Lopes, L. & Liu, X. (2005). An Intelligent Maximum Power Point Tracker Using Peak Current Control. *2005 IEEE 36th Power Electronics Specialists Conference*, pp. 172-. doi: 10.1109/PESC.2005.1581620.

Duduta, M., Ho, B., Wood, V. C., Limthongkul, P., Brunini, V. E., Carter, W. C. & Chiang, Y.-M. (2011). Flow Batteries: Semi-Solid Lithium Rechargeable Flow Battery (Adv. Energy Mater. 4/2011). *Adv. Energy Mater.*, (1), 511-516.

Dykstra, J., R.Zhao, P.M.Biesheuve & der Wal, A. (2016). Resistance identification and rational process design in Capacitive Deionization. *Water Res*, 88(9), 358-370.

Dürr, M., Cruden, A., Gair, S. & McDonald, J. (2006). Dynamic model of a lead acid battery for use in a domestic fuel cell system. *Journal of Power Sources*, 161(2), 1400-1411.

E. Avraham, M. N., Bouhadana, Y., Soffer, A. & Aurbach, D. (2009). Capacitive Deionization of NaCl Solutions at Non-Steady-State Conditions: Inversion Functionality of the Carbon Electrodes. *J. Electrochem. Soc.*, (156), 157–162.

Elshafei, M. & seleym, A. (2017). New Energy Efficient Topology for solar powered capacitive Deionization systems.

Esram, T. & Chapman, P. L. (2007). Comparison of Photovoltaic Array Maximum Power Point Tracking Techniques. *IEEE Transactions on Energy Conversion*, 22(2), 439-449. doi: 10.1109/TEC.2006.874230.

Farmer, J. C., Fix, D. V., Mack, G. V., Pekala, R. W. & Poco, J. F. (1995a). Capacitive deionization of NH4ClO4 solutions with carbon aerogel electrodes. *Low Level Waste Conference and Orlando*, (16), 13.

Farmer, J. C., Fix, D. V., Mack, G. V., Poco, J. F., Nielsen, J. K., Pekala, R. W. & Richardson, J. H. (1995b). Capacitive deionization system. *Pacific Rim Environmental Conference and San Francisco*, (2), 125-127.

Farmer, J. C., Fix, D. V., Mack, G. V., Pekala, R. W. & Poco, J. F. (1996a). Capacitive deionization of NH4ClO4 solutions with carbon aerogel electrodes. *J. Electrochem. Soc.*, (143), 159-169.

Farmer, J. C., Fix, D. V., Mack, G. V., Pekala, R. W. & Poco, J. F. (1996b). Capacitive, deionization with carbon aerogel electrodes: Carbonate, sulfate, and phosphate. *J. Appl. Electrochem.*, (26), 1007-1018.

Farmer, J. C., Bahowick, S. M., Harrar, J. E., Fix, D. V., Martinelli, R. E., Vu, A. K. & Carroll, K. L. (1997). Electrosorption of chromium ions on carbon aerogel electrodes as a means of remediating ground water. *Energy Fuels*, (11), 337-347.

Femia, N., Petrone, G., Spagnuolo, G. & Vitelli, M. (2005). Optimization of perturb and observe maximum power point tracking method. *IEEE Transactions on Power Electronics*, 20(4), 963-973. doi: 10.1109/TPEL.2005.850975.

Feynman, R. & Vernon Jr., F. (1963). The theory of a general quantum system interacting with a linear dissipative system. *Annals of Physics*, 24, 118–173. doi: 10.1016/0003-4916(63)90068-X.

Firmanza, A. P., Habibi, M. N., Windarko, N. A. & Yanaratri, D. S. (2020). Differential Evolution-based MPPT with Dual Mutation for PV Array under Partial Shading Condition. *2020 10th Electrical Power, Electronics, Communications, Controls and Informatics Seminar (EECCIS)*, pp. 198-203.

Gabelich, C. J., Tran, T. D. & Suffet, I. H. M. (2002). Electrosorption of Inorganic Salts from Aqueous Solution Using Carbon Aerogels. *Environmental Science and Technology*, (36), 3010–3019.

Gao, X., Omosebi, A., Landon, J. & Liu, K. (2015). Surface charge enhanced carbon electrodes for stable and efficient capacitive deionization using inverted adsorption–desorption behavior. *Energy Environ.Sci.*, (8), 897–909.

Gao, Y., Li, H. B., Cheng, Z. J., Zhang, M. C., Zhang, Y. P., Zhang, Z. J., Cheng, Y. W., Pan, L. K. & Sun, Z. (2008). Electrosorption of cupric ions from solutions by carbon nanotubes and nanofibres film electrodes grown on graphite substrates. *Proc. IEEE Nanoelectron. Conf.*, 122–124.

Gasperi, M. (2005). Life Prediction Modeling of Bus Capacitors in AC Variable-Frequency Drives. *IEEE transactions on industry applications*, 41(6), 1430–1435.

Ghamrawi, A., Saad, M. & Mougharbel, I. (2022). Energetic capacitance of the membrane capacitive deionization cells. *Cleaner Energy Systems*, 2, 100012.

Gierst, L. (1966). Double layer and electrode kinetics. *J. Am. Chem. Soc.*, 88, 4768.

Golub, D., Oren, Y. & Soffer, A. (1987). Electro adsorption, the electrical double layer and their relation to dimensional changes of carbon electrodes. *Carbon*, 25(1), 109-117.

Grujicic, D. & Pesic, B. (2002). Electrodeposition of copper: the nucleation mechanisms. *Electrochim. Acta*, (47), 2901–2912.

H. Li, L. Z. (2011). Ion-exchange membrane capacitive deionization: a new strategy for brackish water desalination. *Desalination*, 275, 62–66.

Han, L., Karthikeyan, K., Anderson, M., Wouters, J. & Gregory, K. B. (2013). Mechanistic insights into the use of oxide nanoparticles coated asymmetric electrodes for capacitive deionization. *Electrochimica Acta*, 90, 573-581.

Hassanvand, A., Q.Chen, G., Webly, P. A. & Kentish, S. E. (2016). Improvement of MCDI operation and design through experiment and modeling : Regeneration with brine and optimum residence time. *Desalination*, 417, 36-51.

Hatzell, K. B., Iwama, E., Ferris, A., Daffos, B., K. Urita, T. T., Chauvet, F., Taberna, P.-L., Gogotsi, Y. & Simon, P. (2014). Capacitive deionization concept based on suspension electrodes without ion exchange membranes. *Electrochem. Commun*, (43), 18-21.

Hemmatifar, A., Stadermann, M. & Santiago, J. (2015). Two-Dimensional porous electrode model for capacitive deionization. *Desalination*, 228(1-3), 10–29.

Huang, C.-C. & He, J.-C. (2013). Electrosorptive removal of copper ions from wastewater by using ordered mesoporous carbon electrodes. *Chem. Eng. J.*, (221), 469–475.

Huang, G.-H., Chen, T.-C., Hsu, S.-F., Huang, Y.-H. & Chuang, S.-H. (2013). Capacitive deionization (CDI) for removal of phosphate from aqueous solution. *Desalin. Water Treat.*, (52), 759-765.

Huang, S.-Y., Fan, C.-S. & Hou, C.-H. (2014). Electrosorption of chromium ions on carbon aerogel electrodes as a means of remediating ground water. *J. Hazard. Materl*, (278), 8-15.

Husain, M. A., Tariq, A., Hameed, S., Arif, M. S. B. & Jain, A. (2017). Comparative assessment of maximum power point tracking procedures for photovoltaic systems. *Green Energy and Environment*, 2(1), 5-17. doi: https://doi.org/10.1016/j.gee.2016.11.001.

Huyskens, C., Helsen, J., Groot, W. J. & de Haan, A. B. (2013). Charge efficiency: a functional tool to probe the double-layer structure inside of porous electrodes and application in the modeling of capacitive deionization. *Sep. Purif. Technol.*, (118), 33-39.

Hwang, S. & Hyun, S. (2004). Capacitance control of carbon aerogel electrodes. . *Non-Cryst. Solids*, 347, 238–245.

J., H. R., El-Shahat, A. & Kalaani, Y. (2015). Lead Acid Battery Modeling for PV Applications. *Journal of Electrical Engineering*, 17-24.

Jain, S. & Agarwal, V. (2004). A new algorithm for rapid tracking of approximate maximum power point in photovoltaic systems. *IEEE Power Electronics Letters*, 2(1), 16-19. doi: 10.1109/LPEL.2004.828444.

Jande, Y. & Kim, W. (2013). Desalination using capacitive deionization at constant current. *Desalination*, 329, 29-34.

Jantharamin, N. & Zhang, L. (2008). A new dynamic model for lead-acid batteries. *2008 4th IET Conference on Power Electronics, Machines and Drives*, pp. 86-90.

JC, F., DV, F., GV, M., RW, P. & JF., P. (1996). Capacitive deionization of NaCl and NaNO3 solutions with carbon aerogel electrodes. *J Electrochem Soc*, 143, 159-69.

Jeon, S.-I., Park, H.-R., Yeo, J.-G., Yang, S., Cho, C. H., Han, M. H. & Kim, D.-K. (2013). Desalination via a new membrane capacitive deionization process utilizing flow-electrodes. *Environmental Science and Technology*, (6), 1471–1475.

Jeon, S.-I., Park, J.-S., Yeo, J.-G., Yang, S., Choi, J. & Kim, D. K. (2014). Ion storage and energy recovery of a flow-electrode capacitive deionization process. *J. Mater. Chem. A*, (2), 6378–6383.

Johnson, A. M. & Newman, J. (1971). Desalting by means of porous carbon electrodes. *J. Electrochem. Soc.*, (118), 510-517.

Johnson, A. M., Venolia, A. W., Wilbourne, R. G., Newman, J., Wong, C. M., Gilliam, W. S., Johnson, S. & Horowitz, R. H. (1970). Electrosorb Process for Desalting Water, Office of Saline Water Research and Development Progress Report No. 516. *U. S. Dept. of the Interior,Washington,US*, (1), 184.

Jung, H., Hwang, S., Hyun, S., Lee, K. & Kim, G. (2007). Capacitative deionization characteristics of nanostructured carbon aerogel electrodes synthesized via ambient drying. *Desalination*, 216(1-3), 377–385.

Jung, S.-M., Choi, J.-H. & Kim, J.-H. (2012). Application of capacitive deionization (CDI) technology to insulin purification process. *Sep. Purif. Technol.*, (98), 31-35.

Kamarzaman, N. A. & Tan, C. W. (2014). A comprehensive review of maximum power point tracking algorithms for photovoltaic systems. *Renewable and Sustainable Energy Reviews*, 37, 585-598.

Kang, J., Kim, T., Jo, K. & Yoon, J. (2014). Comparison of salt adsorption capacity and energy consumption between constant current and constant voltage operation in capacitive deionization. *Desalination*, 352, 52-57.

Kedem, O. & Robinson, T. (1980). Electrodialysis device. *US Pat., 4,226,688*, 1.

Khaehintung, N., Pramotung, K., Tuvirat, B. & Sirisuk, P. (2004). RISC-microcontroller built-in fuzzy logic controller of maximum power point tracking for solar-powered light-flasher applications. *30th Annual Conference of IEEE Industrial Electronics Society, 2004. IECON 2004*, 3, 2673-2678 Vol. 3. doi: 10.1109/IECON.2004.1432228.

Khan, F. H., Tolber, L. & E.Webb, W. (2010). Start-up and dynamic modeling of the multilevel modular capacitor-clamped converter. *IEEE Trans. Power Electron*, 25(2), 519–531.

Kim, J.-S., Kim, J.-H., Park, J.-M., Park, S.-M., Choe, W.-Y. & Heo, H. (2008). Auto Tuning PID Controller based on Improved Genetic Algorithm for Reverse Osmosis Plant. *World Academy of Science, Engineering and Technology*, 47.

Kim, N., Lee, J., Kim, S., Hong, S. P., Lee, C., Yoon, J. & Kim, C. (2020). Short Review of Multichannel Membrane Capacitive Deionization: Principle, Current Status, and Future Prospect. *Applied Sciences*, 10, 2076-3417.

Kim, S.-J., Choi, J.-H. & Kim, J.-H. (2012). Removal of acetic acid and sulfuric acid from biomass hydrolyzate using a lime addition–capacitive deionization (CDI) hybrid process. *Process Biochem.*, (47), 2051–2057.

Kim, T. & Yoon, J. (2015). CDI ragone plot as a functional tool to evaluate desalination performance in capacitive deionization. *RSC Adv.*, (5), 1456–1461.

Kim, T., Dykstra, J., Porada, S., van der Wal, A., Yoon, J. & Biesheuvel, P. (2015). Enhanced charge efficiency and reduced energy use in capacitive deionization by increasing the discharge voltage. *J. Colloid Interface Sci.*, 446(1), 317–326.

Kim, T.-Y., Ahn, H.-G., Park, S. K. & Lee, Y.-K. (2001). A novel maximum power point tracking control for photovoltaic power system under rapidly changing solar radiation. *ISIE 2001. 2001 IEEE International Symposium on Industrial Electronics Proceedings (Cat. No.01TH8570)*, 2, 1011-1014 vol.2.

Kim, Y.-J. & Choi, J.-H. (2010a). Improvement of desalination efficiency in capacitive deionization using a carbon electrode coated with an ion-exchange polymer. *Water Ressources*, (44), 990-996.

Kim, Y.-J. & Choi, J.-H. (2012). Enhanced desalination efficiency in capacitive deionization with an ion-selective membrane. *Water Ressources*, (46), 6033-6039.

Kim, Y. & Choi, J. (2010b). Enhanced desalination efficiency in capacitive deionization with an ion-selective membrane. *Sep. Purif. Technol.*, 71, 70–75.

KK, P., JB, L., PY, P., SW, Y., JS, M. & HM, E. (2007). Development of a carbon sheet electrode for electrosorption desalination. *Desalination*, 206, 86-91.

Kobayashi, K., Takano, I. & Sawada, Y. (2003). A study on a two stage maximum power point tracking control of a photovoltaic system under partially shaded insolation conditions. *2003 IEEE Power Engineering Society General Meeting (IEEE Cat. No.03CH37491)*, 4, 2612-2617 Vol. 4.

Kwak, N.-S., Koo, J., Hwang, T. & Choi, E. (2011). Synthesis and electrical properties of NaSS–MAA–MMA cation exchange membranes for membrane capacitive deionization (MCDI). *Desalination*, 285, 138–146.

KY, F. & BH., H. (2009). A short review of activated carbon electrosorption process: an overview, current stage and future prospects. *J Hazard Mater*, 170, 552e9.

Lai, J.-S. & Peng, F. Z. (1996). Multilevel converters-a new breed of power converters. *IEEE transactions on industry applications*, 32(3), 509–517.

Laily, Z. & Abdul Rahman, S. (2016). Performance Comparison of PID Tuning by Using Ziegler-Nichols And Particle Swarm Optimization Approaches in a Water Control System. *Journal of Information and Communication Technology*, 15, 203-224.

Landon, J., Gao, X., Omosebi, A. & Liu, K. (2019). Progress and outlook for capacitive deionization technology. *Current Opinion in Chemical Engineering*, 25, 1-8.

Lee, J., Kim, S., Kim, C. & Yoon, J. (2014). Hybrid capacitive deionization to enhance the desalination performance of capacitive techniques. *Energy Environ. Sci.*, (7), 3683–3689.

Lee, J.-H., Bae, W.-S. & Choi, J.-H. (2010). Electrode reactions and adsorption/desorption performance related to the applied potential in a capacitive deionization process. *Desalination*, (258), 159-163.

Lee, J.-Y., Seo, S.-J., Yun, S.-H. & Moon, S.-H. (2011a). *Water Ressorces*, (41), 5375–5380.

Lee, J.-B., Park, K.-K., Yoon, S.-W., Park, P.-Y., Park, K.-I. & Lee, C.-W. (2009a). Desalination performance of a carbon-based composite electrode. *Desalination*, 237(1), 155-161. Issue 1: Water Resources Management: New Approaches and Technologies.

Lee, J., Kim, Y., Kim, J., Chung, S., Ji, D. & Lee, J. (2011b). Comparable mono and bipolar connection of capacitive deionization stack in NaCl treatment. *J. Ind. Eng. Chem.*, 34, 763–766.

Lee, Y., Khaligh, A. & Emadi, A. (2009b). Compensation technique for smooth transitions in a noninverting buck–boost converter. *IEEE Trans. Ind. Electron.*, 24(4), 1002–1015.

Legrand, L., Shu, Q., Tedesco, M., Dykstra, J. & Hamelers, H. (2020). Role of ion exchange membranes and capacitive electrodes in membrane capacitive deionization (MCDI) for CO2 capture. *Journal of Colloid and Interface Science*, 564, 478-490.

Leonard, K., Genthe, J., Sanfilippo, J., Zeltner, W. & Anderson, M. (2009). Synthesis and characterization of asymmetric electrochemical capacitive deionization materials using nanoporous silicon dioxide and magnesium doped aluminum oxide. *Electrochimica Acta*, 54(22), 5286-5291.

Li, H., Gao, Y., Pan, L., Zhang, Y., Chen, Y. & Sun, Z. (2008a). Electrosorptive desalination by carbon nanotubes and nanofibres electrodes and ion-exchange membranes. *Water Ressources*, (42), 4923–4928.

Li, H., Zou, L., Pan, L. & Sun, Z. (2010). Novel graphene-like electrodes for capacitive deionization. *Environ. Sci. Technol.*, (44), 8692–8697.

Li, H., Nie, C., Pan, L. & Sun, Z. (2012). The study of membrane capacitive deionization from charge efficiency. *Desalin. Water Treat.*, 42, 210-215.

Li, H., Gao, Y., Pan, L., Zhang, Y., Chen, Y. & Sun, Z. (2008b). Electrosorptive desalination by carbon nanotubes and nanofibres electrodes and ion-exchange membranes. *Water Research*, 42(20), 4923-4928.

Lim, J.-A., Park, N.-S., Park, J.-S. & Choi, J.-H. (2009). Fabrication and characterization of a porous carbon electrode for desalination of brackish water. *Desalination*, 238(1), 37-42.

Linzen, D., Buller, S., Karden, E. & Doncker, R. W. D. (2005). Analysis and evaluation of chargebalancing circuits on performance, reliability, and lifetime of supercapacitor systems. *IEEE transactions on industry applications*, 41(5), 1135–1141.

Liu, E., Lee, L. Y., Ong, S. L. & Ng, H. Y. (2020). Treatment of industrial brine using capacitive deionization (CDI) towards zero liquid discharge – challenges and optimization. *Water Research*, 183, 116059.

Liu, Y., Pan, L., Xu, X., Lu, T. & Sun, Z. (2013). Selective lithium recovery from aqueous solution using a modified membrane capacitive deionization system. *RSC Adv.*, (3), 16932–16935.

Lorenzo, E. (1994). Solar Electricity: Engineering of Photovoltaic System. *Progensa, Sevilla*, 1.

Lu, R., Tian, L., Zhu, C. & Yu, H. (2008). A new topology of switched capacitor circuit for the balance system of ultracapacitor stacks. *IEEE Vehicle Power Propulsion Conf.*, 1-5.

M., A. (2011). Flow through capacitor basics. *Sep Purif Technol*, 80, 262-9.

MA, A., AL, C. & J., P. (2010). Capacitive deionization as an electrochemical means of saving energy and delivering clean water. Comparison to present desalination practices: will it complete. *Electrochim Acta*, 55, 3845-56.

Macı´as, C., Lavela, P., Rasines, G., Zafra, M. C., Tirado, J. L. & Ania, C. O. (2014). N-doped monolithic carbon aerogel electrodes with optimized features for the electrosorption of ions. *J. Appl. Electrochem.*, (44), 963–976.

Markvart, T. (1994). Solar Electricity. *John Wiley and Sons, Chichester*, 322.

Miao, L., Deng, W., Chen, X., Gao, M., Chen, W. & Ao, T. (2021). Selective adsorption of phosphate by carboxyl-modified activated carbon electrodes for capacitive deionization. *Water Science and Technology*, 84(7), 1757-1773.

Midya, P., Krein, P., Turnbull, R., Reppa, R. & Kimball, J. (1996). Dynamic maximum power point tracker for photovoltaic applications. *PESC Record. 27th Annual IEEE Power Electronics Specialists Conference*, 2, 1710-1716 vol.2. doi: 10.1109/PESC.1996.548811.

Mohandes, M. A. (2012). Modeling global solar radiation using Particle Swarm Optimization (PSO). *Solar Energy*, 86(11), 3137-3145. doi: https://doi.org/10.1016/j.solener.2012.08.005.

M.Pernia, A., Alvarez-Gonzalez, F. J., Diaz, J., J.Villegas, P. & Nuno, Y. F. (2014). Optimum peak current hysteresis control for energy recovering converter in MCDI desalination. *Energies*, 7, 3823–3839.

Nelson, J. (2003). The Physics of Solar Cells. *Imperial College Press*, 111.

Oh, H.-J., Lee, J.-H., Ahn, H.-J., Jeong, Y., Kim, Y.-J. & Chi, C.-S. (2006). Nanoporous activated carbon cloth for capacitive deionization of aqueous solution. *Thin Solid Films*, 515(1), 220-225.

Omosebi, A., Gao, X., Landon, J. & Liu, K. (2014). Asymmetric electrode configuration for enhanced membrane capacitive deionization. *ACS Appl. Mater. Interfaces*, (6), 12640–12649.

Oren, Y. (2008). Capacitive deionization (CDI) for desalination and water treatment—Past, present and future (a review). *Desalination*, 228(1-3), 10–29.

Oren, Y. & Soffer, A. (1983). Water desalting by means of electrochemical parametric pumping: I. The equilibrium properties of a batch unit cell. *J. Appl. Electrochem.*, (13), 473–487.

Park, S.-H., Kim, T.-S., Park, J.-S., Moon, G.-W. & Yoon, M.-J. (2009). A new buck–boost type battery equalizer. *Proc. 24th Annu. IEEE Appl. Power Electron. Conf. Expo.*, 1246–1250.

Pasta, M., Wessells, C. D., Cui, Y. & Mantia, F. L. (2012). A desalination battery. *Nano Lett.*, (12), 839-843.

Patcharaprakiti, N. & Premrudeepreechacharn, S. (2002). Maximum power point tracking using adaptive fuzzy logic control for grid-connected photovoltaic system. *2002 IEEE Power Engineering Society Winter Meeting. Conference Proceedings (Cat. No.02CH37309)*, 1, 372-377 vol.1. doi: 10.1109/PESW.2002.985022.

Pernía, A. M., Alvarez-González, F. J., Díaz, J., Villegas, P. J. & Nuño, Y. F. (2014). Optimum peak current hysteresis control for energy recovering converter in CDI desalination. *Energies*, 7(6), 3823–3839.

Pernía, A. M., Norniella, J. G., Martín-Ramos, J. A., Díaz, J. & Martínez, J. A. (2012). Up–Down Converter for Energy Recovery in a CDI Desalination System. *IEEE Transactions on Power Electronics*, 27(7), 3257-3265.

Planes, G. A., Miras, M. C. & Barbero, C. A. (2005). Double layer properties of carbon aerogel electrodes measured by probe beam deflection and AC impedance techniques. *Chem. Commun.*, 2146–2148.

Porada, S., Sales, B. B., Hamelers, H. V. M. & M.Biesheuvel, P. (2012a). Water Desalination with Wires. *J. Phys. Chem. Lett.*, (3), 1613–1618.

Porada, S., Weinstein, L., Dash, R., van der Wal, A., Bryjak, M., Gogotsi, Y. & Biesheuvel, P. M. (2012b). Water Desalination Using Capacitive Deionization with Microporous Carbon Electrodes. *ACS Appl. Mater. Interfaces*, (4), 1194–1199.

Porada, S., Borchardt, L., Oschatz, M., Bryjak, M., Atchison, J., Keesman, K. J., Kaskel, S., Biesheuvel, P. M. & Presser, V. (2013a). Direct prediction of the desalination performance of porous carbon electrodes for capacitive deionization. *Energy Environ. Sci.*, (6), 3700–3712.

Porada, S., Zhao, R., van der Wal, A., Presser, V. & Biesheuvel, P. (2013b). Review on the science and technology of water desalination by capacitive deionization. *Progress in Materials Science*, 58(8), 1388-1442.

Porada, S., Weingarth, D., Hamelers, H. V. M., Bryjak, M., Presser, V. & Biesheuvel, P. M. (2014). Carbon flow electrodes for continuous operation of capacitive deionization and capacitive mixing energy generation. *J. Mater. Chem. A*, (2), 9313–9321.

Porada, S., Biesheuvel, P. M. & Presser, V. (2015). Comment on" Sponge-templated preparation of high surface area graphene with ultrahigh capacitive deionization performance". *Adv. Funct.Mater.*, (25), 179-181.

Presser, V., Dennison, C. R., Campos, J., Knehr, K. W., Kumbur, E. C. & Gogotsi, Y. (2012). The electrochemical flow capacitor: A new concept for rapid energy storage and recovery. *Adv. Energy Mater.*, (2), 895–902.

Qu, Yatian, Baumann, F.Theodore, Santiago, G. J. & M.Stadermann. (2015). Characterization of Resistances of a Capacitive Deionization System. *Environmental Science and Technology*, 49(19), 9699-9706.

Quismondo, E. G., Santos, C., Soria, J. & Anderson, M. (2015). New operational modes to increase energy efficiency in capacitive deionization system. *Environ. Sci.*, 8, 2296-2319.

Rao, C. S., Santosh, S. & V, D. R. (2020). Tuning optimal PID controllers for open loop unstable first order plus time delay systems by minimizing ITAE criterion. *IFAC-PapersOnLine*, 53(1), 123-128.

Rizoug, N., Bartholomeus, P. & Le Moigne, P. (2010). Modeling and Characterizing Supercapacitors Using an Online Method. *IEEE Transactions on Industrial Electronics*, 57(12), 3980-3990.

Roelofs, S. H., Kim, B., Eijkel, J. C. T., Han, J., van den Berg, A. & Odijk, M. (2015). Capacitive deionization on-chip as a method for microfluidic sample preparation. *Lab Chip*, (15), 1458-1464.

Ryoo, M.-W., Kim, J.-H. & Seo, G. (2003). Role of titania incorporated on activated carbon cloth for capacitive deionization of NaCl solution. *Journal of colloid and interface science*, 264(2), 414—419. doi: 10.1016/s0021-9797(03)00375-8.

Ryu, T., Lee, D.-H., Ryu, J. C., Shin, J., Chung, K.-S. & Kim, Y. H. (2015). *Hydrometallurgy*, (151), 78-83.

Salameh, Z., Casacca, M. & Lynch, W. (1992). A mathematical model for lead-acid batteries. *IEEE Transactions on Energy Conversion*, 7(1), 93-98.

Saleem, M. W., Jande, Y. A. C., Asif, M. & Kim, W.-S. (2016). Hybrid CV-CC operation of capacitive deionization in comparison with constant current and constant voltage. *Separation Science and Technology*, 51(6), 1063-1069.

Samosir, A. S. & Yatim, A. H. M. (2010). Implementation of dynamic evolution control of bidirectional dc–dc converter for interfacing ultracapacitor energy storage to fuel cell system. *IEEE Trans. Ind. Appl.*, 57(10), 3468–3473.

Senjyu, T. & Uezato, K. (1994). Maximum power point tracker using fuzzy control for photovoltaic arrays. *Proceedings of 1994 IEEE International Conference on Industrial Technology - ICIT '94*, pp. 143-147. doi: 10.1109/ICIT.1994.467196.

Seo, S.-J., Jeon, H., Lee, J. K., Kim, G.-Y., Park, D., Nojima, H., Lee, J. & Moon, S.-H. (2010). Investigation on removal of hardness ions by capacitive deionization (CDI) for water softening applications. *Water Research*, 44(7), 2267-2275.

Shukang, C., Hailong, G., Cuiping, L., Bin, G. & Peng, Z. (2008). Research on electric mesh grid for seawater desalination based on capacitive deionization. *Proc. Int. Conf. Electr. Mach. Syst.*, 3854–3857.

Soffer, A. & Folman, M. (1972). The electrical double layer of high surface porous carbon electrode. *J. Electroanal. Chem. Interfacial Electrochem.*, (38), 25-43.

Soto, W. D., Klein, S. & Beckman, W. (2006). Improvement and Validation of a Model for Photovoltaic Array Performance. *Solar Energy*, 80(1), 78 - 88.

Sreekumar, C. & Agarwal, V. (2008). A hybrid control algorithm for voltage regulation in dc–dc boost converter. *IEEE Trans. Ind. Electron.*, 55(6), 2530–2538.

Stoller, M. D. & Ruoff, R. S. (2010). Best practice methods for determining an electrode material's performance for ultracapacitors. *Energy Environ. Sci.*, (3), 1294–1301.

Suss, T.F.Baumann, M.a.Worsley, K.a.Rose, T.F.Jaramillo, M.Stadermann & J.G.Santiago. (2013). Impedance-based study of capacitive porous carbon electrodes with hierarchical and bimodal porosity. *Journal of Power Sources*, 241(19), 266-273.

Suss, M. E., Baumann, T. F., Bourcier, W. L., Spadaccini, C. M., Rose, K. A., Santiago, J. G. & Stadermann, M. (2012). Capacitive desalination with flow-through electrodes. *Energy Environ. Sci.*, (5), 9511-9519.

Suss, M. E., Biesheuvel, P., Baumann, T. F., Stadermann, M. & Santiago, J. G. (2014). In Situ Spatially and Temporally Resolved Measurements of Salt Concentration between charging Porous Electrodes for Desalination by Capacitive Deionization. *Environ. Sci. Technol.*, (48), 2008–2015.

Suss, M. E., Porada, S., Sun, X., Biesheuvel, P. M., Yoonf, J. & Presser, V. (2015). Water desalination via capacitive deionization:what is it and what can we expect from it? *Energy Environ. Sci.*, 8(2296), 11.

Tafticht, T. & Agbossou, K. (2004). Development of a MPPT method for photovoltaic systems. *Canadian Conference on Electrical and Computer Engineering 2004 (IEEE Cat. No. 04CH37513)*, 2, 1123-1126 Vol.2. doi: 10.1109/CCECE.2004.1345317.

Tan, C., He, C., Tang, W., Kovalsky, P., Fletcher, J. & Waite, T. D. (2018). Integration of photovoltaic energy supply with membrane capacitive deionization (MCDI) for salt removal from brackish waters. *Water Research*, 147, 276-286.

UN. (2018). Rapport mondial des Nations Unies sur la mise en valeur des ressources en eau. Retrieved from: https://www.un.org/fr/sections/issues-depth/water/index.htmla.

UNESCO. (2021). The United Nations world water development report 2021: valuing water. Retrieved from: https://unesdoc.unesco.org/ark:/48223/pf0000375724/PDF/375724eng.pdf.multi.

van Limpt, B. & van der Wal, A. (2014). Water and chemical savings in cooling towers by using membrane capacitive deionization. *Desalination*, (342), 148-155.

Wang, G., Dong, Q., Ling, Z., Pan, C., Yu, C. & Qiu, J. (2012). Hierarchical activated carbon nanofiber webs with tuned structure fabricated by electrospinning for capacitive deionization. *J. Mater. Chem.*, (22), 21819–21823.

Wang, G., Qian, B., Dong, Q., Yang, J., Zhao, Z. & Qiu, J. (2013). Highly mesoporous activated carbon electrode for capacitive deionization. *Sep. Purif. Technol.*, (103), 216-221.

Wang, H. & Na, C. (2014). Binder-free carbon nanotube electrode for electrochemical removal of chromium. *ACS Appl. Mater. Interfaces*, (6), 20309–20316.

Wang, H., Shi, L.-Y., Yan, T., Zhang, J., Zhong, Q. & Zhang, D. (2014). Three-dimensional macroporous graphene architectures as high performance electrodes for capacitive deionization. *J. Mater. Chem.*, (2), 4739–4750.

Wang, X. Z., Li, M. G., Chen, Y. W., Cheng, R. M., M.Huang, S., Pan, L. K. & Sun, Z. (2006). Electrosorption of ions from aqueous solutions with carbon nanotubes and nanofibers composite film electrodes. *Electrochem. Solid-State Lett.*, (9), E23–E26.

Wang, Z., Lin, W., Wang, W., Wang, Z., Li, J., Xu, J. & Yu, J. (2021). Research on performance optimization and mechanism of electrochemical water softening applied by pulse power supply. *Water Science and Technology*, 84(9), 2432-2445.

Welgemoed, T. J. & Schutte, C. F. (2005a). Capacitive deionization technology: An alternatif desalination solution. *Desalination*, 183(1-3), 327–340.

Welgemoed, T. & Schutte, C. (2005b). Capacitive Deionization Technology: An alternative desalination solution. *Desalination*, 183(1), 327-340. Desalination and the Environment.

WWAP. (2018). Le Programme mondial des Nations Unies pour l'évaluation des ressources en eau. Retrieved from: https://www.un.org/fr/sections/issues-depth/water/index.htmla.

Xiao, W. & Dunford, W. (2004). A modified adaptive hill climbing MPPT method for photovoltaic power systems. *2004 IEEE 35th Annual Power Electronics Specialists Conference (IEEE Cat. No.04CH37551)*, 3, 1957-1963 Vol.3. doi: 10.1109/PESC.2004.1355417.

Xu, P., Drewes, J. E., Heil, D. & Wang, G. (2008). Treatment of brackish produced water using carbon aerogel-based capacitive deionization technology. *Water Research*, 42(10), 2605-2617.

Y., O. (2008). Capacitive deionization (CDI) for desalination and water treatment e past, present and future (a review). *Desalination*, 228, 10-29.

Yang, K., Ying, T., Yiacoumi, S., Tsouris, C. & Vittoratos, E. (2001). Electrosorption of ions from aqueous solutions by carbon aerogel: an electrical double-layer model. *Langmuir*, 17, 1961–1969.

Yang, L. F., Shi, Z. & Yang, W. H. (2014). Enhanced capacitive deionization of lead ions using air-plasma treated carbon nanotube electrode. *Surf. Coat. Technol.*, (251), 122-127.

Yeo, J.-H. & Choi, J.-H. (2013). Enhancement of nitrate removal from a solution of mixed nitrate, chloride and sulfate ions using a nitrate-selective carbon electrode. *Desalination*, (320), 10-16.

Ying, T.-Y., Yang, K.-L., Yiacoumi, S. & Tsouris, C. (2002). Electrosorption of Ions from Aqueous Solutions by Nanostructured Carbon Aerogel. *Journal of Colloid and Interface Science*, 250(1), 18-27.

Zhang, D., Shi, L., Fang, J., Dai, K. & Li, X. (2006). co-doped hollow carbon polyhedra derived from MOF-based core–shell nanocomposites for capacitive deionization. *Mater. Chem.Phys.*, (97), 415-419.

Zhang, L., Bai, Y. & Al-Amoudi, A. (2002). GA-RBF neural network based maximum power point tracking for grid-connected photovoltaic systems. *2002 International Conference on Power Electronics, Machines and Drives (Conf. Publ. No. 487)*, pp. 18-23. doi: 10.1049/cp:20020083.

Zhang, S. & Pan, N. (2015). Supercapacitors performance evaluation. *Adv. Energy Mater*, (5), 10.1002.

Zhao, R., Biesheuvel, P. M., Miedema, H., Bruning, H. & van der Wal, A. (2010). Charge efficiency: a functional tool to probe the double-layer structure inside of porous electrodes and application in the modeling of capacitive deionization. *J. Phys. Chem. Lett.*, (1), 205-210.

Zhao, R., Biesheuvel, M. & der Wal, B. V. (2012a). Energy consumption and constant current operation in membrane capacitive deionization. *Energy Environ. Sci.*, 5, 9520–9527.

Zhao, R., van Soestbergen, M., Rijnaarts, H., van der Wal, A., Bazant, M. & Biesheuvel, P. (2012b). Time-dependent ion selectivity in capacitive charging of porous electrodes. *Journal of Colloid and Interface Science*, 384(1), 38-44.

Zhao, R., Porada, S., Biesheuvel, P. M. & van der Wal, A. (2013a). Energy consumption in membrane capacitive deionization for different water recoveries and flow rates, and comparison with reverse osmosis. *Desalination*, (330), 35-41.

Zhao, R., Satpradit, O., Rijnaarts, H., Biesheuvel, P. & vanderWal, A. (2013b). Optimization of salt adsorption rate in membrane capacitive deionization. *Water Res.*, 47, 1941–1952.

Zhao, Y., Wang, Y., Wang, R., Wu, Y., Xu, S. & Wang, J. (2013c). Performance comparison and energy consumption analysis of capacitive deionization and membrane capacitive deionization processes. *Desalination*, 324, 127-133.

Zou, L., Li, L., Song, H. & Morris, G. (2008a). Using mesoporous carbon electrodes for brackish water desalination. *Water Research*, 42(8), 2340-2348.

Zou, L., Morris, G. & Qi, D. (2008b). Using activated carbon electrode in electrosorptive deionisation of brackish water. *Desalination*, 225(1), 329-340.

Álvarez González, F. J., Martín-Ramos, J. A., Díaz, J., Martínez, J. A. & Pernía, A. M. (2016). Energy-Recovery Optimization of an Experimental CDI Desalination System. *IEEE Transactions on Industrial Electronics*, 63(3), 1586-1597.

Çetinkaya, A. Y. (2020). Life cycle assessment of environmental effects and nitrate removal for membrane capacitive deionization technology. *Environmental Monitoring and Assessment*, 543, 192.